

**FLOTATION OF AURIFEROUS PYRITE USING A MIXTURE OF
COLLECTORS**

By

ANTONY TAPIWA MAKANZA

Submitted in partial fulfilment of the requirements for the degree

**Master of Engineering
(Metallurgical Engineering)**

in the

Faculty of Engineering, Built Environment and Information Technology
University of Pretoria

December 2005

*...now unto Him that is able to do exceeding abundantly above
all that we ask or think, according to the power that worketh in
us....*

ACKNOWLEDGEMENTS

First of all, I would like to extend my greatest appreciation to Anglogold Ashanti for providing the financial support for this project. To Sarah Havenga and Professor Chris Pistorius, your commitment cannot be summarised in a few words. Thank you for all the support that you gave me during my time as a student in the department. You will always be remembered for your kindness. Professor John Davidtz, words cannot express how grateful I am for your unwavering support and guidance throughout the project. You've got loads of patience I must say, going through all that nonsense I used to send you and for listening to me all those times I used to make unfounded arguments. It's a quality that many would desire to have, but is often elusive. To Tham, thank you for being a source of inspiration. "I am free at last". To all my friends from His People Church, thank you for all the encouragement in all those times when it looked like the end was endless. Last but not least, I would like to thank my wife Ennie and our daughter Mutsawashe for being there when I needed them and when I desperately did not need them.

Antony T. Makanza

November 2005

Pretoria, South Africa

FLOTATION OF AURIFEROUS PYRITE USING A MIXTURE OF
COLLECTORS

By

ANTONY TAPIWA MAKANZA

Supervisors: Professor John C. Davidtz
Doctor Thys (MKG) Vermaak
Department: Materials Science and Metallurgical Engineering
Degree: Master of Engineering

ABSTRACT

The effects SIBX/C₁₀ (or C₁₂) TTC mixtures on flotation response of pyrite, gold and uranium from AngloGold Ashanti's No 2 Gold Plant feed were investigated. In batch flotation tests where TTC was dosed from aged 1% wt stock solutions, synergism was shown to occur in gold flotation at 25 mole percent C₁₂ TTC and in uranium flotation at a similar dosage of C₁₀ TTC. With commercial C₁₂ TTC, 8 mole percent recorded the highest uranium and gold recoveries. The SIBX/C₁₂ TTC mixture had a greater effect on gold than on uranium. When C₁₂ mercaptan replaced the TTC in SIBX mixtures, rates and recoveries decreased at all levels.

Kinetics and recovery with a mixture of 92 mole percent SIBX and 8 mole percent commercial C₁₂ TTC gave a better flotation activity than obtained with SIBX alone. A combination of SIBX and an aged 1% wt solution of TTC lost activity when compared to that of SIBX and commercial TTC. This was attributed to the hydrolysis of TTC.

Micro-probe analysis, back-scattered electron images, and EDS analysis showed that all the uranium recovered in flotation concentrates was associated with either pyrite, galena or a carbonaceous material (karogen). This was attributed to the flotation of the uranium oxide minerals brannerite and uraninite.

Conditioning at pH values between 1.9-3.7 improved kinetics of gold, sulphur and uranium collection, but sulphur and uranium final recoveries were lower and gold final recovery was higher than the standard.

In the presence of 0.001M cyanide, equivalent to 70g/t copper sulphate failed to activate pyrite at both pH 5.5 and pH 7.2. At a similar molar dosage lead nitrate did activate pyrite at pH 5.5 but not at pH 7.2.

Keywords: Froth flotation, Auriferous Pyrite, Trithiocarbonate collectors, Cyanide, Lead nitrate, Copper sulphate, Mineralogy, pH

TABLE OF CONTENTS

Acknowledgements	iii
Abstract	iv
Chapter 1 Introduction	1
Chapter 2 Literature Review	3
2.1 Introduction	3
2.2 Operations at No. 2 Gold Plant – An Overview	3
2.3. Mineralogy of No 2 Gold Plant Feed	8
2.3.1 Introduction	8
2.3.2 Mineralogy of the Vaal Reef	8
2.4. Fundamentals of Froth Flotation	13
24.1 An Overview of the Flotation Process	13
2.4.2 Thermodynamic Considerations	14
2.4.3 Contact Angle	17
2.4.3 Flotation Rate	19
2.5. Collectors for Auriferous Pyrite Flotation	23
2.5.1 Xanthate (Dithiocarbonate) Collectors	26
2.5.2 Xanthate – Pyrite Interactions	29
2.5.3 Trithiocarbonate Collectors	31
2.5.4 TTC – Pyrite Interactions	32
2.5.5 Synergism in SIBX/TTC Mixtures	35
2.5.6 Mechanisms of Synergism	35
2.6. Activators for Auriferous Pyrite Flotation	37
2.6.1 Adsorption of Lead (II) Ions on Pyrite	39
2.6.2 Copper Sulphate	42
2.6.3 Adsorption of Copper (II) ions on Pyrite	44
2.6.4 Cyanide and Activation of Pyrite with Copper and Lead Ions	46
2.6.5 Iron ions and Surface Charge	53

Chapter 3 Materials and Methods	55
3.1 Materials	55
3.1.1 Ore	55
3.1.2 Reagents	57
3.1.3 Apparatus	57
3.2 Methods	59
3.2.1 Single-Point Flotation Tests	59
3.2.2 Release Curve Measurements	60
Chapter 4 Effect of SIBX dosage level on single point batch flotation	61
4.1 Introduction	61
4.2 Results and Discussion	62
4.2.1 Mass Recovery	62
4.2.2 Sulphur	63
4.2.3 Uranium	64
4.2.4 Gold	64
4.2.5 Optimum SIBX Dosage	65
4.2.6 Conclusions	66
Chapter 5 Effect of SIBX/TTC mixtures on single point batch flotation	67
5.1 Introduction	67
5.2 SIBX and C ₁₀ TTC	68
5.2.1 Results and Discussion	68
5.2.1.1 Mass Recovery	68
5.2.1.2 Sulphur	69
5.2.1.3 Uranium	70
5.2.1.4 Gold	72
5.2.1.5 Conclusions	73
5.3 SIBX and C ₁₂ TTC	74
5.3.1 Results and Discussion	74
5.3.1.1 Mass Recovery	74
5.3.1.2 Sulphur	75
5.3.1.3 Gold	76

5.3.1.4 Uranium	78
5.3.1.5 Conclusions	79
5.4 Auriferous Pyrite Flotation with SIBX/Fresh TTC Mixtures	80
5.4.1 Introduction	80
5.4.2 Results and Discussion	81
5.4.2.1 Water Recovery	81
5.4.2.2 Mass Recovery	82
5.4.2.3 Sulphur	83
5.4.2.4 Uranium	84
5.4.2.5 Gold	86
5.4.2.6 Conclusions	87
Chapter 6 Effect of Diluted and Aged TTC on Sulphur, gold and uranium flotation	88
6.1 Introduction	88
6.2 Results and Discussion	88
6.2.1 Water and Mass recovery	85
6.2.2 Sulphur Recovery	90
6.2.3 Uranium Recovery	91
6.2.5 Gold	92
6.2.6 Conclusions	93
Chapter 7 Effect of Conditioning pH on Sulphur, Gold and Uranium Flotation	95
7.1 Introduction	95
7.2 Results and Discussion	96
7.2.1 Sulphur	96
7.2.2 Uranium	101
7.2.3 Gold	111
7.2.4 Conclusions	113
Chapter 8 Activation of Pyrite by Pb ²⁺ and Cu ²⁺ in the Presence of Cyanide	114
8.1 Introduction	114

8.2 Results and Discussion	114
8.2.1 Copper Sulphate	114
8.2.2 Lead Nitrate	117
8.2.3 Copper Sulphate at pH 5.5	119
8.2.4 Lead Nitrate at pH 5.5	119
8.2.5 Conclusions	121
Chapter 5 Conclusions and Recommendations	125
References	121
Appendix A – Back-scattered electron images	131

LIST OF FIGURES

Figure 2.1	An XRD pattern for typical No. 2 Gold Plant feed	4
Figure 2.2	Flow sheet of No. 2 Gold Plant flotation circuit	7
Figure 2.3	Conglomerate comprised of pebbles of quartz embedded in a quartz rich matrix.	9
Figure 2.4	Photomicrograph showing uraniferous karogen containing inter- and intra-columnar gold	10
Figure 2.5	The radioactive decay of U^{238} to Pb^{206}	12
Figure 2.6	Processes occurring in a flotation cell	13
Figure 2.7	Mineral surface–collector–water interactions	15
Figure 2.8	Initial rate- G^{ex} relationship for DTC's and TTC's on copper	16
Figure 2.9	Relationship between G^{ex} and recovery for covalent TTC collector molecules	16
Figure 2.10	A summary of interacting variables in flotation	17
Figure 2.11	Schematic representation of the equilibrium contact between an air bubble and a solid immersed in a liquid	18
Figure 2.12	Typical curves obtained by fitting recovery-time data to a two parameter model.	21
Figure 2.13	Thiol collectors (a) dithiocarbonates, (b) trithiocarbonates	25
Figure 2.14	Illustration of different surfactant self-assembly structures	26
Figure 2.15	Hydrolysis and oxidation of ethyl xanthate in aqueous solution	27
Figure 2.16	Infrared spectrum of diamyl dixanthogen and pyrite conditioned in the absence and presence of PAX	29
Figure 2.17	Differential IR spectrum of pyrite after reacting with EX at pH 6	31
Figure 2.18	FTIR of (a) EX_2 and (b) $Fe(EX)_3$	31

Figure 2.19	Chemical structure of TTCs	32
Figure 2.20	Oxidation of Trithiocarbonates to their corresponding dimmers	33
Figure 2.21	Comparison between FTIR transmission spectra the n-amyl TTC dimer and that of pyrite treated with potassium n-amyl trithiocarbonate	33
Figure 2.22	Standard reduction potentials for thiocarbonate collectors as a function of alkyl chain length	34
Figure 2.23	Auriferous pyrite grade–recovery curves for DTC and 25% TTC / 75% DTC mixture	35
Figure 2.24	Electrochemically controlled contact angle measurements as a function of lead concentration for pyrite in PAX	37
Figure 2.25	(a) A Pobaix diagram for the Pb-H ₂ O (b) Lead (II) speciation at 1 x 10 ⁻³ M [Pb ²⁺]	38
Figure 2.26	Speciation of cyanide as a function of pH at 2 x 10 ⁻³ [CN ⁻].	39
Figure 2.27	Effect of copper sulphate on recovery of pyrite	43
Figure 2.28	Effect of copper sulphate on pyrite flotation	43
Figure 2.29	Effect of copper sulphate on gangue recovery	44
Figure 2.30	A Pourbaix diagram for the Fe-S-CN-H ₂ O system	47
Figure 2.31	Copper (II) speciation at different pH values.	47
Figure 2.32	Speciation diagram for 2 x 10 ⁻³ M Fe(III) as a function of pH at 25°C.	51
Figure 2.33	Speciation diagram for 2 x 10 ⁻³ M Fe(II) as a function of pH at 25°C.	51
Figure 2.34	Effect of pH and reagent addition order on the flotation of pyrite in the absence and presence of Fe ³⁺ ions	52
Figure 2.35	Effect of pH and reagent addition order on the flotation of ore-pyrite in the absence and presence of Fe ²⁺ ions	53

Figure 3.1	Typical particle size distribution of ore samples treated in this investigation.	56
Figure 3.2	A Denver D12 laboratory flotation machine	58
Figure 4.1	Response of mass recovery to different SIBX dosages	62
Figure 4.2	Change of (a) concentrate sulphur grade and (b) the corresponding recoveries with SIBX dosage	63
Figure 4.3	Variation of (a) uranium grade (b) uranium recovery with SIBX	64
Figure 4.4	Variation of (a) gold grade and (b) gold recovery with SIBX dosage	65
Figure 4.5	(a) sulphur, gold and uranium grades and (b) their corresponding recoveries plotted versus SIBX	66
Figure 5.1	Variation of mass recovery with mole percent of C ₁₀ TTC	68
Figure 5.2	Variation of (a) sulphur grade (b) sulphur recovery with C ₁₀ TTC mole ratio	70
Figure 5.3	Sulphur grade-recovery combinations for the different SIBX/C ₁₀ TTC mixtures tested	70
Fig. 5.4	Response of (a) uranium grade and (b) uranium recovery to different SIBX/ C ₁₀ TTC mixtures. (c) Corresponding uranium grade-recovery relationships	71
Fig. 5.5	(a) Gold grade and (b) recovery for SIBX/C ₁₀ TTC mixtures	73
Figure 5.6	Gold grade-recovery relationships for SIBX/C ₁₀ TTC combinations	73
Figure 5.7	Response of mass recovery to increased C ₁₂ TTC mole percent	75
Figure 5.8	Sulphur (a) grade and (b) recovery plotted against C ₁₂ TTC mole percent in the collector mixture	76
Figure 5.9	Response of gold (a) grade, and (b) gold recovery change in C ₁₂ TTC mole percent in the collector	77

Figure 5.10	Gold recoveries and their corresponding grades for SIBX/C ₁₂ mixtures	77
Figure 5.11	Response of uranium (a) grade and (b) recovery to change in C ₁₂ TTC mole percent	78
Figure 5.12	The response of water recovery to mole percent C ₁₂ TTC	81
Figure 5.13	Variation of mass recovery with mole percent C ₁₂ TTC of the mixture dosed	82
Figure 5.14	(a) Variation of sulphur grade with TTC mole percent and (b) the linear relationship between sulphur grade and mass recovery	83
Figure 5.15	(a) Plot of sulphur recovery versus TTC mole percent (b) Sulphur recoveries and their corresponding grades	84
Figure 5.16	(a) Variation of uranium grade and recovery with C ₁₂ TTC mole percent	85
Figure 5.17	Change in (a) gold grade and (b) gold recovery with mole percent C ₁₂ TTC	87
Figure 5.18	A summary of gold flotation responses for the different collector mixtures tested	87
Figure 6.1	Sulphur recovery-grade curves	91
Figure 6.2	Uranium recovery-grade curves	92
Figure 6.3	Gold recovery-grade curves	93
Figure 7.1	A Pourbaix diagram for the Fe-S-H ₂ O system at 25°C	97
Figure 7.2	Sulphur recovery-grade curves	98
Figure 7.3	Speciation diagram for 2 × 10 ⁻³ M Fe(III) as a function of pH at 25°C.	99
Figure 7.4	Speciation diagram for 2 × 10 ⁻³ M Fe(II) as a function of pH at 25°C	99
Figure 7.5	Uranium grade-recovery curves for conditioning at pH 1.9 and 7.2	102

Figure 7.6	A back-scattered electron image of a concentrate recovered with 20g/t SIBX	103
Figure 7.7	EDS spectra of phases in Figure 4.32.	104
Figure 7.8	Lead and uranium recoveries for C ₁₀ TTC/SIBX mixtures	105
Figure 7.9	Lead and uranium recoveries for C ₁₂ TTC/SIBX mixtures	105
Figure 7.10	A dispersion of fine uranium-containing particles embedded in a larger particle	106
Figure 7.11	A BEI taken from the micro-probe analysis of concentrates floated with 20g/t SIBX	106
Figure 7.12	EDS spectra generated from the microprobe analysis of an iron sulphide	108
Figure 7.13	EDS spectra generated from the microprobe analysis of the dark phase found in concentrates	109
Figure 7.14	Gold recovery–grade curves for two conditioning pHs: pH 1.9 and pH 7.5	111
Figure 8.1	A Pourbaix diagram for the Fe-S-CN-H ₂ O system	112
Figure 8.2	Copper (II) speciation at different pH values.	115
Figure 8.3	Lead (II) speciation at 2 × 10 ⁻⁴ M [Pb ²⁺].	116
Figure 8.4	(a) Sulphur (b) uranium and (c) gold recovery-time graphs recorded for 440mmol/t Pb(NO ₃) ₂ in NaCN	118
		120

LIST OF TABLES

Table 2.1	Typical minerals found in No. 2 Gold Plant Feed	5
Table 2.2	Chemical composition of calcine water	5
Table 2.3	Typical reagent suite used at No. 2 Gold Plant	6
Table 2.4	Vaal Reef pebble cementing matrix	9
Table 2.5	Application of Selected Thiol Collectors	23
Table 2.6	Selected Thiol Collector Structures	24
Table 2.7	Response of sulphide minerals to xanthate collectors	28
Table 2.8	Half-life times for SIBX and iC3-TTC	39
Table 2.9	Basic chemistry of the INCO SO ₂ /AIR process	49
Table 3.1	Typical minerals found in No. 2 Gold Plant Feed	55
Table 3.2	Chemical composition of the ore sample	56
Table 3.3	Collectors used in the study	57
Table 4.1	Mass recovery	62
Table 4.2	Sulphur flotation data for each SIBX dosage	63
Table 4.3	Uranium flotation responses for different SIBX dosages	64
Table 4.4	Gold flotation data for each SIBX dosage tested	65
Table 5.1	SIBX/C ₁₀ TTC combinations and reagent volumes	67
Table 5.2	SIBX/C ₁₂ TTC combinations and reagent volumes	67
Table 5.3	Mass recovery	68
Table 5.4	Sulphur flotation responses for SIBX/C ₁₀ TTC mixtures	69
Table 5.5	Uranium flotation responses for SIBX/C ₁₀ TTC mixtures	71
Table 5.6	Gold flotation data for SIBX/C ₁₀ TTC mixtures tested	72
Table 5.7	Mass recovery	74
Table 5.8	Sulphur flotation responses for SIBX/C ₁₂ TTC mixtures	75
Table 5.9	Gold flotation data for SIBX/C ₁₂ TTC mixtures tested	76
Table 5.10	Uranium flotation responses for SIBX/C ₁₂ TTC mixtures	78
Table 5.11	SIBX/C ₁₂ TTC combinations and reagent volumes	80
Table 5.12	Water recoveries	81
Table 5.13	Mass recovery	82

Table 5.14	Sulphur flotation responses for SIBX/C ₁₂ TTC mixtures	83
Table 5.15	Uranium flotation responses for SIBX/C ₁₂ TTC mixtures	85
Table 5.16	Gold flotation data for SIBX/C ₁₂ TTC mixtures	86
Table 6.1	Water initial rates and final recoveries	89
Table 6.2	Mass final recoveries and initial rates	89
Table 6.3	Sulphur initial rates and final recoveries	90
Table 6.4	Uranium final recoveries and initial rates	91
Table 6.5	Gold flotation responses for 8 mole percent TTC	93
Table 7.1	Sulphur final recoveries and initial rates	96
Table 7.2	Pulp pH and potentials recorded during conditioning	96
Table 7.3	Uranium final recoveries and initial rates	101
Table 7.4	Gold final recoveries and initial rates	111
Table 8.1	Flotation responses recorded with lead nitrate at pH 5.5	120

CHAPTER 1

INTRODUCTION

Gold in the feed to AngloGold Ashanti's North No. 2 Gold Plant is recovered by floating its pyrite host using sodium *iso*-butyl xanthate (SIBX) as a collector, Dowfroth 200 as a frother, copper sulphate as an activator, GEMPOLYM GM4 as a depressant and SO₂-containing calcine water as a cyanide oxidant and pH modifier.

Trial runs using a combination of 96.5 mole % SIBX and 3.7 mole % C₁₂ trithiocarbonate (TTC) collector, firstly in the laboratory and then at a full plant scale were conducted over a ten-month period (Davidtz, 2002). Results recorded from this work showed an increase in the recovery, of gold, uranium, and sulphur. Interest in the role played by the TTC collectors has led to research by The Department of Materials Science and Metallurgical Engineering at the University of Pretoria in conjunction with the Department of Metallurgy at the University of Utah. Some of the areas of interest include the effect of functional group changes O-CS₂ (xanthates) versus S-CS₂ (trithiocarbonates) with respect to auriferous pyrite flotation response and definition of relevant mechanisms using electrochemistry and spectroscopy. The present study is aimed at quantifying the effect of SIBX/TTC collector mixtures in the flotation of pyrite, gold and uranium from No. 2 Gold Plant feed. Attention is also given to the factors contributing to the flotation of uranium. The objectives of this work are:

1. To optimise the SIBX/TTC (C₁₀ and C₁₂) mixtures for oxidised pyrite flotation and study the effect of ageing TTC on flotation response.
2. To compare the activation of pyrite by Cu (II) and Pb (II) in the presence of cyanide.

3. To determine the probable mechanisms contributing to uranium flotation.
4. To determine the effect of conditioning pH on flotation

CHAPTER 2

LITERATURE REVIEW

2.1 Introduction

In this section, an overview of the operations at AngloGold Ashanti's No 2 Gold Plant operation is given. This is followed by a review of the mineralogy of the ore, collectors and activators used in this investigation. The thermodynamics of collector adsorption and mathematical models used the described the kinetics of flotation are examined as well.

2.2 Operations at No. 2 Gold Plant – An Overview

The feed to the plant originates from two sources:

- Tailings from No. 2 Pumpcell Plant, which leaches reclaimed West Pay Dam material. Slimes are sluiced using a hydraulic gun. The resulting pulp is treated with lime and cyanide, and leached while being transported in an 11km pipeline. At the plant, it is stripped of any dissolved gold by contacting with carbon in a Carbon-In-Leach (CIL) circuit.
- Gold leached material from No. 9 Gold Plant, which is fed with run-of-mine ore from No. 9 Shaft at Tau Lekoa Mine.

The two tailings streams are combined and de-slimes using cluster cyclones. The mineralogy of the composite feed varies but a typical analysis derived from Figure 2.1 is shown in Table 2.1.

CHAPTER 2. LITERATURE REVIEW

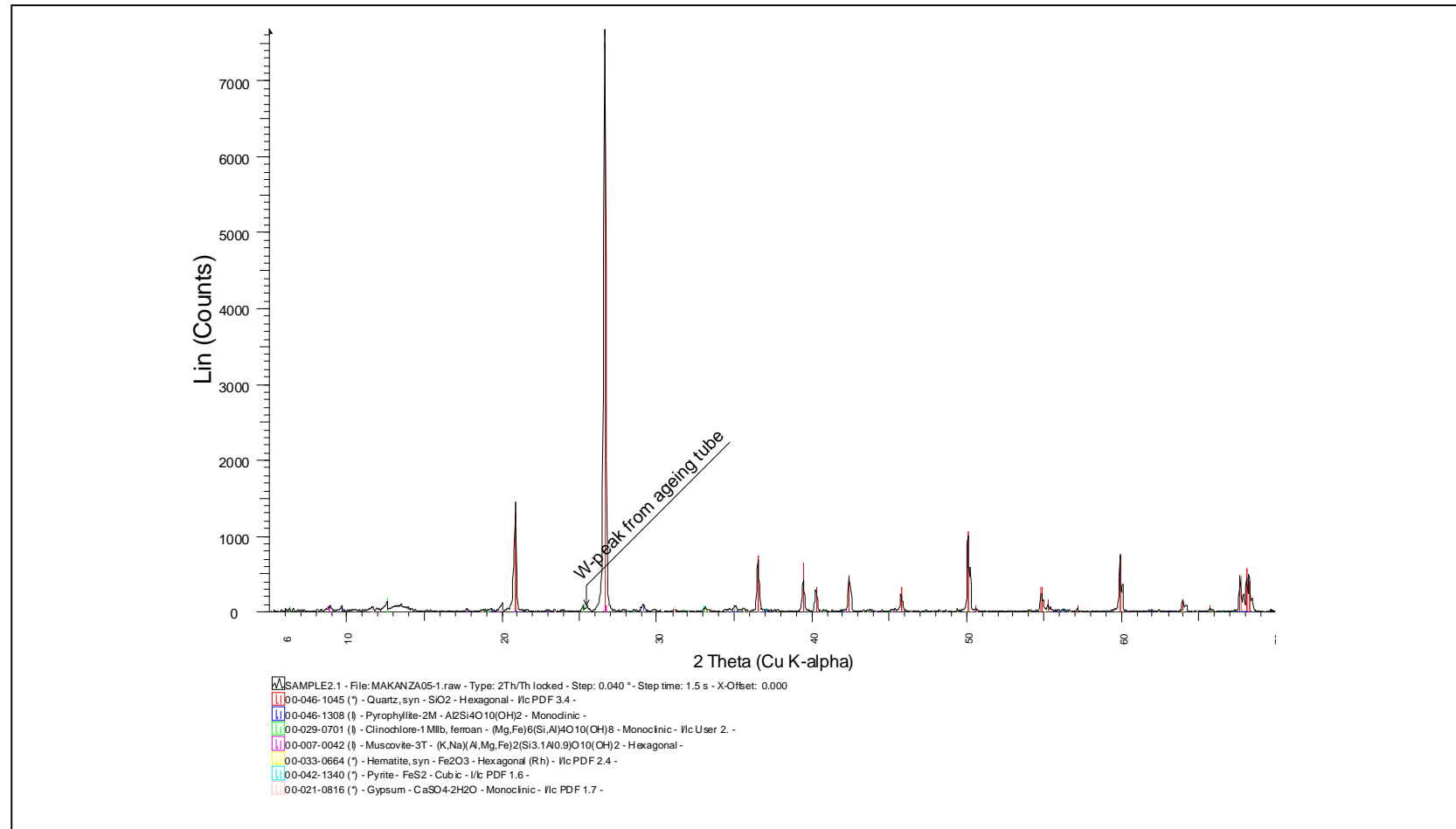


Figure 2.1 An XRD pattern for typical No. 2 Gold Plant feed

The main features are:

- Pyrite occurs in cubic form and can be either coarse or fine grained.
- Pyrophyllite is a naturally floatable clay mineral that comes from freshly mined material at No. 9 Shaft (Tau Lekoa Mine). It is removed from the feed by de-sliming.

Table 2.1 Typical minerals found in No. 2 Gold Plant Feed

Mineral	Chemical Formula
Quartz	SiO ₂
Pyrophyllite	Al ₂ Si ₄ O ₁₀ (OH) ₂
Clinocllore	(Mg,Fe) ₆ (Si,Al) ₄ O ₁₀ (OH) ₈
Muscovite	(K,Na)(Al,Mg,Fe) ₂ (Si _{3.1} Al _{0.9})O ₁₀ (OH) ₂
Hematite	Fe ₂ O ₃
Pyrite (cubic)	FeS ₂
Gypsum	CaSO ₄ .2H ₂ O

The overflow from de-sliming cyclones is sent to the Back-fill Plant while the underflow is conditioned with copper sulphate at a pH of 9.5 for about 10 hours. Thereafter, it is pumped to the float stock tank where it is reacted with an SO₂ containing solution called calcine water (Table 2.2) from the acid plant and additional copper sulphate.

Table 2.2 Chemical composition of calcine water (Dumisa, 2002)

Component	Pb	S	Fe	Al	Cu	Ni	Ca	Mg	Zn	U	SO ₄
Concentration (mg l ⁻¹)	2.5	1000	130	31	18	3.2	400	83	50	1.75	3410

At the end of the treatment, pulp pH is about 7.2. Mine water is added to achieve a final pulp specific gravity of 1.3. The pulp is divided into two streams. Each is treated with flotation reagents before being fed to flotation cells (Figure 2.2). Typical reagent dosages are shown in Table 2.3. The flotation circuit contains four rougher and two cleaner banks, which consist of eighteen and twelve cells in series respectively.

Table 2.3 *Typical reagent suite used at No. 2 Gold Plant (Dumisa, 2002)*

Reagent	Function	Dosage (g/t)
Copper Sulphate	Activator	70
SIBX	Collector	16
Dow200	Frother	16
GEMPOLYM GM4	Depressant	20

Concentrates collected from the first fourteen rougher cells are sent to the cleaner circuit while those from the last four are recycled to the float stock tank. The feed to the latter is treated with additional collector. All rougher tails are sent to the Back-fill Plant. In the cleaner bank, depressant is dosed into the first flotation cell. Concentrates collected from the first six cells (typically 28% sulphur) are thickened and sent to the acid plant while those from the last six are recycled to the cleaner bank's feed box. All cleaner tailings are recycled to the float stock tank (Dumisa, 2002).

CHAPTER 2. LITERATURE REVIEW

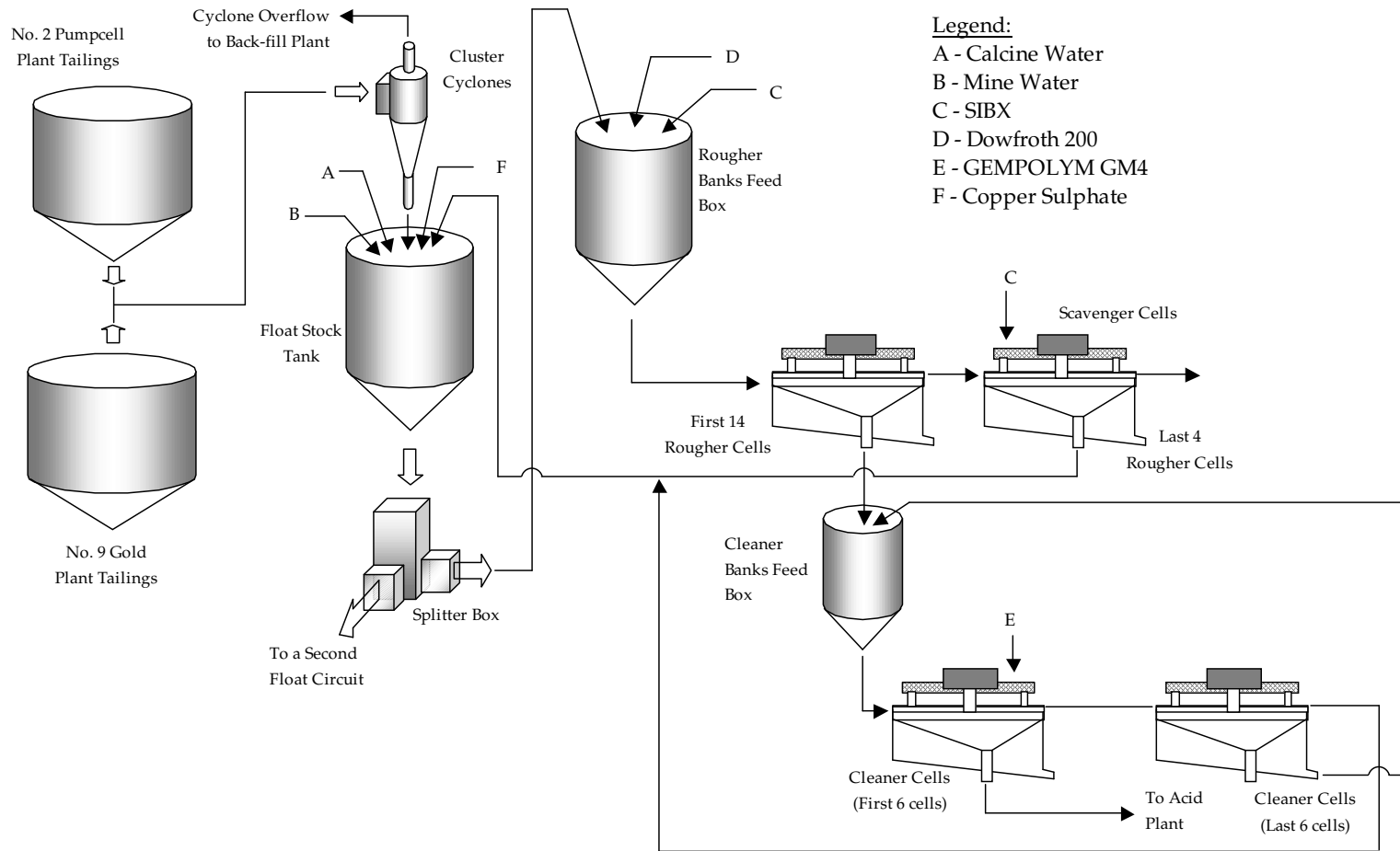


Figure 2.2 Flow sheet of the flotation circuit at AngloGold Ashanti's No. 2 Gold Plant (Dumisa, 2002)

2.3. Mineralogy of No. 2 Gold Plant Feed

2.3.1 Introduction

No. 2 Plant feed consists of reclaimed material from West Pay Dam and leach tails from No 9 Gold Plant (Dumisa, 2002). The latter treats ore received from Tau Lekoa and Kopanang Mines in separate streams. The two mining operations are exploiting the Ventersdorp Contact Reef and the Vaal Reef respectively (Browne, 2002). This section provides an overview of the geology of the latter. The focus is on mineralogy because of the significant impact it has on the flotation behaviour of the ore.

2.3.2 Mineralogy of the Vaal Reef

Like the rest of the Witwatersrand basin hosting it, the Vaal Reef is believed to originate from the Archaean granite-greenstone terrains that surround it (Anhaeusser et al., 1987). Its sediments range from coarse conglomerates to coarse arenites. Cemented by a fine-grained matrix of re-crystallised quartz and phyllosilicates^ψ, the former predominate. They are greyish metamorphosed sedimentary rocks that consist of mainly muffin-shaped pebbles of quartz ($\approx 80\%$ by mass) (Figure 2.3). The pebbles vary in composition, size and colour. The larger ones of vein quartz averaging about 40 to 50mm predominate and are sometimes accompanied by pebbles of other materials such as quartzite, chert, red jasper, and quartz porphyry (Robb and Meyer, 1995). Except for occasional veinlets and inclusions of sulphides and rare gold, the pebbles are barren. The matrix (Table 2.4) invariably contains visible pyrite, accompanied by other sulphides such as pentlandite, pyrrhotite, galena, sphalerite and chalcopyrite in diminutive amounts. Visible gold is rare (Ford, 1993).

^ψ A mixture of muscovite and chlorite and sometimes pyrophyllite and/or chloritoid

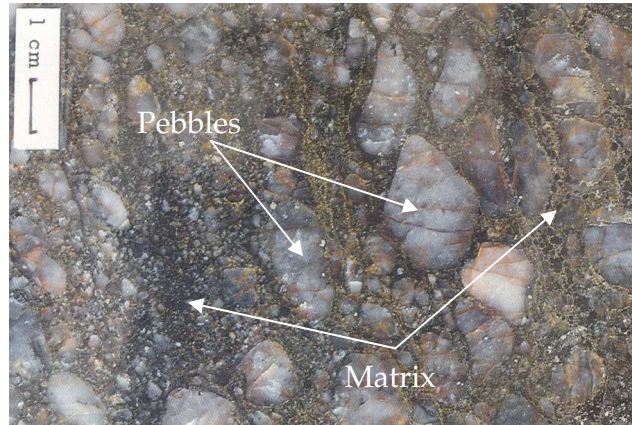


Figure 2.3 Conglomerate comprised of pebbles of quartz embedded in an essentially quartz rich matrix. Grain boundaries are outlined by phyllosilicates and fractures by recent oxidation of pyrite to iron oxides. Macrophotograph, linear magnification $\times 0.6$ (after Anhaeusser et al., 1987)

Table 2.4 Vaal Reef pebble cementing matrix (Ford, 1993)

Major Constituents		Minor Constituents		Rare Constituents	
Pyrite		Arsenopyrite Cobaltite Gersdorffite	Sulpharsenides	Gold	
Rutile Leucoxene	As separate or composite grains	Pyrrhotite Sphalerite Galena Chalcopyrite	Sulphides	Platinum Group Minerals	
Chromite		Anatase U-bearing minerals		Marcasite Pentlandite Mackinawite Millerite	Sulphides
Zircon		Chloritoid		Tucekite	
Sericite Pyrophyllite Chlorite	Phyllosilicates			Illite Kaolinite	Phyllosilicates
				Tormaline	
				Churchite Xenotime	Yttrium Phosphates
				Apatite	

The reef is characterised by the presence of discontinuous patches of carbonaceous matter, intimately associated with uraninite and gold. Occasionally, the uraninite is found in the form of round compact grains, enveloped and/or partially replaced by the carbonaceous matter (also called karogen). The latter has been sometimes referred to as bitumen since it is

largely regarded as organic material that was once a mobile viscous liquid and has since solidified (Simpson and Bowels, 1977). During sedimentation, the enveloped uraninite must have escaped oxidation but not dissolution. This conclusion is drawn from some grains found in the matrix. Because of lack of protection, they formed a brannerite species, most probably through leaching of their uranium content by hydrothermal fluid. Based on their optical characteristics, two distinct species of the brannerite are recognised. One resembles leucoxene^{9†} and the other, brannerite of hydrothermal origin. The optical differences between the two varieties are linked to a compositional delimitation that can be expressed as a ratio between the oxides of uranium and those of titanium. The species with a ratio below 1 are referred to as uraniferous leucoxene and those above this value, brannerite.

Karogen may also occur as isolated round nodules within which an association with uranium is less obvious. Gold is very often intimately associated with such karogen seams both along the edges and within the hydrocarbon (Figure 2.4).

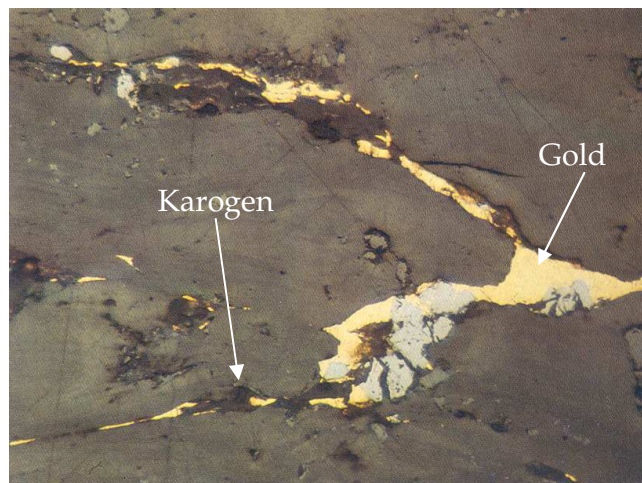


Figure 2.4 Photomicrograph showing uraniferous karogen containing inter- and intra-columnar gold, Carbon Leader Reef, Doornfontein Mine. Linear magnification $\times 135$ (Anhaeusser et al., 1987)

^{9†} The earthly variety of rutile

A distinction is made between detrital⁸ gold and that which was deposited, dissolved, transported and re-precipitated elsewhere (Robb and Meyer, 1995) Due to exclusion during crystallisation, the latter is found at pyrite grain boundaries. Consequently, the association existing between pyrite and the metals uranium (in the form of uraninite) and gold is of a purely sedimentological nature. Concentrations of pyrite do not always carry uraninite and/or gold. Their presence depends chiefly on the supply from the source rock at the time of sedimentation in addition to post-depositional reactions. The other sulphides *viz.* (pyrrhotite, sphalerite, galena chalcopyrite, marcasite and pentlandite) were all precipitated after the detritus had been deposited. The following uranium-bearing minerals (all containing tetravalent uranium) contribute to the mineralisation in the reef:

Uraninite	UO ₂ , enclosed in the matrix or by karogen
Brannerite type minerals	U _{1-x} Ti _{2+x} O ₆
Coffinite	(U,Th)SiO ₄
Uraniferous Zircon	ZrSiO ₄

The uranium content of the uraniferous zircon is negligible and coffinite is rare. The most important carriers of uranium are primary uraninite and minerals of the brannerite type. The former may contain minute specks of up to 20% by mass of galena per grain (Ford, 1993). This is thought to have formed from lead, a product of the radioactive decay of uranium. An example involving the U²³⁸ isotope is shown in Figure 2.5.

⁸ Transportation of discrete grains from their place of origin, followed by deposition

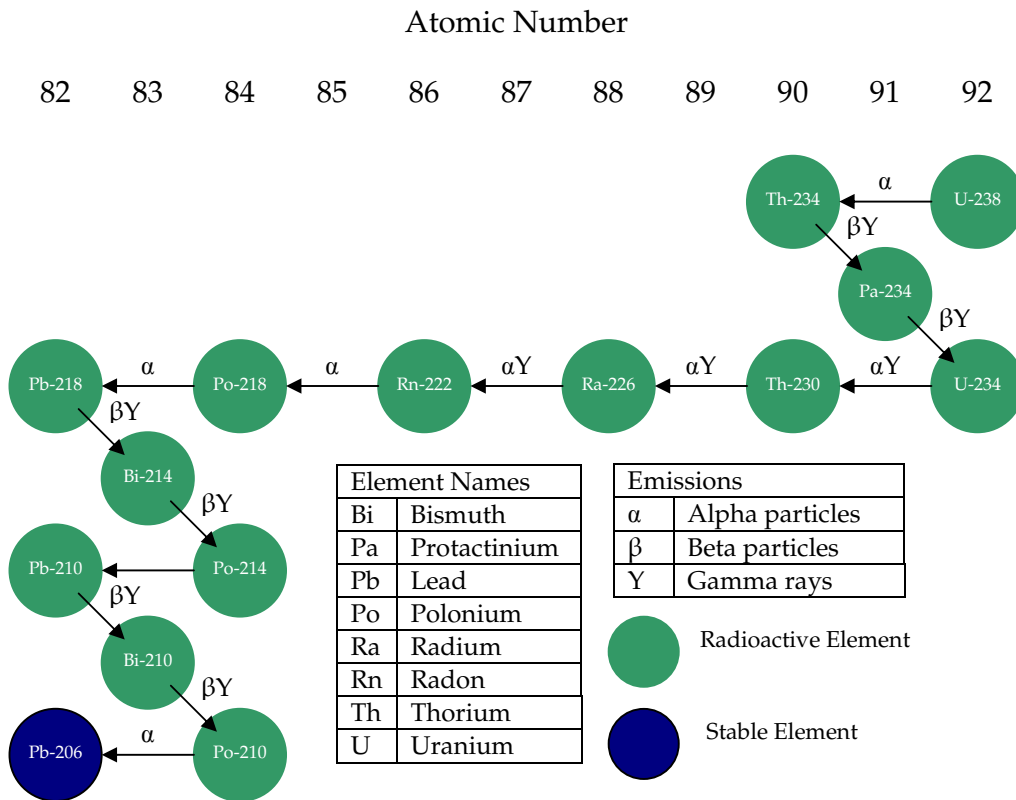


Figure 2.5 The radioactive decay of U^{238} to Pb^{206} (The Nuclear History Site, 2002)

2.4. Fundamentals of Froth Flotation

2.4.1 An Overview of the Flotation Process

Froth flotation is a beneficiation process that utilises the differences in physico-chemical surface properties of minerals, finely divided and suspended in an aqueous medium to effect separation. It involves the attachment of air bubbles to mineral particles that have been selectively rendered hydrophobic. The aggregates formed then rise to the surface where they form a metastable froth phase (Crozier, 1992). Ores generally consist of valuable mineral particles that are intimately associated with gangue. After milling and liberation of mineral values and adjustment of pulp density, various chemical constituents are added to modify constituent minerals. For effective collection of valuables from gangue, a concentration process by froth flotation follows.

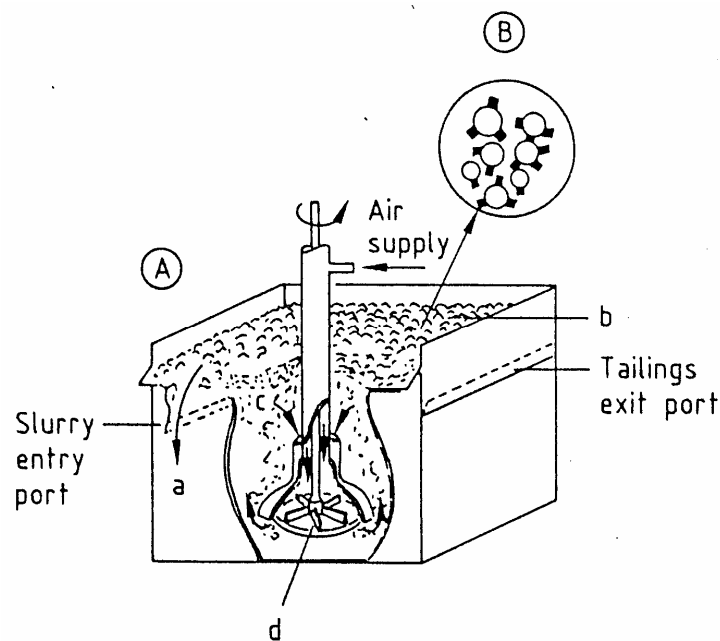


Figure 2.6 Processes occurring in a flotation cell (A) Flotation cell a) Froth overflow; b) Froth layer; c) Pulp; d) Rotor for pulp agitation; (B) Mineralised air bubbles within flotation cell (Yarar, 1985).

Sulphydryl collectors have the role of selectively attaching to sulphide minerals and producing a water repellent film. A frother is used to impart an internal hydrophobic character to a bubble which after an effective collision with a coated valuable particle allows certain stability to mineral-laden air bubbles after they reach the surface. Depressants are added to exclude undesirable minerals called gangue from attaching to the air bubble by imparting a hydrophilic character to them.

2.4.2 Thermodynamic Considerations

Based on thermodynamic phase equilibrium, Davidtz (1999) proposed the use of activity coefficients to quantify the degree of hydrophobicity of surfaces coated with surfactant molecules. Under surface coverage conditions that do not exceed monolayer coverage, and where chain length and concentration of collector molecules were below the critical micelle concentration, it was possible to quantify the thermodynamic factors involved in the phase separation between water and a suspended particle.

The conclusion reached was that for a given particle size and temperature, only the amount (X_i) and type of collector functional groups reflected in the activity coefficients of interacting water and functional groups (γ_i) determined the degree of phase separation between a particle and water. Furthermore, the greater the degree of phase separation, as reflected by the Excess Gibbs Free Energy, the more readily the particle floated. Effectively, it was assumed that a freshly exposed surface would be hydrated and hydrophilic, and that progressively, this would become more hydrophobic as collector coverage increased. Eventually, a two-phase region is formed in which surface adsorbed collector molecules (phase α) are surrounded by water (phase β). (Figure 2.7 (b))

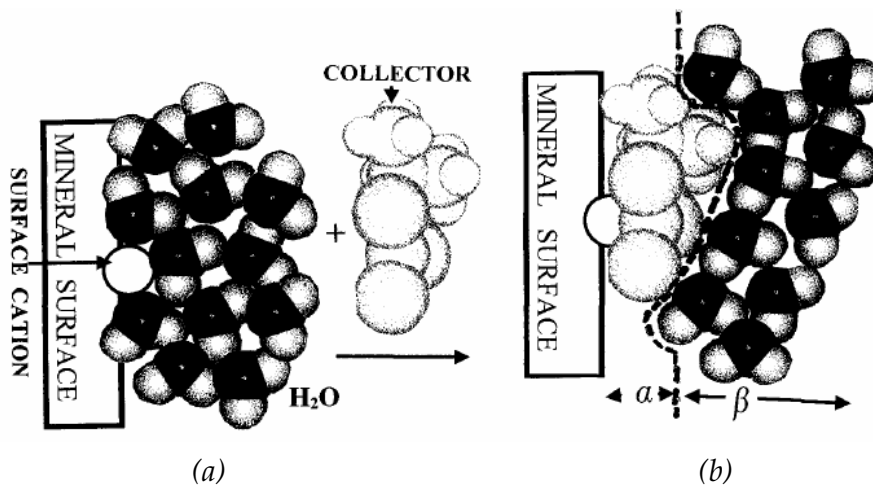


Figure 2.7 Zone where mineral surface-collector-water interactions take place (Davidtz, 1999)

The Excess Gibbs Free Energy (G^{ex}) is defined by:

$$G^{ex} = RT \sum x_i \ln \gamma_i \quad [2.1]$$

Where x_i = mole fraction

γ_i = activity coefficient for the i^{th} component

Support to the method was claimed by comparing G^{ex} values calculated with the UNIFAC method to experimental data from batch flotation tests using a copper ore at starvation reagent dosages. Time-recovery data obtained were used to determine cumulative recovery (R) and mean initial rate (K). Fitting a linear relationship between the calculated G^{ex} values and K gave R-squared values very close to 1, implying a strong correlation (Figure 2.8). Similarly, results from the flotation of a mixed sulphide ore containing chalcopyrite, galena, sphalerite, pyrrhotite with covalent TTC also showed a strong linear correlation between G^{ex} and fractional recovery (Figure 2.9). From these findings, Davidtz (1999) concluded that Gibbs excess free energy is directly

proportional to both initial rate and fractional recovery. In other words, for different collectors, G^{ex} can be used to predict flotation performance.

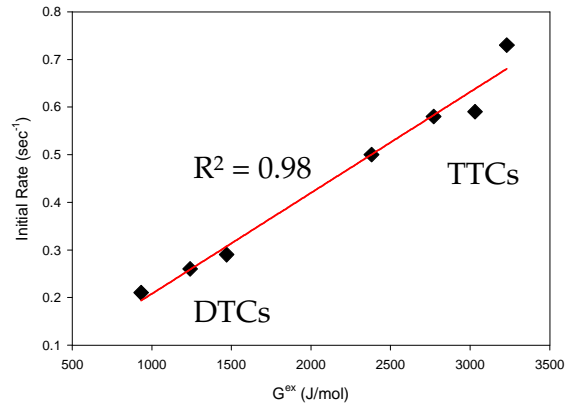


Figure 2.8 Initial rate- G^{ex} relationship for DTCs and TTCs on copper (Davidtz, 1999)

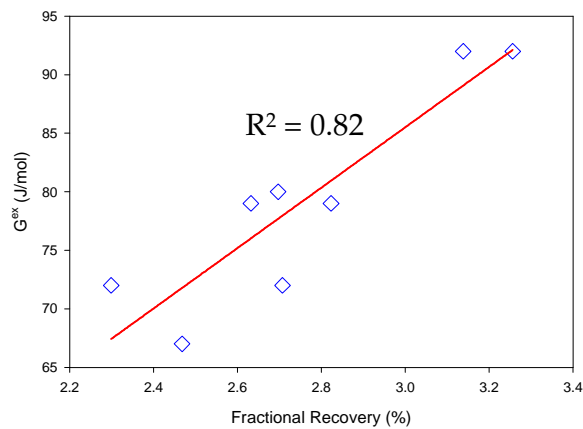


Figure 2.9 Relationship between G^{ex} and recovery for covalent TTC collector molecules (Davidtz, 1999)

Davidtz (2005) summarized the interacting variables as follows:

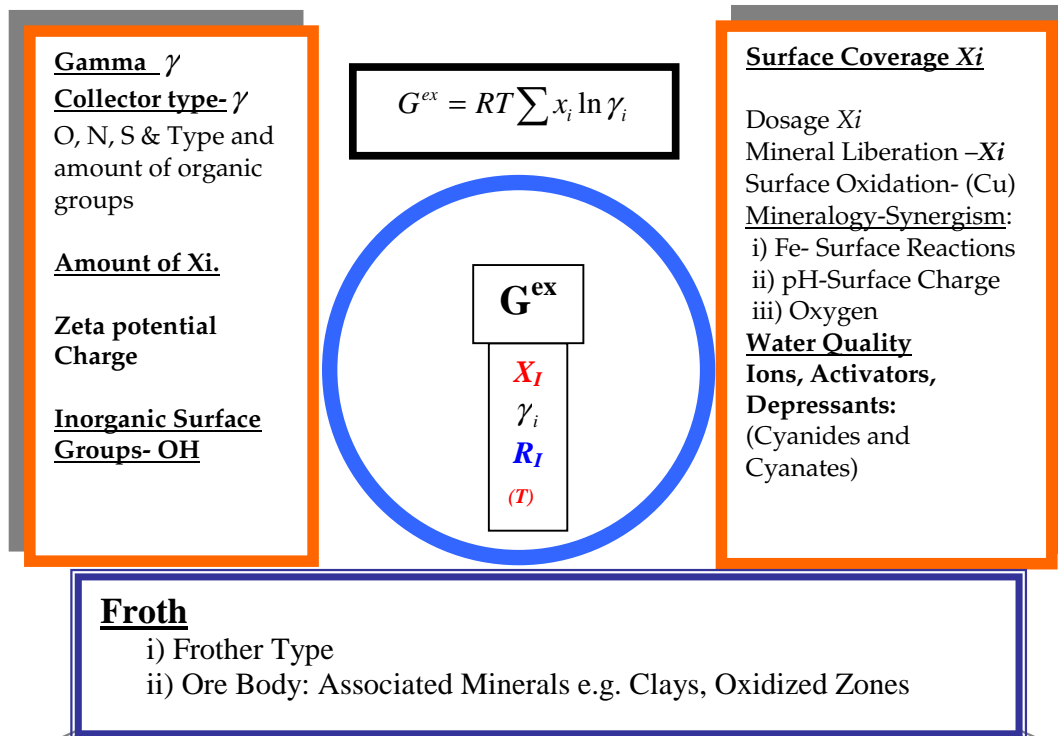


Figure 2.10 A summary of interacting variables in flotation (Davidtz, 2005)

2.4.3 Contact Angle

Particle-bubble attachment is known to occur when a solid surface is hydrophobic. The stability of the attachment is measured by the contact angle, θ (Figure 2.11) developed between the two phases: the air bubble (gas) and the surface of the mineral (solid). When an air bubble does not displace the aqueous phase, the contact angle is zero. On the other hand, complete displacement represents a contact angle of 180° . Values of contact angles between these two extremes provide an indication of the degree of surface polarity, or conversely, the hydrophobic character of the surface.

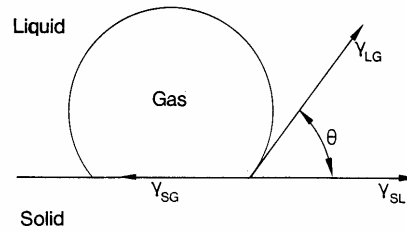


Figure 2.11 Schematic representation of the equilibrium contact between an air bubble and a solid immersed in a liquid (Fuerstenau and Raghavan, 1976)

The maximum free energy change per unit area, G^{ex} , corresponding to the attachment process (the displacement of the water by the air bubble) can be expressed by:

$$\Delta G = \pi_{SG} - (\pi_{SL} + \pi_{LG}) \quad [2.2]$$

Where π_{SG} , π_{SL} and π_{LG} are surface energies between the solid-gas, solid-liquid and liquid-gas phases respectively. Since the three-phase equilibrium existing in the system can be described in terms of the respective interfacial tensions according to:

$$\pi_{SG} = \pi_{SL} + \pi_{LG} \cos \theta \quad [2.3]$$

Where θ is the contact angle between the mineral surface and the air bubble, the free energy change can be expressed as:

$$\Delta G = \pi_{LG} (\cos \theta - 1) \quad [2.4]$$

Further support for Gibbs Excess Free Energy is in its relationship to contact angle and hence hydrophobicity: At constant temperature and composition, the change in G^{ex} is the product of the surface area and the change in surface tension, π .

$$dG^{ex} = A d\pi \quad [2.5]$$

2.4.3 Flotation Rate

The flotation response of minerals at different experimental conditions has been traditionally studied through laboratory batch tests in which the recovery of the target mineral is measured at the end of a certain period of time. Klimpel (1980) drew attention to the loss of valuable information on the recovery kinetics as a drawback associated with this method. Instead, the author proposed the use of release curves. This approach is based on the fact that flotation is primarily a rate process that can be described by a first-order rate equation. Concentrates are collected over preset time intervals. The recovery-time data obtained are fitted into a model that describes recovery as a function of time. According to Klimpel (1984a), using models makes it is easier to compare and statistically test differences between recovery-time profiles by studying their model parameters instead of actually testing the profiles themselves. The more the conditions tested, the more the profiles involved, and the more difficult it will be to recognise trends and test significant differences using profiles only. The author also emphasised that the most suitable models are those that have two curve-fitting parameters. Since optimal parameters from curve fitting have broad confidence ranges, models having more than two curve-fitting parameters result in over-fitting of data, making the parameters loose their physical meaning.

Slabbert (1985) listed various equations that have been developed for describing the flotation process:

$$\text{Klimpel's Equation:} \quad R = R_{\max} \left(1 - \frac{1}{Kt} (1 - e^{-kt}) \right) \quad [2.6]$$

$$\text{Gamma Equation:} \quad R = R_{\max} \left(1 - \frac{\gamma}{(\gamma + t)^p} \right) \quad [2.7]$$

$$\text{Simplified Gamma:} \quad R = 1 - \frac{\gamma}{(\gamma + t)^p} \quad [2.8]$$

$$R = \frac{t}{g + t} \quad [2.9]$$

$$R = R_{\max} (1 - e^{-kt}) \quad [2.10]$$

$$\text{Fermentation model:} \quad R = \frac{R_{\max}}{(1 + k/t)} \quad [2.11]$$

R denotes cumulative recovery at time t and R_{\max} , k , γ , g and p are curve fitting parameters. As long as the chosen equation fits the data reasonably well with only two curve-fitting parameters, the choice of a particular model is often not critical (Klimpel, 1984b). This present work adopts expression [2.10] in which k is interpreted as the initial rate (min^{-1}) and R_{\max} the equilibrium recovery at long flotation times (the asymptote of the cumulative recovery-time curve at high t -values). According to Agar et al. (1980), this relationship can be applied to all the components of the flotation system including water. Through its use, a continuous circuit can be simulated from batch data, and all the more, the treatment time in the various stages can be optimised.

Despite the general awareness that flotation rate is an important variable, performance between different systems, for example reagent schemes have been generally assessed by only looking at differences in R_{\max} . Klimpel (1984a) has argued that this approach implies that flotation is an equilibrium process. Also, such an assumption suggests that differences in recovery measured in the laboratory will indicate recovery differences in the plant, regardless of the time-scale differences between the two. This is inconsistent with the findings of a testing program he conducted in order to determine some general guidelines for the use of chemicals in flotation plants. Klimpel (1984a) showed that the laboratory-scale time value (time equivalency value) to be used for comparing laboratory flotation results to the behaviour of the plant could be anywhere in the laboratory time scale. The time equivalency

value can be viewed as the time in the laboratory time-recovery profile that corresponds to the measured plant final recovery in the section under study. In some work conducted by this author, the appropriate laboratory time value was found to be considerably less than normally associated with equilibrium recovery. Figure 2.12 illustrates the fitting of typical lab data to the Klimpel model (equation [2.6] above) so as to characterise each profile by appropriate R and K parameters. If the plant being simulated corresponds to a laboratory time less than t_k , the settings associated with System 1 are preferred, while the converse is true if the laboratory equivalence value is greater than t_k (denoted as the R/K trade-off).

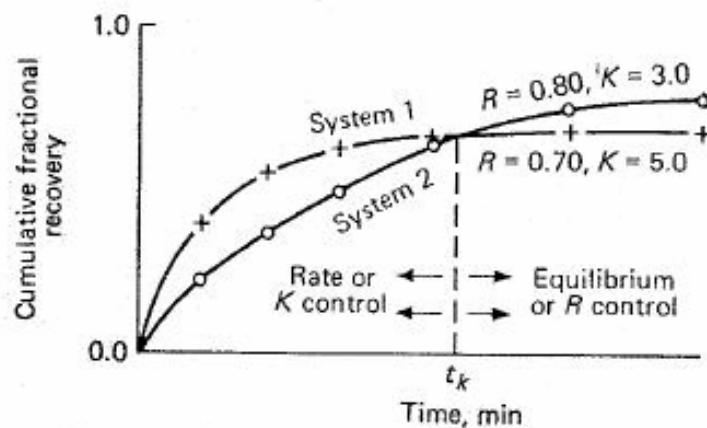


Figure 2.12 Typical curves obtained by fitting recovery-time data to a two parameter model. System 1 shows a high rate and low equilibrium recovery; System 2 shows the reverse (Klimpel, 1984b)

The recovery-time profiles in Figure 2.12 can be divided into two regions; the first where recovery is sensitive to the time of flotation is called rate control. The second is under equilibrium control and is where curve flattens and the recovery is not sensitive to time. Experience has shown that different reagent schemes used on the same ore give different curve shapes when their recovery-time data are fitted into a model such as shown in Figure 2.12. According to Klimpel (1984a), this is important because plant performance is often correlated with lab results for lapses of times considerably less than those corresponding to equilibrium recovery. The author concluded that the

most important difference between tests is often in the rate at which the valuable mineral can be removed from the cell. The K difference is crucial and can sometimes overwhelm the importance of the associated R difference.

2.5. Collectors for Auriferous Pyrite Flotation

Thiols are the collectors most widely in used in the flotation of pyrite (O'connor and Dunne, 1994). Examples include dithiocarbonates, trithiocarbonates, dithiophosphates, dithiocarbamates, thionocarbamates and mercaptobenzothiazoles. Tables 2.5 and 2.6 show a summary of properties and applications of these reagents.

Table 2.5 *Application of Selected Thiol Collectors* (after Bradshaw, 1997)

Collector	Application and Properties
Dithiocarbonates (Xanthates)	- Used in a pH range of 8-12 - Undergo hydrolysis at low pH
Dithiophosphates	- More resistant to oxidation than xanthates and less stable than xanthates in moist conditions, and are usually stabilised with soda ash - Generally used at high pH, effective in the pH range 4-12 and used in mixtures with other collectors for high recoveries
Thionocarbamates	- Reasonably stable but hydrolyse in acidic conditions - Less sensitive to water chemistry than xanthates and dithiophosphates - Generally applied in the pH range 4-9
Thiocarbamates	- They have been known for a while but have not achieved much commercial success because they decompose readily in acidic conditions
Mercaptobenzothiazoles	Mostly used in combinations with DTP and/or xanthate for flotation of tarnished and oxidised ores and cyanidation tailings at low pH. These conditions promote removal of oxide and cyanide, which could interfere with interaction with reagents. The costly neutralisation step is not necessary because the collector operates efficiently at low pH.

Table 2.6 Selected Thiol Collector Structures (after du Plessis, 2003)

Collector	Structure
Monothiocarbonates	
Dithiocarbonates	
Trithiocarbonates	
Dithiophosphates	
Thionocarbamates	
Thiocarbamates	
Mercaptobenzothiazoles	

Dithiocarbonate and trithiocarbonate collectors, which are the focus of this present work, differ in the isomorphous substitution of sulphur for oxygen (Figure 2.13)

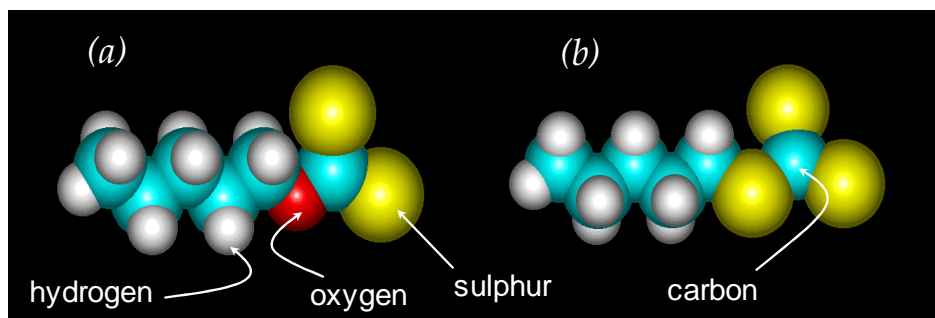


Figure 2.13 Thiol collectors (a) dithiocarbonates, (b) trithiocarbonates (Miller, 2003)

According to Fuerstaenau (1982a), increasing the length of the hydrocarbon group of collector molecules:

- Increases recovery power, frothing properties, mass recovery, water repulsion and the tendency to form micelles.
- Lowers selectivity and solubility

Micelles are stable reversible aggregates that are formed spontaneously when collector concentrations exceed a certain threshold known as the critical micelle concentration (CMC). In solution a three dimensional, regular array of the molecules results from intermolecular bonding. The shape taken by the assemblages depends primarily on surfactant architecture, the solvent, presence of added components (such as co-surfactants and salts) and temperature. Examples of assemblies are shown in Figure 2.14. In order to lower solution free energy, surfactants self-assemble by creating an interface separating the aqueous phase from the hydrophobic portions of the surfactant. The hydrophobic portions aggregate to form an oily interpenetrating assembly that is separated from the aqueous solvent by the hydrophilic head-group. The head-groups serve to define a boundary for double layer structure between the aqueous and oily pseudo-phases.

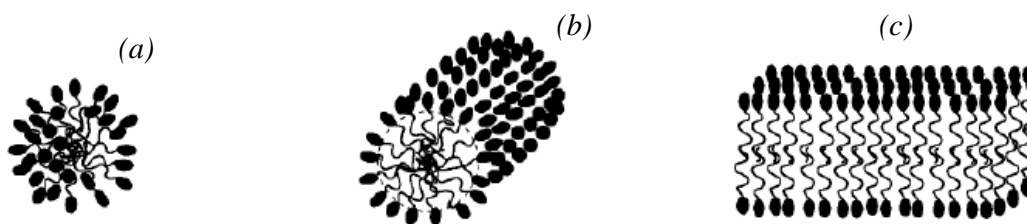


Figure 2.14 Illustration of different surfactant self-assembly structures (a) spherical micelle, (b) cylindrical micelle and (c) lamellar micelle (Boschkova, 2002).

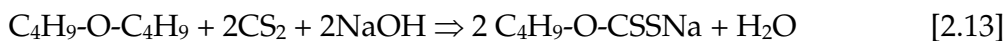
When collector molecules are bonded to a surface, three dimensional arrays are not possible. Instead hydrophobic bonding dominates intermolecular attraction. In solution, dodecyl structures typically form micelles around 0.08M solutions (Davidtz, 2005). A typical monolayer surface of thiocarbonate collector is so dense that it can be compared with a solution at concentrations around 8M, three orders of magnitude higher than the CMC. For a nC_6 xanthate, interaction between neighbouring collector species begins at a surface density of coverage of about 0.7 (Slabbert 1985)

2.5.1 Xanthate (Dithiocarbonate) Collectors

The xanthates, first patented in 1925 are the most widely used flotation collectors and account for over 80% of world usage of thiol collectors (Crozier, 1992). Some factors contributing to this wide application are: they possess good water solubility and they are very stable in alkaline conditions. Xanthates are also inexpensive, easy to manufacture, transport, store and handle and they are very effective in the non-selective flotation of sulphides. This investigation uses SIBX, which is synthesised by reacting carbon bisulphide (CS_2), butyl alcohol (C_4H_9OH) and a strong alkali (NaOH):



The xanthate can also be produced by reacting ether with the alkali and carbon disulphide:



Xanthates undergo different reactions dependant on the environment they are exposed to (Figure 5.3). They may decompose via the hydrolysis reaction to xanthic acid and then to the original reactants, carbon bisulphide and alcohol (de Donato et al. (1989)).

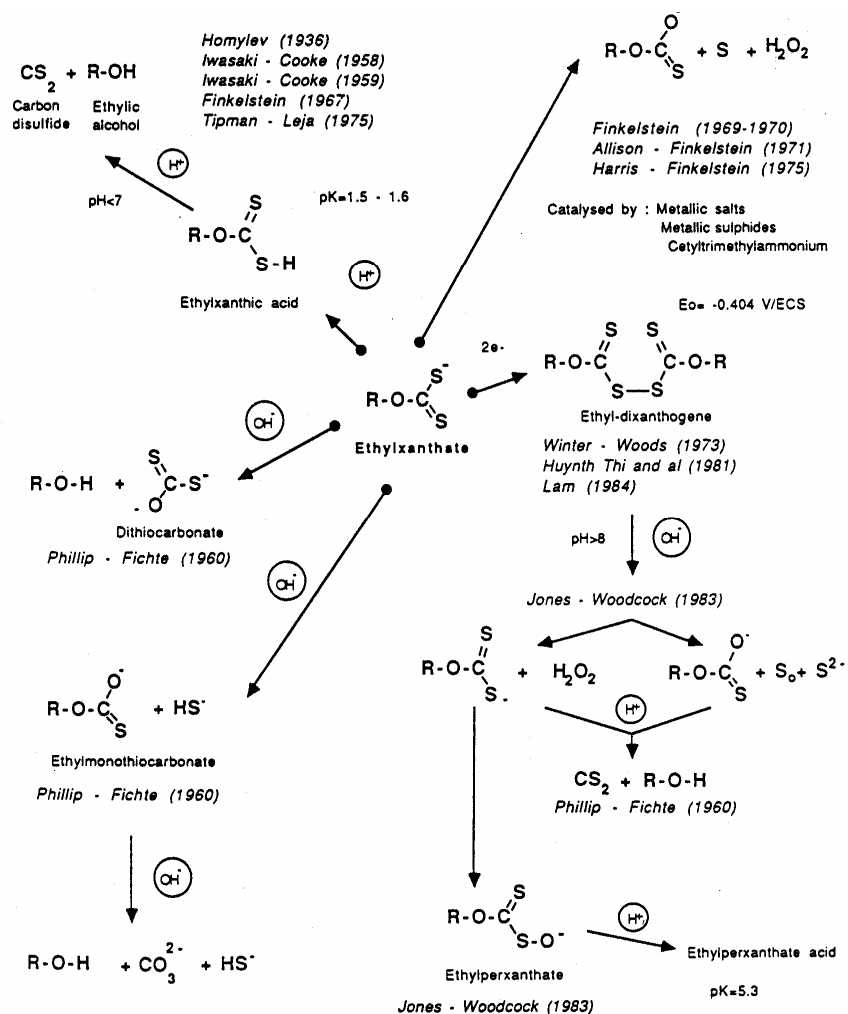


Figure 2.15 Hydrolysis and oxidation of ethyl xanthate in aqueous solution: the different reactive paths. R is the ethyl radical (de Donato et al., 1989)

The stability of xanthates in aqueous solutions depends on solution pH, the rate of decomposition decreasing with increasing pH. The flotation circuit at No 2 Gold Plant is run at a near neutral pH of 7.2 for which SIBX is expected to be stable.

Metallic sulphides and metal ions may catalyse the oxidation of xanthates to dixanthogen (Bradshaw, 1997). Xanthates are reducing agents that form ferrous and cuprous salts in the presence of iron and copper ions respectively. In cases where the iron is present in the ferric state, Fe^{3+} , the ferric xanthate that is initially formed is quickly reduced to ferrous xanthate (Sutherland and Wark, 1955). In practice, the effectiveness of xanthates increases with the molecular weight of their alcohol radical (Table 2.7).

Methyl xanthates are more effective on Cu, Hg and Ag minerals, and iron sulphides. Ethyl and the C_3 to C_5 xanthates are effective in normal concentrations without the need for activators for all heavy metal sulphides except sphalerite and pyrrhotite. The failure to collect these two is due to the ferrous and zinc compounds formed by C_1 to C_5 xanthates being soluble at economic reagent quantities.

Table 2.7 Response of sulphide minerals to collectors of the xanthate type (Marsden and House, 1992)

Collector \ Mineral	Methyl Xanthate	Sodium Aerofloat	Ethyl Xanthate	Butyl Xanthate	Amyl Xanthate	Hexadecyl Xanthate	Potassium di-amyl dithio-carbamate
Sphalerite Pyrrhotite	Response To Collectors Only In The Presence Of Activators						
Pyrite Galena Chalcopyrite							
Bornite Covellite Chalcocite	Response To Collectors Without Activation						

2.5.2 Xanthate – Pyrite Interactions

The mechanisms by which xanthates float pyrite have been studied extensively over the years and Wang (1994) lists some of this work. The traditional theory considers xanthate adsorption as an electrochemical process that involves the formation of dixanthogen (Chander, 1999). This conclusion has been drawn from spectroscopic (Fuerstenau et al., 1968), electrochemical (Woods, 1976; Usul and Tolun, 1974; Majima and Takeda, 1968) and flotation data (Fuerstenau et al., 1968). The sole presence of dixanthogen on the pyrite surface after contact with xanthate has been demonstrated clearly using infrared spectroscopy (Figure 2.16).

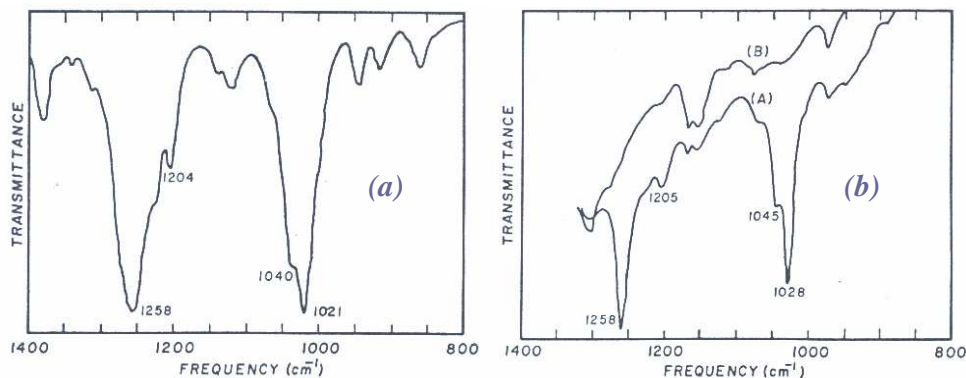


Figure 2.16 Infrared spectrum of (I) diamyl dixanthogen, (II) pyrite conditioned at pH 3.5 in the absence (Curve B) and presence (curve A) of potassium amyl xanthate (after Fuerstenau et al., 1968)

The principal absorption bands of diamyl dixanthogen occur at 1,021 and 1,258 cm^{-1} (Figure 2.16 (a)). After contact with amyl xanthate, the principal absorption bands of pyrite occur at 1,028 and 1,258 cm^{-1} (Figure 2.16 (b)), which correspond closely with those of dixanthogen.

The formation of dixanthogen is also supported by measurements of pyrite rest potentials in various xanthate solutions (Alison and Finkelstein, 1971), which are close to xanthate/dixanthogen redox couples (Crozier, 1991). Electrochemical interactions between sulphides and xanthate collectors that

result in dixanthogen formation were first suggested by Salamy and Nixon (1952). They postulated that oxidation of collector ions occurs at anodic sites according to:



This reaction being supported by a cathodic reduction of adsorbed oxygen:



As emphasised by de Wet et al. (1997), initial attachment of the xanthate onto pyrite before the oxidation to dixanthogen is important. These authors cited the work by Ackerman et al. (1987) in which pyrite responded poorly to flotation with dissolved dixanthogen. They also referred to the findings by Leppinen (1990) who used in-situ spectroscopic techniques to show that a monolayer of iron xanthate initially adsorbed on pyrite, after which dixanthogen formed just above it.

Based on Fourier Transform Infra Red (FTIR) spectroscopic studies, Wang (1994) has shown that pyrite-xanthate interactions result in the formation of ferric xanthate as well. Figure 2.17 shows the differential spectra of ethyl xanthate treated pyrite. Two intense absorption peaks can be observed at 1252 and 1030 cm^{-1} . Comparison of spectra in Figure 2.17 with that of dixanthogen and ferric xanthate in Figure 2.18 shows the presence of diethyl dixanthogen. Other absorption bands at 1250 and 1005 cm^{-1} are close to those of ferric ethyl xanthate (Figure 2.18 (b)), suggesting it is one of the surface products formed when xanthate ions are adsorbed.

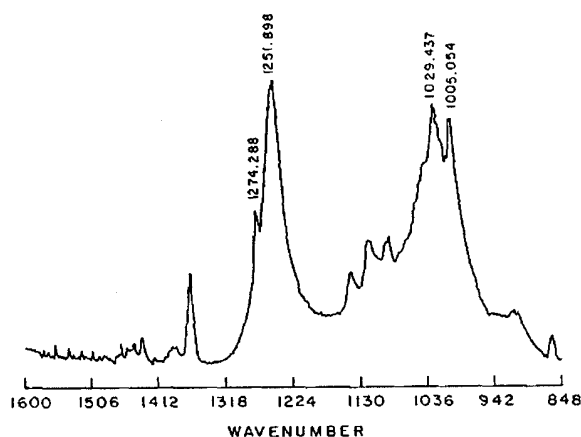


Figure 2.17 Differential IR spectrum of pyrite after reacting with 1.0×10^{-3} mol/l sodium ethyl xanthate solution at pH 6 (after Wang, 1994).

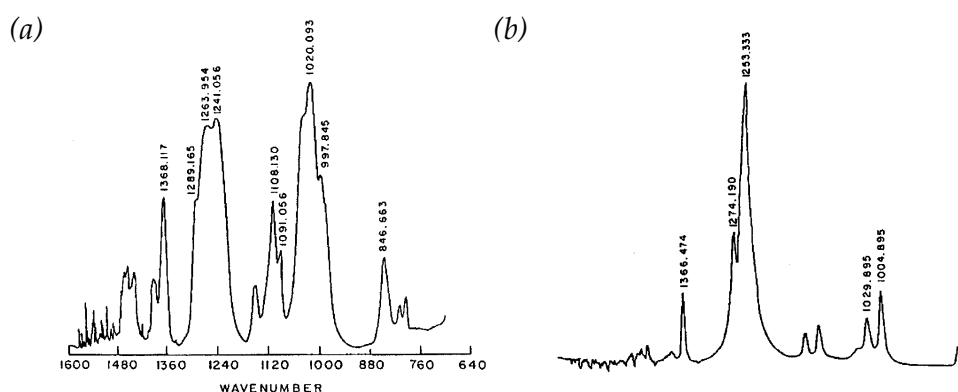


Figure 2.18 FTIR of (a) diethyl dixanthogen and (b) ferric ethyl xanthate, both in KBr (Wang, 1994)

2.5.3 Trithiocarbonate Collectors

TTCs can be of either ionic (Figure 2.19 (a)) or ester (Figure 2.19 (b)) type. The former is chemically known as alkyl trithiocarbonate and both the straight and branched chains are recognized. TTCs are synthesized by dissolving an alkali hydroxide in the appropriate alkyl mercaptan, followed by the addition of carbon disulphide to the resulting metal mercaptide:





Generally, freshly prepared sodium and potassium salts are bright yellow in colour and possess a distinct odour. The differences between the straight and branched chains are not yet fully understood, and the latter seem to be superior, (du Plessis et al., 2000).

Studies have shown that the ester-type TTCs are very effective in the bulk flotation of sulphide minerals (Coetzer and Davidtz, 1989). Their higher cost however seems to discourage their application so that ionic TTCs are preferred.

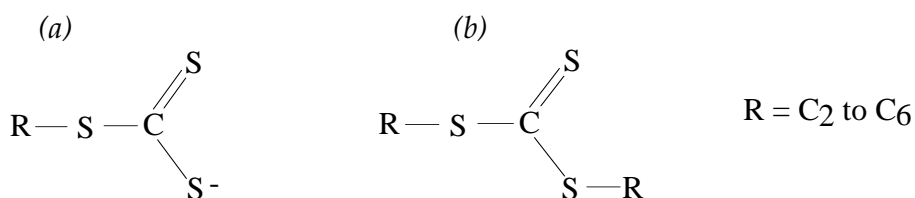


Figure 2.19 Chemical structure of (a) ionic TTCs and (b) ester type ionic TTCs

2.5.4 TTC – Pyrite Interactions

The flotation of pyrite by xanthate collectors is known to occur through the formation of metal xanthates (Wang, 1994) and then dimers (Chander 1999). Oxidation of TTC molecules to their dimers (Figure 2.20), supported by the cathodic reduction of oxygen (equation 2.15), may occur on mineral surfaces, selectively rendering them hydrophobic. Supporting evidence for this assertion can be obtained from FTIR spectroscopy (du Plessis, 2003). Figure 2.21 compares the FTIR transmission spectrum of a TTC dimer with an external reflection FTIR spectrum of a pyrite surface treated with TTC under oxidizing conditions. It is clear that there is good agreement between the two, indicating bulk dimer formation at the pyrite surface.

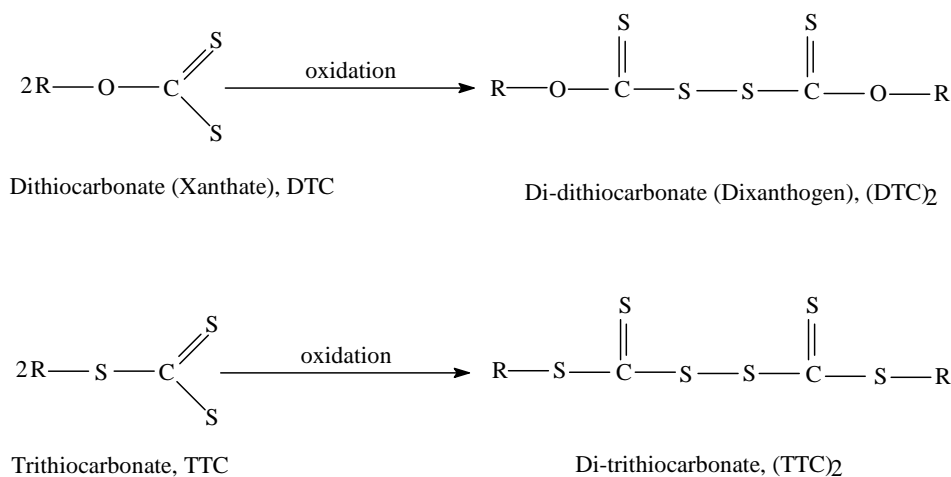


Figure 2.20 Oxidation of Trithiocarbonates to their corresponding dimers (du Plessis et al., 2000)

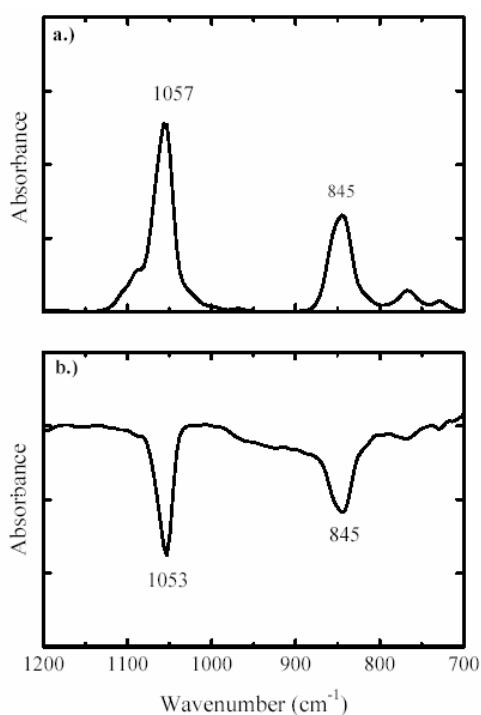


Figure 2.21 (a) FTIR transmission spectrum of the *n*-amyl trithiocarbonate dimer compared to (b) the FTIR external reflection spectrum of pyrite treated with 1 × 10⁻³ M potassium *n*-amyl trithiocarbonate, at 0.1 V for 15 minutes at pH 4.7 in air (45°, *p* polarized) (du Plessis, 2003).

The work conducted by du Plessis *et al.* (2000) has further shown that TTC collectors oxidise more readily^x the higher the number of sulphur atoms in their functional group (Figure 2.22)

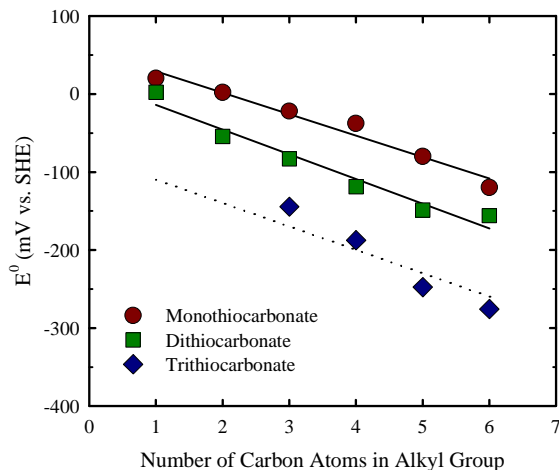


Figure 2.22 Standard reduction potentials for thiocarbonate collectors as a function of alkyl chain length (after du Plessis *et al.*, 2000)

TTCs have been reported to be stronger collectors than DTCs and can be used at lower dosages for near neutral pH slurries (Klimpel, 1999; Coetzer and Davidtz, 1989). Research by Sutherland and Wark (1955) has shown that an increase in the number of sulphur atoms in the functional group of thiol collectors improves their tendency to adsorb on sulphide mineral and metal surfaces. Work conducted by Slabbert (1985) on the flotation of PGMs from a Merensky ore (South Africa) using iC_3 TTC collector showed an increase in recovery relative to a mixture of xanthate and dithiophosphate. A monoalkyl trithiocarbonate (Orfom 800) developed by Philips Petroleum Company has been used as a collector in the flotation of copper ores in the USA and in Spain (Avotins *et al.*, 1994). It is against this background that this work seeks to test the flotation with TTC collectors, of pyrite and gold from leach residues being treated by AngloGold Ashanti's North No. 2 Gold Plant.

^x A lower value of E_h^o indicates that the collector oxidises more readily

2.5.5 Synergism in SIBX/TTC Mixtures

Although benefits have been reported for a wide range of collector mixtures, the mechanisms of enhancement have not been clearly established (Bradshaw, 1997). Some authors have attributed better performance to the summation of individual contributions of the respective collectors (Mitrofanov et al., 1985). Others have however ascribed it to synergism, the working together of two collectors to yield flotation performances greater than the sum of the individual reagents. A typical illustration is the work conducted by du Plessis et al. (2000) in which a mixture of 25% C₁₂ TTC and 75% SIBX gave better sulphide flotation response than SIBX (Figure 2.23).

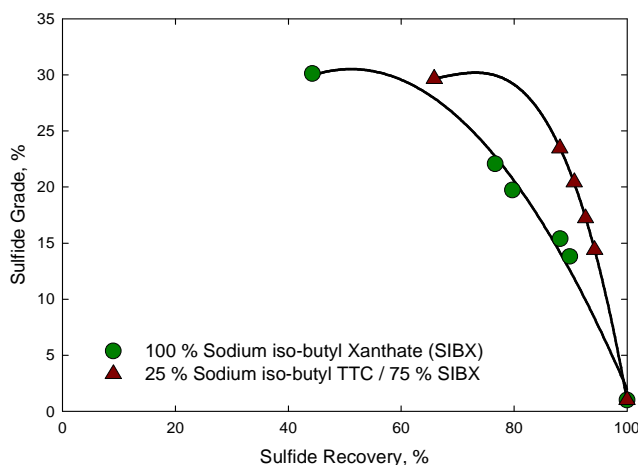


Figure 2.23 Grade–recovery curves evaluating iso-butyl dithiocarbonate and a 25% iso-butyl Trithiocarbonate / 75% iso-butyl dithiocarbonate mixture for auriferous pyrite recovery with air at pH 8 (du Plessis et al., 2000)

2.5.3.1 Mechanisms of Synergism

Early work by Plaskin et al. (1954) into the effect of using blends of ethyl xanthate and amyl xanthate in the flotation of arsenopyrite and galena recorded recoveries that were higher than simple summations of individual effects by pure collectors. The authors attributed this to better adsorption on mineral surfaces that were viewed as inhomogeneous. The improved flotation

responses were also accompanied by higher recovery kinetics for all collector mixtures tested. In single-point flotation tests of a mixed copper ore with various mixtures of dithiophosphates, monothiophosphates and xanthates, Mitrofanov et al. (1985) reported improved collection of fines due to the combination of the frothing properties of dithiophosphates and the “dry” froth produced by xanthates. Critchley and Riaz (1991) reported enhanced microflotation of heazlewoodite with a 1:2 mixture of potassium ethyl xanthate and diethyl dithiocarbamate and ascribed it to enhanced overall extent of collector adsorption. Valdiviezo and Oliveira (1993) used surface tension measurements correlated to contact angle measurements to show that synergism existed between a 3:1 molar ratio of ethyl xanthate and sodium oleate. They attributed this behaviour to a favourable arrangement of the species on mineral surfaces.

A literature survey conducted by Bradshaw (1997) summarised that the synergistic enhancement of flotation observed for many collector blends has been largely attributed to improved adsorption characteristics of the mixed collectors on mineral surfaces as compared to pure collectors. The author highlighted the work conducted by Mellgren (1966) who proposed that when one of the collectors adsorbs by chemisorption, it provides sites on the mineral surface for the subsequent adsorption of the second collector, which is comprised of more hydrophobic neutral molecules, thereby increasing the overall hydrophobic properties of the mineral.

This means that for the SIBX – TTC mixtures being tested in this present work, one of the two, possibly TTC could initially irreversibly adsorb and the dithiolate of SIBX could increase the density of collector packing by physisorption and thereby increase the hydrophobic state of the sulphide surface (Davidtz, 2002).

2.6. Activators for Auriferous Pyrite Flotation

Activators are generally soluble salts that ionise in solution; the ions then react with the mineral surface and promote collector adsorption. Work done by Miller (2003) indicates that lead (II) in lead nitrate can be used to activate auriferous pyrite in pulps containing traces of cyanide. These conclusions are based on contact angle measurements (Figure 2.24) and maybe due to the fact that Pb^{2+} ions do not complex with cyanide. The implication is that Pb ions can activate pyrite promoting xanthate adsorption.

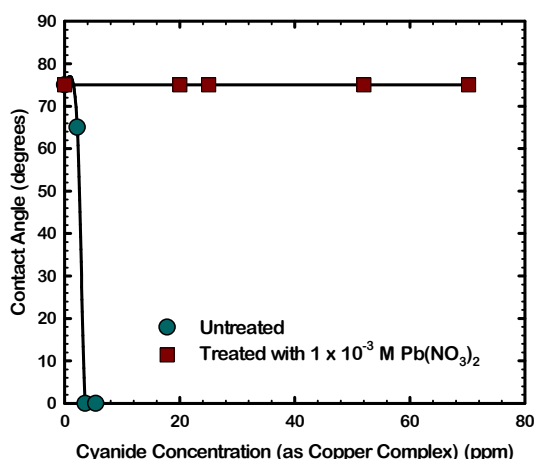


Figure 2.24 Electrochemically controlled contact angle measurements as a function of lead concentration for pyrite in $1 \times 10^{-3} M$ PAX solution, pH 4.7, at a potential of $-300 mV$ vs. SCE (Miller, 2003)

The investigation by Miller (2003) was conducted at pH 4.7 and a potential $-0.300 mV$ (SCE), which translates to $-0.032 V$ (SHE). This coincides with the domain in which Pb^{2+} is thermodynamically stable (Figure 2.25 (a)). The speciation diagram plotted for the lead concentration that Miller (2003) used shows that approximately 90% of lead is in the Pb^{2+} form at pH 4.7.

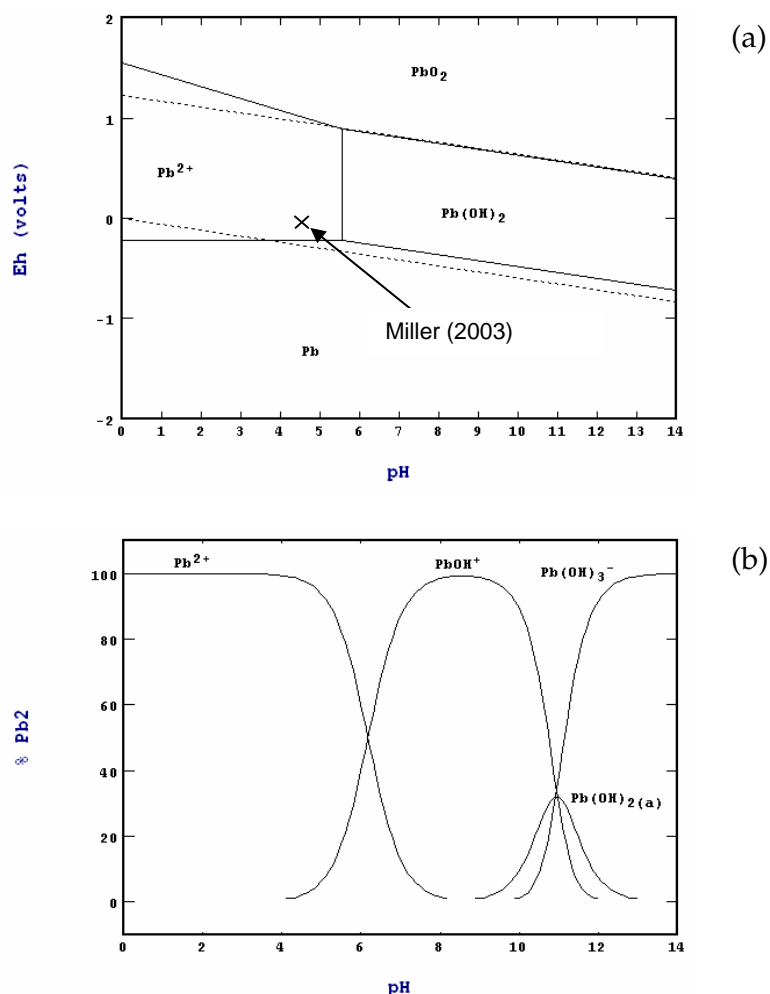


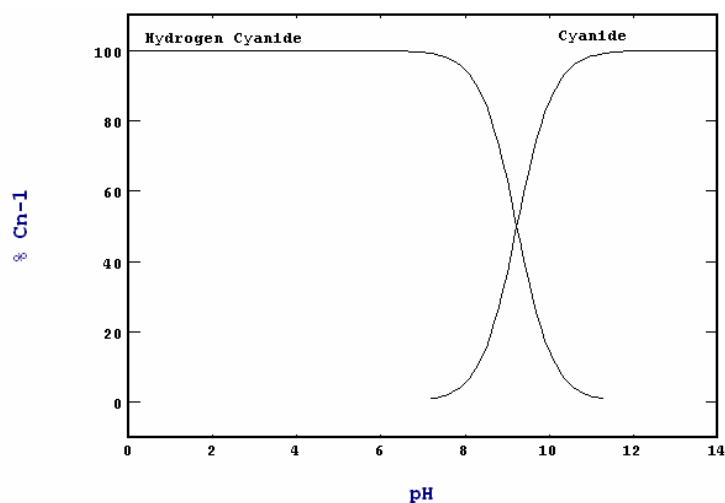
Figure 2.25 (a) A Pourbaix diagram for the Pb-H₂O system at $1 \times 10^{-3} \text{M}$ [Pb²⁺] showing E_h -pH conditions used by Miller (2003), (b) Lead (II) speciation at $1 \times 10^{-3} \text{M}$ [Pb²⁺]. Diagrams drawn with STABCAL software using NBS database

If the Pb²⁺ state is a pre-requisite for lead nitrate to be an effective activator, then flotation must be conducted at relatively low pH (Figure 2.25 (b)). Running a flotation circuit in acidic conditions is however likely to be detrimental to xanthate collectors if residence times are long. The work conducted by Viljoen (1998) shows that in air, the xanthate has a half life of 63.2 hours at pH 6 (Table 2.8). Cyanide too may hydrolyse to give HCN (equation 2.18), a poisonous gas at these low pH values (Figure 2.26).



Table 2.8 Half-life times for SIBX and iC_3 -TTC for different gaseous environments and pH (Viljoen, 1998)

Collector	Half life			
	pH 6		pH 9	
	N ₂	Air	N ₂	Air
SIBX	81.5 hours	63.2 hrs	1172 hours	1193 hours
iC_3 -TTC	25 minutes	36 minutes	40 minutes	63 minutes

**Figure 2.26** Proportion of cyanide species present as a function of pH at $2 \times 10^{-3} [CN^-]$. Diagram drawn using STABCAL Software, NBS Database

2.6.1 Adsorption of Lead (II) Ions on Pyrite

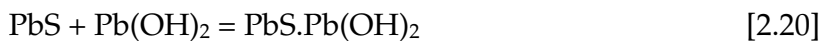
Sui et al. (1997) used cyclic voltammetry at a sweep rate of 20mV/s from -800mV to 300mV (SCE) to compare the behaviour of lead-treated pyrite and clean pyrite at pH 10.5. Both samples yielded similar voltammograms, which was attributed to lack of significant electron transfer between adsorbed lead ions and pyrite within the potentials tested. Based on this finding, the authors concluded that lead-uptake was through physisorption. At low pH, Allison (1982), Wang et al. (1989) and Leppinen et al. (1995) also showed that activation of pyrite did not involve cationic exchange between lead in solution

and the sulphide lattice. Inspection of the lead speciation diagram in Figure 2.35 shows that Pb^{2+} dominates at low pH while at pH 10.5, approximately 60% is in the form of $PbOH^+$, 28% as aqueous $Pb(OH)_2$ and 12% as $Pb(OH)_3^-$. Therefore regardless of pH and the lead species present, uptake of lead by pyrite only involves physisorption. It is important to note that the $Pb(OH)_3^-$ species depresses galena (Fuerstenau, 1982b) so that it should affect pyrite similarly. However, since it only forms 12% of the total lead, its effect could be small. Therefore, the interaction of lead-treated pyrite with xanthate recorded by Sui et al. (1997) could be a result of $PbOH^+$ and aqueous $Pb(OH)_2$ species only.

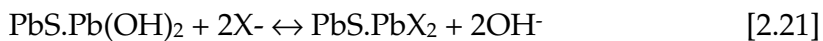
Sui et al. (1997) also showed that at pH 10.5, open circuit potentials (rest potential) of clean pyrite and lead-treated pyrite were similar. They suggested the electrochemical properties of pyrite were not significantly altered by the presence of Pb ions. Compared to clean pyrite, a pyrite electrode treated with 20ppm $PbCl_2$ showed two peaks in the presence of $10^{-3}M$ xanthate at pH 10.5, an anodic peak at 100mV that they attributed to formation of $Pb(OH)X$ and dixanthogen and a cathodic peak at -750mV due to dixanthogen reduction. The magnitude of the current at 100mV did not change for all lead concentrations tested (between 1 and 100ppm), leading to the conclusion that the electrode was already saturated at 1ppm lead. Pyrite contacted with a supernatant from a galena particle bed gave a similar voltammogram with that treated with $PbCl_2$. This means that Pb ions play the same role in promoting pyrite interaction with xanthate irrespective of their source.

Infrared spectra obtained from lead-treated pyrite exposed to xanthate showed a more intense dixanthogen peak compared to clean pyrite, which shows lead activated pyrite and was consistent with voltammetric results in which dixanthogen formation was inferred. The interaction between lead-treated pyrite and xanthate could be similar to the mechanism proposed by O'Dea and co-workers (2001) in their study of xanthate adsorption on galena

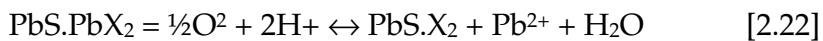
at high pH. Lead (II), which is predominantly in hydroxide form due to hydrolysis is attached to the surface:



An exchange reaction between xanthate and hydroxide may then take place:



Oxidation of xanthate to dixanthogen accompanied by oxygen reduction may follow:



It is likely that $\text{Pb}(\text{OH})_2$, which forms 60% of lead (II) species at pH 10.5 adsorbs onto pyrite and undergoes similar reactions as shown above, with pyrite taking the role played by galena.

2.6.2 Copper Sulphate

Under neutral pH conditions, pyrophyllite or the so-called khaki shales in most ores from the Witwatersrand basin do not float readily. Copper sulphate additions ensure that pyrite flotation is not depressed. Some flotation circuits recovering pyrite together with uranium bearing minerals operate at low pH levels (O'Connor et al., 1988). Under these conditions, the addition of copper sulphate enhances the rate of pyrite flotation, concentrate grade and reduces conditioning time. Typical addition rates vary between 30g/t and 100g/t, (O'Connor and Dunne, 1991), with even higher rates being applied in the treatment of refractory ores. Conditioning times are generally less than 1 minute.

A number of theories have been proposed to explain the mechanism of pyrite activation. O'Connor and co-workers (1988) have drawn attention to some of this work. Livshits and Dudenkov (1965) showed that the insoluble hydrophobic precipitates formed by xanthates in the presence of Cu^{2+} ions destabilise the froth phase. It has often been suggested that the addition of copper sulphate activates pyrite in streams containing traces of cyanide by forming copper-cyanide complexes. Westwood et al. (1970) and Lloyd (1981) however disputed this; with Westwood and co-workers arguing that although copper complexes with cyanide, the addition of copper sulphate alone is insufficient, low pH is also required. Work done by Levin and Veitch (1970) reported poor results from laboratory batch flotation tests in which CuSO_4 was added as compared to ones in which no addition was made, thus suggesting that the presence of copper ions jeopardised the process. In flotation plants however, the exclusion of copper sulphate has been shown to give overall poorer performance (Broekman et al., 1987).

O'Connor et al. (1988) carried out adsorption studies of copper sulphate on onto gravity concentrated pyrite containing quartz and khaki shale gangue.

Their results are shown in Figure 2.27. Tests 1, 2 and 3 were carried out under identical conditions, as were tests 4, 5 and 6. Figure 2.28 shows the grade-recovery data for the same set of tests. Despite the poor reproducibility in tests 4-6, it is clear that the addition of copper sulphate enhanced both pyrite grades and final recoveries. In addition, Figure 2.29 shows that gangue recovery increased due to the dosing of copper sulphate.

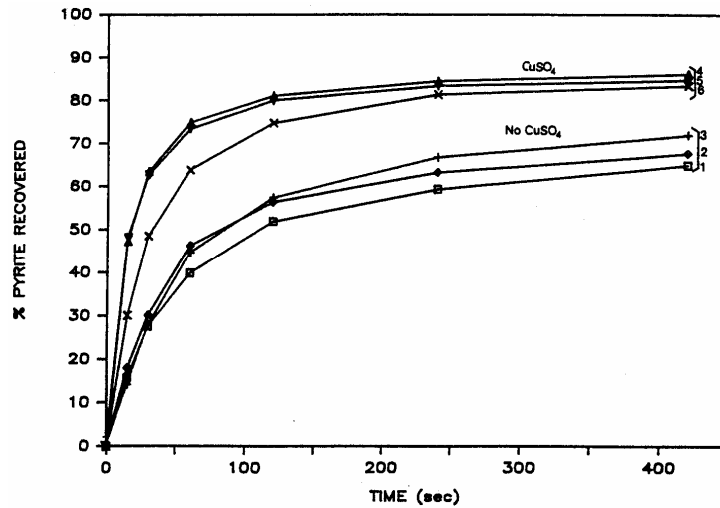


Figure 2.27 Effect of copper sulphate on recovery of pyrite (O'Connor et al., 1988)

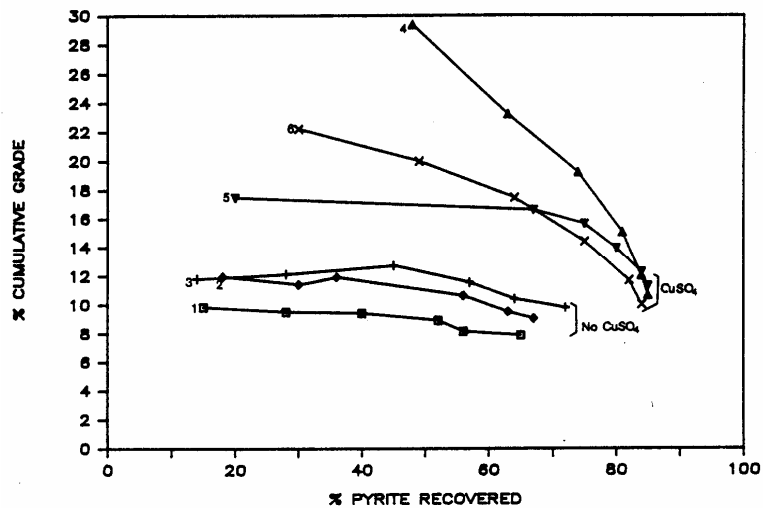


Figure 2.28 Effect of copper sulphate on pyrite flotation (O'Connor et al., 1988)

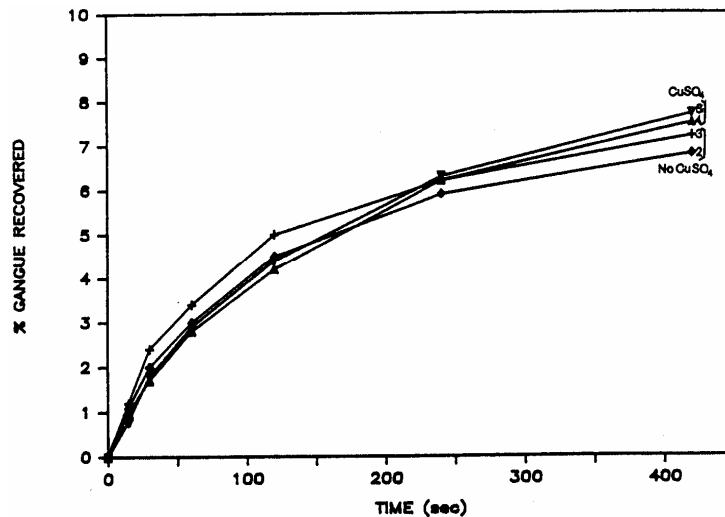


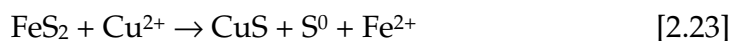
Figure 2.29 Effect of copper sulphate on gangue recovery (O'Connor et al., 1988)

2.6.3 Adsorption of Copper (II) ions on Pyrite

Several theories regarding the mechanism by which copper (II) activates pyrite have been put forward and a literature survey conducted by Chen (1999) lists some of this work. Allison (1982), Wang et al. (1989) and Leppinen et al. (1995) studied the activation of pyrite by heavy metal ions and showed that the adsorption of Cu^{2+} on pyrite did not involve exchange with the lattice cation. They concluded that it was the hydroxides that adsorbed on pyrite during the initial stage of activation. Wang et al. (1989) and Voigt et al. (1994) also agreed that the activation products were CuS_2 or $(\text{Cu}, \text{Fe})\text{S}$, together with surface cupric hydroxide which interacted with ferric hydroxides resulting from the oxidation of the pyrite surface. The adsorbed cupric hydroxide was found to dissolve readily in water. Voigt and his co-workers studied the relationship between the adsorbed cupric hydroxides and cuprous sulphides. They found that the adsorption in the cuprous form was independent of pH, whereas the adsorption of the cupric form rose sharply with the pH and reached a peak at about 9. They also observed that the adsorption of the cupric hydroxide had an induced stage: copper (II) was detected at the surface only after it had been

exposed to the activating solution for about 15 minutes. It took about 2 minutes for copper (II) to reach its maximum density at the surface at pH 5; at pH 10 it took far longer. At pH 10, copper (I) seemed to form in two distinct stages, the second stage started only after the adsorption of the hydroxide had commenced. This study showed that the activation of sulphide minerals under alkaline conditions involves complex interactions between the sulphide products, which are thought to be responsible for activation of the reaction with the collectors, and the hydroxides which are formed through oxidation of the mineral surface and hydrolysis of the activating ion. Voigt et al. (1994) also found the amount of copper adsorbed on pyrite, measured by the atomic surface ratio Cu/S, to be limited. The copper (I) did not exceed a monolayer on pyrite and did not penetrate below the surface.

Bushell et al. (1961), on the other hand, proposed that pyrite is activated with copper (II) by a reaction that essentially involves oxidation of pyrite with the formation of elemental sulphur:



Zhang et al. (1997) observed a significant increase in the zeta potential of pyrite after it was contacted with cupric ions at pHs above 6. Basing their argument on stability diagrams, they attributed this to uptake of $\text{Cu}(\text{OH})^+$. Upon addition of xanthate, the zeta potential decreased significantly. This was thought to be due to either adsorption of a negatively charged species and/or partial removal of adsorbed cupric ions from the pyrite surface. However, they observed increased pyrite recoveries, which suggested that the former was more likely. The presence of a positive charge from adsorbed cupric ions attracts negatively charged xanthate ions. The authors also used infrared spectroscopy to identify the surface species resulting from interactions pyrite treated with cupric ions and xanthate. Compared to

untreated pyrite, treated pyrite showed increased intensity of dixanthogen bands and additional bands which were attributed to cupric xanthate.

2.6.4 Cyanide and Activation of Pyrite with Copper and Lead Ions

The feed to No 2 Gold Plant consists of a mixture of tailings from cyanidation plants treating run-of-mine ore and reclaimed dump material. Leaching is carried out in alkaline conditions, typically above pH 10. The cyanidation reaction requires oxygen and common plant practice involves blowing air into leach pulps. This increases the amount of dissolved oxygen so that any sulphides present are prone to surface oxidation. Consequently, feed to the flotation circuit always contains oxidised pyrite as well cyanide carried over from leaching. The superficial oxide inhibits interaction with flotation reagents (Benzaazoua and Kongolo, 2002) and cyanide depresses pyrite (de Wet et al., 1997; O'Connor et al., 1988; Janetski et al., 1977, Elgillani and Fuerstenau, 1968).

Examination of the Pourbaix diagram of the Fe-S-CN-H₂O system (Figure 2.30) shows that ferricyanide ($\text{Fe}(\text{CN})_6^{3-}$) and ferrocyanide ($\text{Fe}(\text{CN})_6^{4-}$) are the stable species formed at the flotation pH of 7.2 used at No 2 Gold Plant. According to Seke (2005), most flotation processes are run at pulp potentials that thermodynamically favour the formation of ferrocyanide so that when the flotation feed enters the plant, it is likely to be adsorbed on pyrite. Elgillani and Fuerstenau (1968) have attributed the depression of pyrite by cyanide to the formation of this iron cyanide followed by the precipitation of ferric ferrocyanide ($\text{Fe}_4[\text{Fe}(\text{CN})_6]_3$) on the sulphide surface.

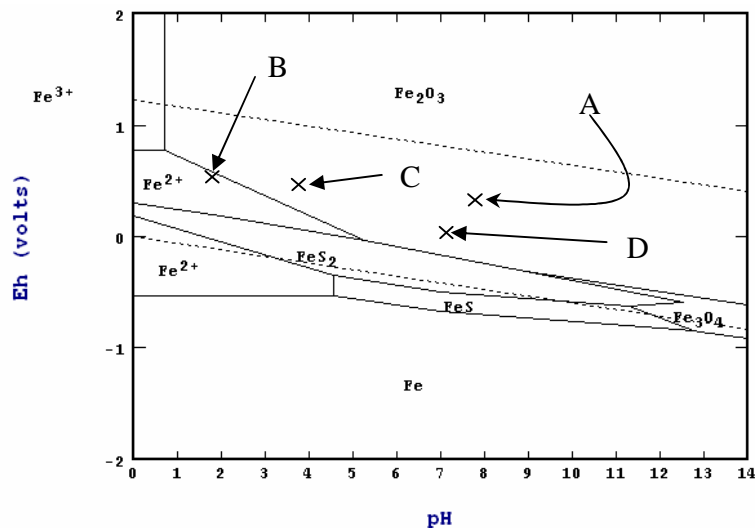


Figure 2.30 A Pourbaix diagram for the Fe-S-CN-H₂O system drawn using STABCAL software for $10^{-4}\text{M} [\text{S}]$, $10^{-4}\text{M} [\text{Fe}]$ and $2 \times 10^{-3}\text{M} [\text{CN}^-]$, NBS Database

The speciation diagram of copper (II) in Figure 2.31 predicts that at the plant flotation pH of 7.2, approximately 80% of the copper is available in the form of Cu^{2+} . Since this species dominates to a large extent, Cu^{2+} is likely to determine the behaviour of copper (II) in the flotation process.

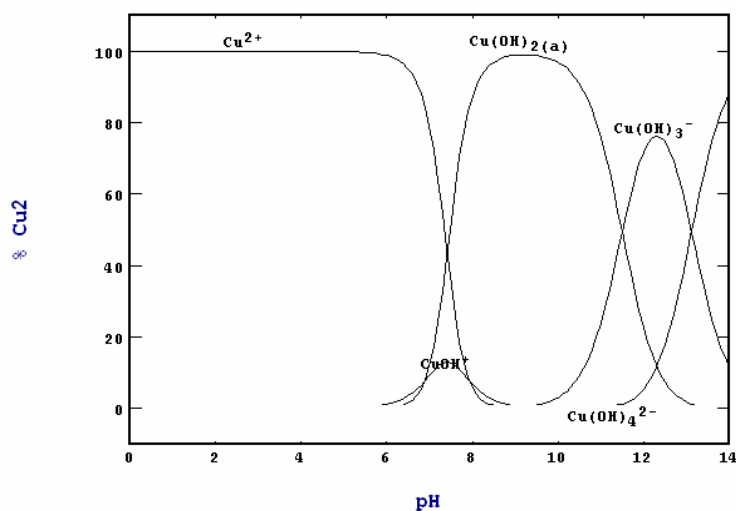


Figure 2.31 Copper (II) speciation at different pH values. Diagram drawn using STABCAL Software for $2 \times 10^{-4}\text{M} [\text{Cu}^{2+}]$, NBS Database

Since ferrocyanide is formed at E_h -pH conditions in which pyrite flotation takes place, any interaction between Cu^{2+} and ferrocyanide will affect the capacity of copper sulphate to activate pyrite. The work conducted by Bellomo (1970) in which copper (II) was titrated with ferrocyanide shows that the two interact to yield a reddish brown precipitate of copper ferrocyanide ($Cu_2Fe(CN)_6$) according to:

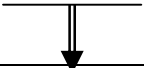
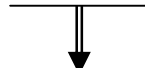


Considering the negative free energy change, it is reasonable to assume that copper ferrocyanide is formed spontaneously when copper sulphate is dosed to the flotation feed. The precipitate has a solubility of 2×10^{-6} mol/L and the plant doses 70g/t copper sulphate (equivalent to 2×10^{-4} M [Cu^{2+}]). Since this is greater than the solubility, some of the salt formed should precipitate. It therefore appears that copper sulphate dosed in the presence of cyanide is likely to be consumed in the formation of copper ferrocyanide salt so that none is available to adsorb on pyrite and activate it. Consequently, xanthate cannot adsorb and pyrite will still be depressed. Perhaps this is the reason why Westwood and co-workers (1970) have emphasised that in flotation feed containing traces of cyanide, treatment with copper sulphate alone is not sufficient to render pyrite floatable. Low pH treatment is essential as well. The low pH probably destroys cyanide (Table 2.2), completely eliminating the participation of ferrocyanide so that Cu^{2+} can adsorb and activate pyrite without any interference from complex ion formation.

At No. 2 Gold Plant, cyanide is destroyed by treating flotation feed with calcine water, a low pH SO_2 -containing solution (Table 2.2) prior to flotation. This reduces cyanide concentrations from about 125ppm to less than 4ppm (Brooks, 2005). The treatment is based on the INCO SO_2 /AIR process

(Davidtz, 2002). Robins (1996) has outlined its basic chemistry and it consists of primary and secondary reactions and is shown in Table 6.2.

Table 2.9 Basic chemistry of the INCO SO₂/AIR process (Robbins, 1996)

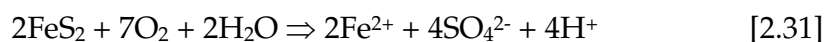
<i>Oxidation</i>	
$\text{CN}^-_{\text{free}} + \text{SO}_2 + \text{O}_2 + \text{H}_2\text{O} \rightarrow \text{OCN}^- + \text{H}_2\text{SO}_4$	[2.24]
$\text{Me}(\text{CN})^{2-}_4 + 4\text{SO}_2 + 4\text{O}_2 + 4\text{H}_2\text{O} \rightarrow 4\text{OCN}^- + 4\text{H}_2\text{SO}_4 + \text{Me}^{2+}$	[2.25]
$\text{Me}^{2+} = \text{Zn}^{2+}, \text{Cu}^{2+}, \text{Ni}^{2+}, \text{Cd}^{2+}, \text{etc}$	[2.26]
<i>Neutralisation</i>	
$\text{H}_2\text{SO}_4 + \text{Ca}(\text{OH})_2 \rightarrow \text{CaSO}_4 \cdot 2\text{H}_2\text{O}$	[2.27]
<i>Precipitation</i>	
$\text{Me}^{2+} + \text{Ca}(\text{OH})_2 \leftrightarrow \text{Me}(\text{OH})_2 + \text{Ca}^{2+}$	[2.28]
	
$2\text{Me}^{2+} + \text{Fe}(\text{CN})^{2-}_6 \leftrightarrow \text{Me}_2\text{Fe}(\text{CN})_6$	[2.29]
	
Reactions catalysed by copper in solution	
$\frac{\text{SO}_2}{\text{CN}_{\text{WAD}}} = 2.46\text{g/g}$	[2.30]

Weak dissociable cyanide (CN_{WAD}), which includes free cyanide and weakly complexed metal cyanides is oxidised to produce cyanate (OCN^-) and sulphuric acid. This reaction requires a small amount of copper in solution to serve as catalyst. Acid produced in the oxidation reactions is neutralised with lime.

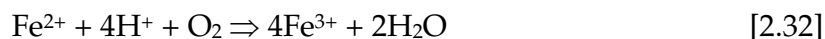
Due to the characteristic low pH of calcine water (typically 1.8), dosing it to plant feed also aids pyrite flotation by removing superficial oxide. This is formed during cyanidation and more significantly, during the period prior to excavation of the fraction of feed coming from old slimes dams (Dumisa, 2002). Examination of the Pourbaix diagram for the Fe-S-CN-H₂O system (Figure 2.30) shows that if E_h -pH conditions are adjusted to suit the domains in which ferric and ferrous ions are thermodynamically stable, then iron (III)

oxide (Fe_2O_3) should dissolve, exposing fresh sulphide that can interact freely with flotation reagents.

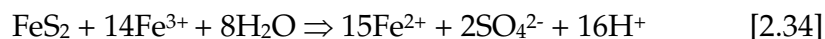
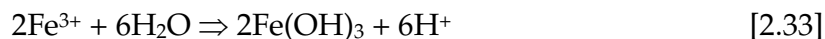
Apart from the beneficial destruction of cyanide and 'polishing' of sulphides, addition of calcine water introduces ferric and ferrous ions. In the presence of water, pyrite also undergoes oxidation. Jiang et al. (1998) have outlined the chemistry of the process, and the initial stage involves the production of ferrous ions:



The ferrous ions are oxidised to ferric ions due to the presence of dissolved oxygen and acid:



Ferric iron may undergo hydrolysis to form ferric hydroxide (equation 6.16), or it may oxidise pyrite to release more ferrous ions into solution (equation 6.17):



The oxidation reactions can take place within a very short time of exposure and considering that calcine water comes with high iron concentrations (Table 2.2), ferrous and ferric ions are ubiquitous on the pyrite surface and in solution. Examination of speciation diagrams for both ferrous and ferric ions (Figures 2.32 and 2.33) shows that at the plant flotation pH of 7.2, all the ferric iron is present as ferric hydroxide ($\text{Fe}(\text{OH})_3$) while approximately 70% of ferrous iron is in complex form (FeOH^+) and 30% is available as Fe^{2+} . The

effect of iron ions on pyrite flotation with SIBX is therefore dependant on interaction between SIBX and each of the three species.

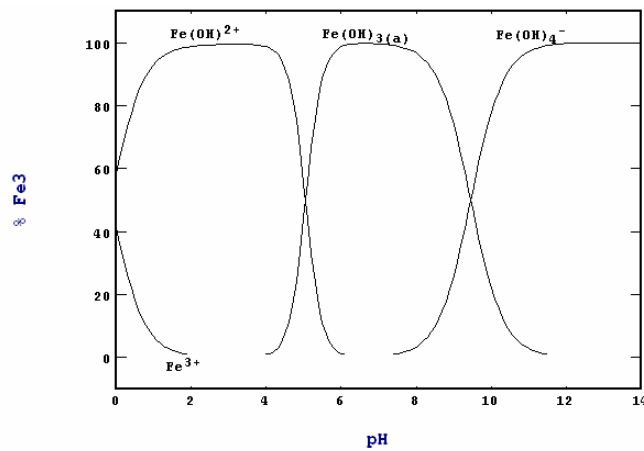


Figure 2.32 Speciation diagram for $2 \times 10^{-3}M$ Fe(III) as a function of pH at 25°C. STABCAL Software, NBS Database

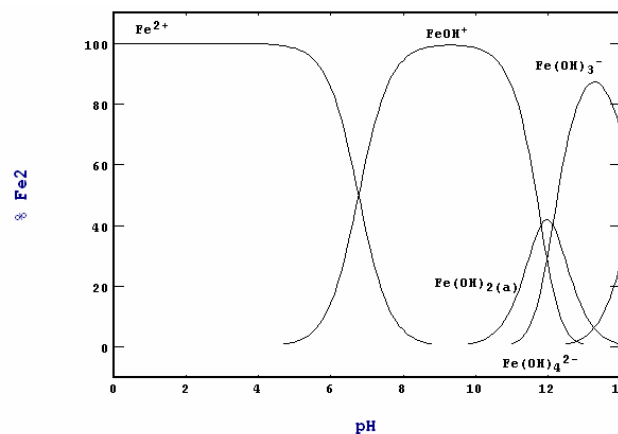


Figure 2.33 Speciation diagram for $2 \times 10^{-3}M$ Fe(II) as a function of pH at 25°C. STABCAL Software, NBS Database

Jiang and co-workers (1998) have investigated the effect of ferric and ferrous ions on the flotation behaviour of ore-pyrite as a function of pH. While xanthate alone gave complete flotation in acidic and alkaline regions, the presence of ferric ions gave partial flotation in the intermediate pH range (Figure 2.34). This is the region in which ferric hydroxide is stable (Figure 2.32). By using distribution diagrams of the iron-xanthate-water system, the authors were able to show that a weakly hydrophobic and insoluble ferric

dihydroxy xanthate complex ($\text{Fe}(\text{OH})\text{X}_2$) is formed. The sequence of reagent addition and pH adjustment was found to have a remarkable effect on pyrite flotation response in the neutral pH region. In the presence of ferric ions, adjustment of solution pH before addition of xanthate gave more significant depression that the reverse-order. This is important as it predicts the behaviour of ferric ions released into solution by a low pH treatment aimed at “polishing” oxidised pyrite prior to flotation.

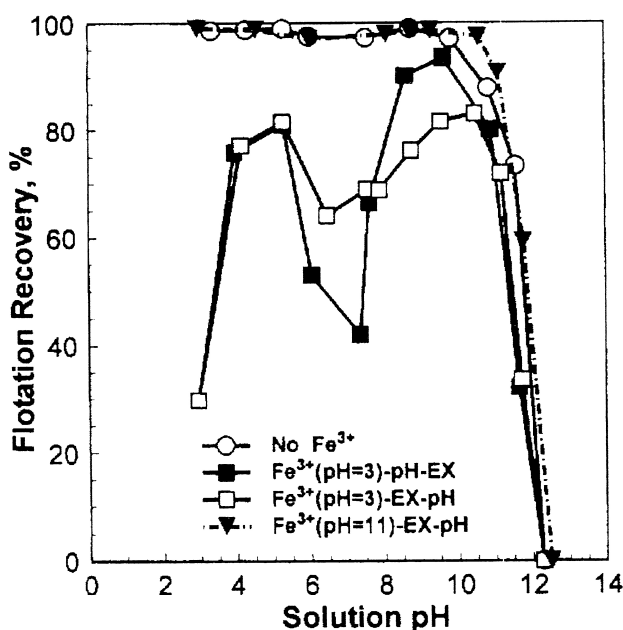


Figure 2.34 Effect of pH and reagent addition order on the flotation of ore-pyrite in the absence and presence of $2 \times 10^{-3} \text{M}$ Fe^{3+} ions using $3.3 \times 10^{-4} \text{M}$ ethyl xanthate (EX) and 50mg l^{-1} MIBC. Conditioning time and reagent addition order: (■) Fe^{3+} (2 min) at pH 3 → pH adjustment (2 min) → EX (2 min); (□) Fe^{3+} (2 min) at pH 3 → EX (2 min) → pH adjustment (2 min); (▼) Fe^{3+} (2 min) at pH 11 → EX (2 min) → pH adjustment (2 min) (Jiang et al., 1998)

In Figure 2.35, ferrous ions too were shown to significantly affect pyrite flotation in neutral to weakly alkaline solutions. The authors observed that in the presence of ferrous ions, complete flotation was observed below about pH 5-6 irrespective of reagent addition order. This behaviour was attributed to the solubility of ferrous xanthate being high in acidic pH so that no significant

side-reactions between ferrous and xanthate ions occurred during flotation. The drastic decrease in pyrite flotation at about pH 6 was attributed to reactions between ferrous iron with xanthate to form a weakly hydrophobic compound on pyrite and in the solution. The authors assumed this to be ferric di-hydroxy xanthate.

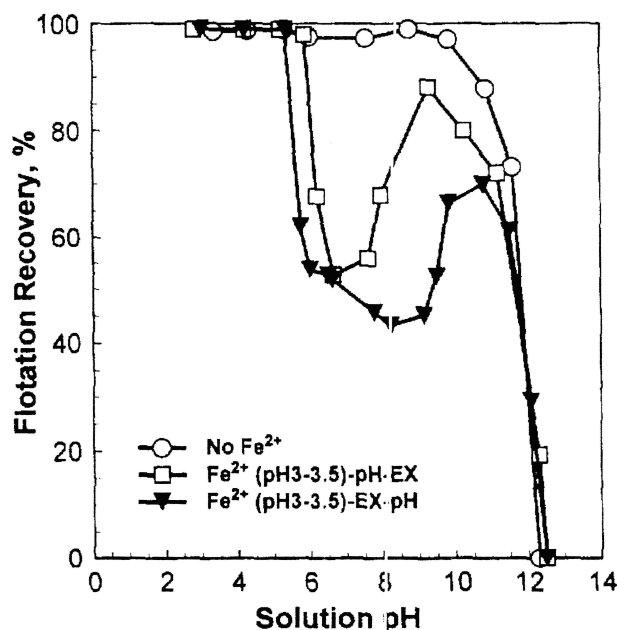


Figure 2.35 Effect of pH and reagent addition order on the flotation of ore-pyrite in the absence and presence of $2 \times 10^{-3} \text{M}$ Fe^{2+} ions using $3.3 \times 10^{-4} \text{M}$ ethyl xanthate (EX) and 50mg l^{-1} MIBC. Conditioning time and reagent addition order: (\square) Fe^{3+} (2 min) at pH 3.0-3.5 \rightarrow pH adjustment \rightarrow EX (2 min); (\blacktriangledown) Fe^{2+} (2 min) at pH 3.0-3.5 \rightarrow EX (2 min) \rightarrow pH adjustment (2 min) (after Jiang et al., 1998)

2.6.5 Iron Ions and Surface Charge

The oxidation products formed on the surface such as ferrous ions, and the hydroxyl complexes produced after the addition of caustic to neutralise pH also play an important role in influencing surface electrical properties and hence, floatation of pyrite with xanthate. As highlighted by Fuerstenau (1982c), when the inorganic species are adsorbed on the surface, they affect the sign and magnitude of surface charge, thereby controlling the adsorption

of physically adsorbing flotation agents. Once a surface charge exists, other ions from the bulk solution must be adsorbed as counter-ions for electro-neutrality. This gives rise to an electrical double layer. In a system involving pyrite and its oxidation products, hydrogen and hydroxyl ions are free to pass between the solid phase and the liquid phase and are therefore called potential determining ions. The activity of these ions at which surface charge is zero is called the point of zero charge (PZC). The importance of this parameter is that the sign of surface charge has a major effect on the adsorption of all other ions and particularly those charged oppositely to the surface because they function as counter ions to maintain electro-neutrality.

Jiang et al. (1998) have showed that at a modest degree of oxidation; pyrite surfaces behave like iron oxide with a PZC at pH 7. This is due to the presence of ferric hydroxide formed during oxidation. The surface will acquire electro-kinetic features of the iron hydroxide. The authors showed that in the presence of 2×10^{-3} M ferric ions and 5.6×10^{-4} M ethyl xanthate, the zeta potential of pyrite exhibited less positive charge below pH 7.5 compared with that in the presence of ferric xanthate alone. At pH > 7.5, there was no noticeable difference between the two. This implies that in the presence of ferric ions, adsorption of xanthate onto pyrite is favoured in acidic conditions only.

Jiang and co-workers also showed that the PZC of pyrite in the presence of 2×10^{-3} M ferrous ions is pH 9. Addition of 5.6×10^{-4} M ethyl xanthate reduced it to pH 6. The authors observed that at pH < 6, the zeta potential curve was identical to that in the presence of xanthate only and at pH > 6, it was identical to that in the presence of only ferrous ions. From these results, they concluded that ferrous ions do not undergo significant reaction with xanthate at pH < 6 and the flotation of pyrite in this region is mainly due to the adsorption of xanthate on the surface. At pH > 6, the adsorption of xanthate was reduced, which was in agreement with their flotation results.

CHAPTER 3

MATERIALS AND METHODS

3.1 Materials**3.1.1 Ore**

The auriferous pyrite ore samples used in this study were collected from the feed stream to the flotation circuit at No. 2 Gold Plant at Vaal Reefs. The feed consists of a de-slimed mixture of cyanide leach tailings from two circuits, one treating reclaimed tailings from West Pay Dam and the other, run-of-mine ore from Kopanang Mine. The latter treats feed augmented with reclaimed dump material as well. After filtration and drying at 60°C, about 350kg of the bulk feed sample collected was screened through an 850µm screen; thoroughly mixed and divided first into 50kg batches, and then down to 2kg samples. To avoid dust losses, the cone and quartering technique was used throughout.

Typical mineralogical composition of the feed is shown in Table 3.1 and was determined using X-Ray Diffraction Spectrometry. The accompanying XRD pattern is shown in Figure 2.1

Table 3.1 *Typical minerals found in No. 2 Gold Plant Feed*

Mineral	Chemical Formula
Quartz	SiO ₂
Pyrophyllite	Al ₂ Si ₄ O ₁₀ (OH) ₂
Clinochlore	(Mg,Fe) ₆ (Si,Al) ₄ O ₁₀ (OH) ₈
Muscovite	(K,Na)(Al,Mg,Fe) ₂ (Si _{3.1} Al _{0.9})O ₁₀ (OH) ₂
Hematite	Fe ₂ O ₃
Pyrite (Cubic)	FeS ₂
Gypsum	CaSO ₄ .2H ₂ O

Typical chemical composition of the material is shown in Table 3.2. The gold content was assessed using fire assay while a sequential XRF spectrometer ARL 9400-241 XP+ was used for determining the concentrations of the other constituents. Particle size distribution (Figure 3.1) was determined using a Malvern Mastersizer 2000 instrument.

Table 3.2 Typical chemical composition of the bulk ore sample used in this study

	Composition								
	%					ppm			
Element	Si	Ca	Fe	S	Zr	Au	Pb	U ₃ O ₈	Zn
Content	39.62	0.46	3.06	1.03	0.03	0.4	109	140	213

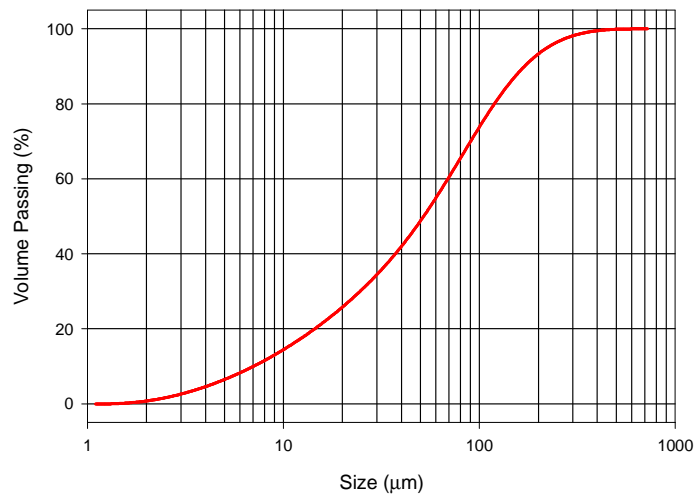


Figure 3.1 Typical particle size distribution of ore samples treated in this investigation.

3.1.2 Reagents

The pH was adjusted by adding either reagent grade sulphuric acid or analytical grade caustic soda. GEMPOLYM GM4, a guar based depressant was used for depressing pyrophyllite present in the feed and Dowfroth 200 was used as the frother. The three collectors (Table 3.3) tested in this work were sodium *iso*-butyl xanthate, C₁₀ and C₁₂ trithiocarbonate (TTC). Copper sulphate and lead nitrate and sodium cyanide were used as modifiers. All reagents were dosed from 1% wt solutions. Tap water was used in all the experiments.

Table 3.3 *Collectors used in the study*

Name	Abbreviation	Chemical Formula	Molecular Weight (a. m. u)
Sodium <i>iso</i> -butyl xanthate	SIBX	C ₄ H ₉ OCS ₂ Na	172
Sodium <i>n</i> -decyl trithiocarbonate	C ₁₀ TTC	C ₁₀ H ₂₁ SCS ₂ Na	272
Sodium <i>n</i> -dodecyl trithiocarbonate	C ₁₂ TTC	C ₁₂ H ₂₅ SCS ₂ Na	300

3.1.3 Apparatus

A Denver D12 flotation machine (Figure 3.2) fitted with either a 5L or 10L cell was used for all the batch flotation experiments. The machine was run at 1200rpm and 1500rpm for the 5L and 10L cells respectively. The pH was monitored using an Orion pH meter-model 420.

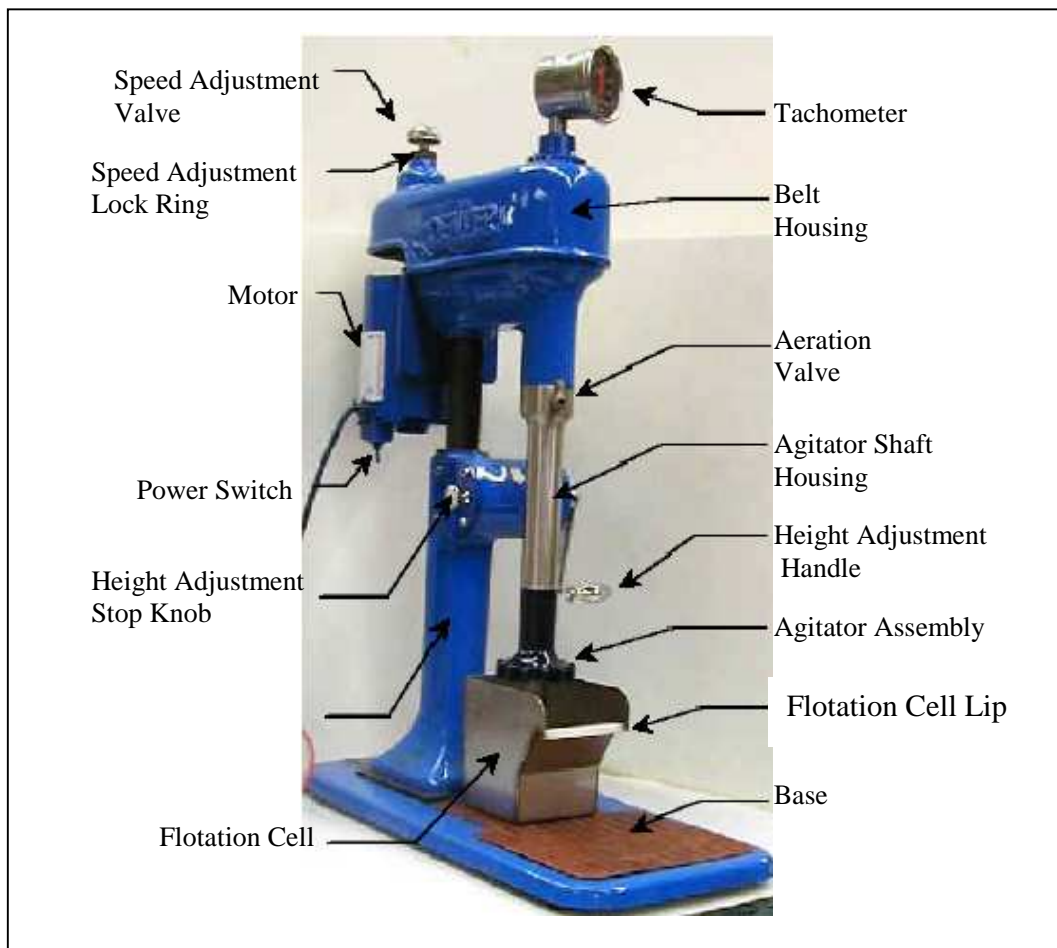


Figure 3.2 A Denver-D12 laboratory flotation machine fitted with a flotation cell

3.2 Methods

3.2.1 Single-Point Flotation Tests

Batch flotation tests were used to firstly establish the optimum SIBX dosage (called the standard) by studying the effect of SIBX dosage level; and to evaluate the effect of SIBX/TTC mixtures on gold, pyrite and uranium flotation.

A 2kg sample of dried plant feed was mixed with 3kg of water in a 5-litre flotation cell to give a pulp of 40% wt solids at a natural pH of 7.8. This was conditioned at 1200 rpm for 1 minute to ensure homogenous slurry before any reagents were added. Firstly copper sulphate ($\text{CuSO}_4 \cdot 5\text{H}_2\text{O}$) was dosed at 70g/t and the pulp conditioned for 5 minutes. This was followed by the collector (SIBX or a mixture of TTC and SIBX) and another 5 minutes of conditioning. The frother (16g/t Dow 200) and lastly the depressant (20g/t GEMPOLYM GM4) was added, each followed by 1 minute of conditioning. Thereafter, the pulp was aerated. Froth was allowed to build up, after which it was scrapped at 15 second intervals for 6 minutes. During the experiment, the pH of the pulp was maintained at 7.2 by adding either sulphuric acid or a caustic solution. Froth height was not controlled. All tests at a given set of conditions were repeated in triplicates.

Concentrates and tailings were filtered, dried at 70°C and weighed. Individual samples were then sent for chemical analysis. Sulphur content was determined using a 114 Series Leco Analyser located within The Department of Materials Science and Metallurgical Engineering at The University of Pretoria. Gold, lead and uranium were assayed by SGS Lakefield Research Africa (Pvt) Ltd in Johannesburg. Gold was analysed by fire assay while lead and uranium were done using XRF

3.2.2 Release Curve Measurements

Release curves were used to compare the standard and the optimum SIBX/TTC mixtures, the effect of acid conditioning prior to flotation and the effect of activating with copper sulphate or lead nitrate in the presence of sodium cyanide.

A dry 4kg ore sample was placed into a 10-litre flotation cell. It was then re-pulped with 6kg of tap water to give a pulp of 40% wt solids. 70g/t of the activator, copper sulphate, was added and conditioned for 5 minutes. From this point onwards, pH was maintained at 7.2 using either sulphuric acid or a caustic solution. The collector (SIBX or combinations with either C₁₀ or C₁₂ TTC) were added and the pulp conditioned for 5 minutes. This was followed by the frother (16g/t) and the depressant (20g/t), each accompanied by 1 minute of conditioning. Air was then introduced into the cell and scrapping of the froth was initiated every 15 seconds. Concentrates were collected after 1, 2, 4, 8 and 20 minutes of flotation. At the end of the each test, the concentrates and tailings were dried and analysed for sulphur, uranium and gold. Experiments were repeated to assure reproducibility and establish the magnitude of statistical error. All experimental data were fitted using empirical first order kinetics outlined by Cullinan et al. (1999) and Agar and Barrett (1983):

$$R = R_{\max} [1 - e^{-kt}] \quad [3.1]$$

Where R (%) is the recovery at time t (min), k (min⁻¹) is the initial rate and R_{\max} (%) is the final recovery. Sigma Plot 2001® was used for fitting experimental data and for determining the k and R_{\max} terms in equation 3.1. In the fitting of all the data into this first-order rate equation, an R-squared value was quoted. The closer the value is to 1, the better the data could be described in terms of the model.

CHAPTER 4

**EFFECT OF SIBX DOSAGE LEVEL ON SINGLE-POINT
BATCH FLOTATION**

4.1 Introduction

The current practice at No 2 Gold Plant is to dose SIBX at a rate of 16g/t. The following experiments were conducted to establish the optimum dosage level of SIBX on gold, sulphur and uranium grades and recoveries. This information was needed so that chemicals could be compared in terms of rate and recovery data obtained from release curves. These curves would be generated with information obtained from batch flotation tests results that are to follow.

The materials and methods used are described in Chapter 3. Single-point batch flotation tests in which SIBX dosages were varied from 10 to 40g/t were performed at the plant operating flotation of pH 7.2. $\text{CuSO}_4 \cdot 5\text{H}_2\text{O}$ was maintained at 70g/t, Dow 200 at 16g/t and GEMPOLYM GM4 at 20g/t. The concentrate was collected for 6 minutes. The results recorded are shown in Tables 4.1 to 4.4 and Figures 4.1 to 4.4. The standard error associated with each set of data is shown in the form of error bars in all the graphs that were plotted from the data.

4.2. Results and Discussion

4.2.1 Mass Recovery

Table 4.1 shows the mass recoveries recorded for each of the SIBX dosages tested. They increased from 10g/t to 30g/t SIBX, after there was a slight decrease at 40g/t. This trend is evident in Figure 4.1, which shows a plot of mass recovery against SIBX dosage. The initial trend can be attributed to more sulphide being floated by the increased amount of collector added. This is supported by variation in sulphur recovery with collector dosage (Figure 4.2 (b)).

Table 4.1 *Mass recovery*

SIBX (g/t)	Mass Recovery (%)	Standard Error
10	2.6	0.11
20	2.8	0.11
30	3.1	0.06
40	3.0	0.10

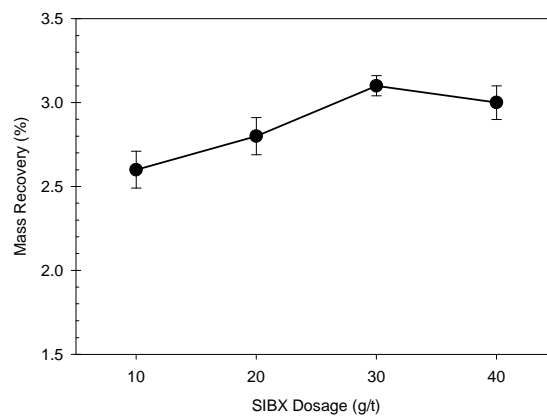


Figure 4.1 *Response of mass recovery to different SIBX dosages*

4.2.2 Sulphur

Table 4.2 shows sulphur recoveries and grades of concentrates and tailings obtained at each of the SIBX dosages tested. Sulphur grades decreased from 10g/t SIBX to 30g/t and then increased slightly at 40g/t (Figure 4.2 (a)). This is an opposite trend to mass recovery (Figure 4.1) and could be attributed to dilution from, presumably increased gangue flotation.

Table 4.2 Sulphur flotation data for each SIBX dosage

SIBX (g/t)	Concentrates		Tails		Sulphur Recovery (%)	Std Error
	Sulphur Grade (%)	Std Error	Sulphur Grade (%)	Std Error		
10	31.1	1.01	0.26	0.01	75.9	1.14
20	29.3	1.08	0.22	0.01	78.9	0.85
30	27.2	0.63	0.22	0.01	79.7	0.48
40	27.9	0.84	0.22	0.01	79.6	0.58

The grade of the tails did not vary significantly with TTC mole percent. Sulphur recoveries increased from 10g/t to 30g/t and almost levelled at 40g/t (Figure 4.2 (b)). The only significant change was between 10g/t and 20g/t. For the last three data points, sulphur recoveries were almost similar.

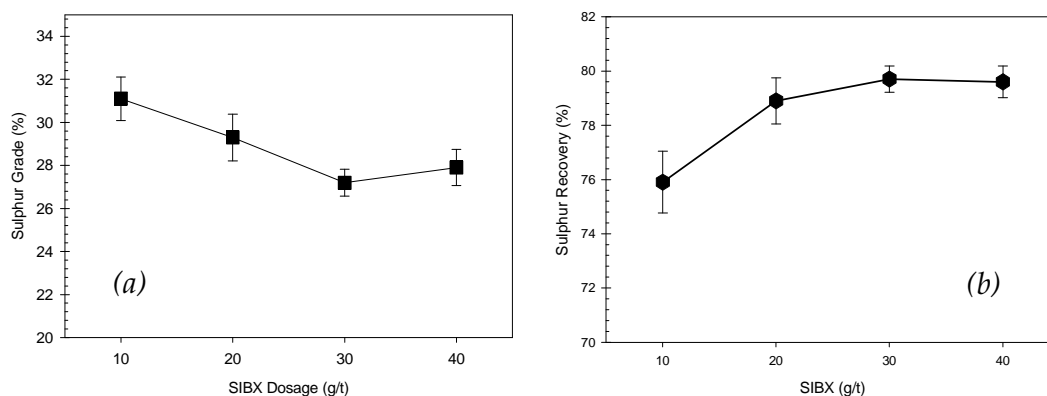


Figure 4.2 Change of (a) concentrate sulphur grade and (b) the corresponding recoveries with SIBX dosage

4.2.3 Uranium

Uranium recoveries, tailings and concentrate grades are shown in Table 4.3. A plot of uranium grade versus SIBX dosage in Figure 4.3 (a) shows a decrease from 10g/t SIBX to 30 g/t. This was followed by a slight increase at 40g/t. Taking into account experimental error, the latter may be insignificant. As for the recovery, the gradual increase from 10 to 40g/t SIBX is also small but there is a trend (Figure 4.3 (b)).

Table 4.3 Uranium flotation responses for the SIBX concentrations tested

SIBX (g/t)	Concentrates		Tails		Uranium Recovery (%)	Std Error
	Uranium (ppm)	Std Error	Uranium Grade (ppm)	Std Error		
10	888.3	65.5	140.0	1.4	14.2	0.6
20	884.0	71.5	141.7	2.3	15.2	0.9
30	796.3	16.1	140.7	6.0	15.3	0.6
40	813.3	3.5	136.3	4.0	15.7	0.8

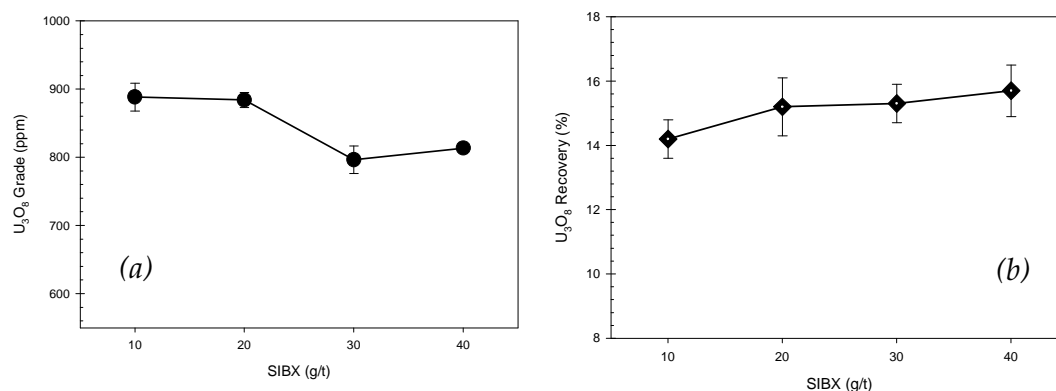


Figure 4.3 Variation of (a) uranium grade (b) uranium recovery with SIBX

4.2.4 Gold

Gold tailings and concentrate grades and recoveries are shown in Table 4.4. Statistically, gold grade was not affected by SIBX dosage (Figure 4.4(a)). However recovery (Figure 4.4 (b)) increased steadily from 10g/t to 40g/t collector and the tails showed the correspondence. With experimental error

taken into account, the differences in these responses become small, leading to the conclusion that gold recoveries and grades varied marginally, but again, there is a trend.

Table 4.4 Gold flotation data for each SIBX dosage tested

SIBX (g/t)	Concentrates		Tails		Gold Recovery (%)	Std Error
	Gold Grade (g/t)	Std Error	Gold Grade (g/t)	Std Error		
10	5.4	0.3	0.26	0.02	35.0	1.2
20	5.2	0.1	0.23	0.01	39.5	3.8
30	5.8	0.6	0.25	0.03	40.8	1.9
40	5.3	0.1	0.22	0.01	43.1	3.6

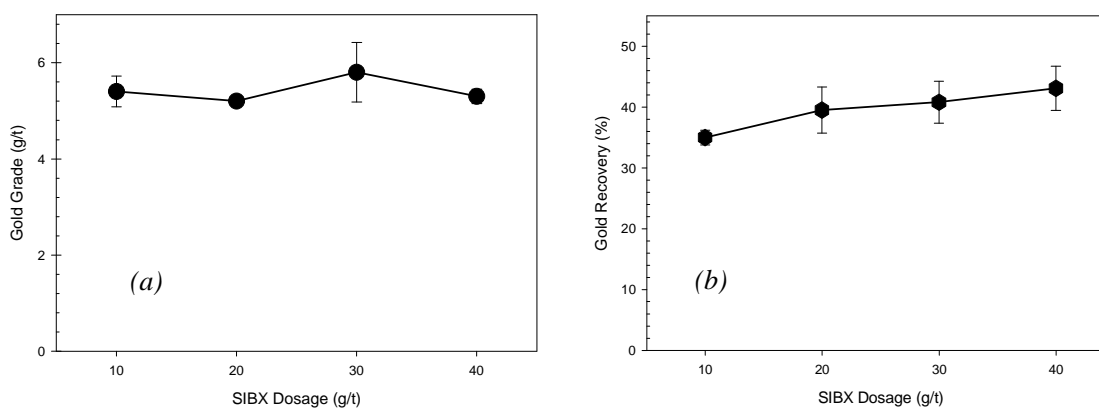


Figure 4.4 Variation of (a) gold grade and (b) gold recovery with SIBX dosage

4.2.5 Optimum SIBX Dosage

Figure 4.5 shows the recoveries and grades of all three minerals plotted on the same axis. In order to stay close to plant operating conditions, a level of 20g/t SIBX was selected.

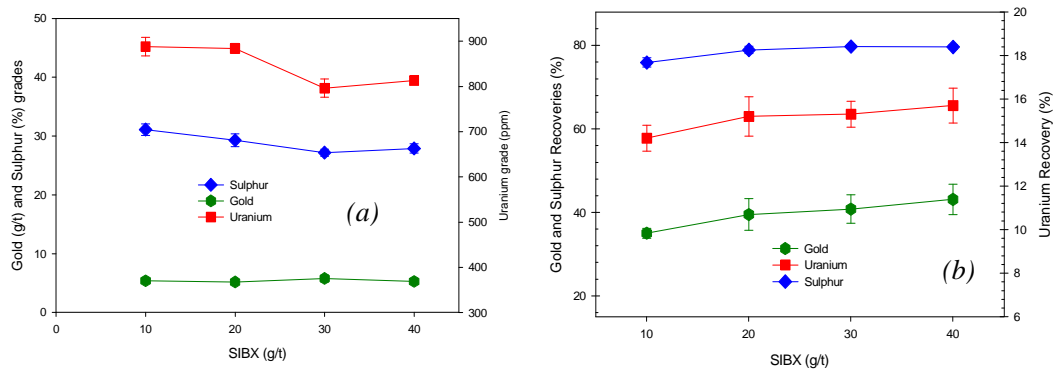


Figure 4.5 (a) sulphur, gold and uranium grades and (b) their corresponding recoveries plotted versus SIBX

4.2.6 Conclusions:

A steady increase in sulphur, uranium and gold recovery was found in SIBX doses from 10g/t to 40g/t. The gold grade seemed unaffected by dosage between the limits described.

CHAPTER 5

EFFECT OF SIBX/TTC MIXTURES ON SINGLE-POINT BATCH FLOTATION

5.1 Introduction

This section presents experiments that were conducted in order to study the flotation response of sulphur, gold and uranium to substitution of SIBX with C₁₀ or C₁₂ TTC. The percent replacement of the standard (20g/t SIBX) was expressed on a molar basis. For each combination, both SIBX and TTC were dosed from 1%wt stock solutions, the volumes of which are shown in Tables 5.1 and 5.2. These were all calculated for a 2kg-dry ore sample used per batch flotation experiment. As in previous experiments, SIBX/TTC mole ratios were tested at pH 7.2, 16g/t Dowfroth 200, 70g/t CuSO₄.5H₂O, 20g/t GEMPOLY GM4 and 6 minutes of flotation

Table 5.1 SIBX/C₁₀ TTC combinations and their corresponding reagent volumes

Test	SIBX			C ₁₀ TTC		
	%	μmol	1% wt Solution (ml)	%	μmol	1% wt Solution (ml)
1	100	233	4.0	0	0	0.0
2	92	214	3.7	8	19	0.5
3	84	195	3.4	16	37	1.0
4	75	174	3.0	25	58	1.6

Table 5.2 SIBX/C₁₂ TTC combinations and their corresponding reagent volumes

Test	SIBX			C ₁₂ TTC		
	%	μmol	1% wt Solution (ml)	%	μmol	1% wt Solution (ml)
1	100	233	4.0	0	0	0.0
2	92	214	3.7	8	19	0.6
3	84	195	3.4	16	37	1.1
4	75	174	3.0	25	58	1.7

5.2 SIBX and C₁₀ TTC

5.2.1 Results and Discussion

Flotation responses to the different SIBX/C₁₀ TTC combinations tested are shown in Tables 5.3 to 5.6 and Figures 5.1 to 5.6.

5.2.1.1 Mass Recovery

Table 5.3 shows mass recoveries for the SIBX/C₁₀ TTC mole ratios tested. There was no significant variation with mole percent TTC dosed (Figure 5.1).

Table 5.3 *Mass recovery*

C ₁₀ TTC (<i>mole percent</i>)	Mass Recovery (%)	Standard Error
0	3.21	0.06
8	3.27	0.05
16	3.27	0.07
25	3.36	0.03

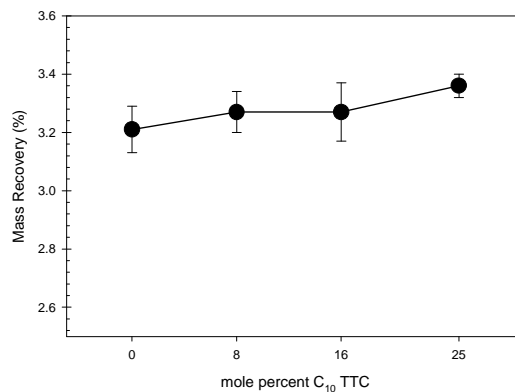


Figure 5.1 *Variation of mass recovery with mole percent of C₁₀ TTC*

5.2.1.2 Sulphur

Concentrate and tailings sulphur grades and recoveries are shown in Table 5.4 below. Even though sulphur grade decreased with each increase in C_{10} TTC mole ratio dosed, the change was small (Figure 5.2 (a)). Sulphur recovery however increased from the standard (0 mole percent TTC) to 8 mole percent TTC, after which it decreased at 16 mole percent and increased again at 25 mole percent TTC (Figure 5.2(b)).

Table 5.4 Sulphur flotation responses for SIBX/ C_{10} TTC mole ratios tested

C_{10} TTC (mole percent)	Concentrates		Tails		Sulphur Recovery (%)	Std Error
	Sulphur Grade (%)	Std Error	Sulphur Grade (%)	Std Error		
0	25.12	0.41	0.23	0.00	78.64	0.03
8	24.77	0.50	0.21	0.00	79.40	0.35
16	24.84	0.66	0.23	0.00	78.17	0.11
25	24.06	0.24	0.22	0.00	78.91	0.03

Sulphur flotation response is best illustrated in Figure 5.3. All the collector mixtures gave almost similar effects. The difference between the highest recovery (at 8 mole percent TTC) and the lowest (at 16 mole percent TTC) is only 1.23%. Regardless of this, it appears that 8 mole percent TTC gave the highest sulphur recovery and hence the best performance. This was followed by 25 mole percent TTC, the standard and lastly 16 mole percent TTC.

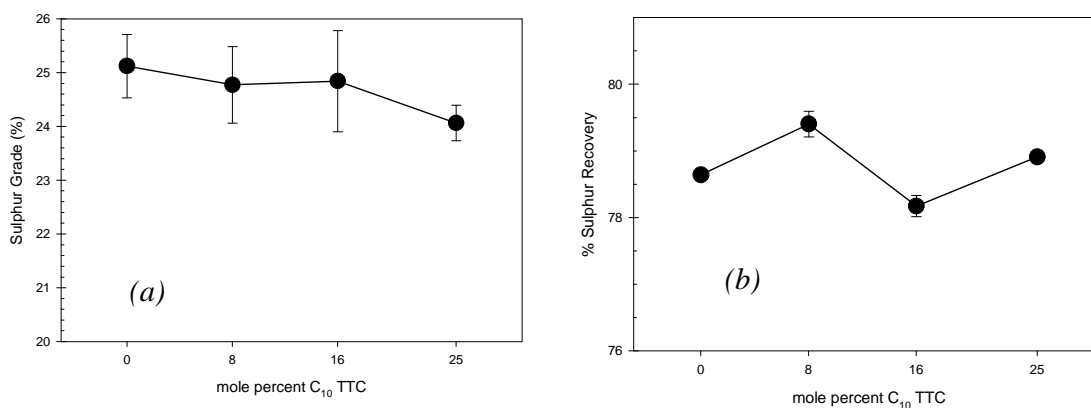


Figure 5.2 Variation of (a) sulphur grade (b) sulphur recovery with C₁₀ TTC mole ratio

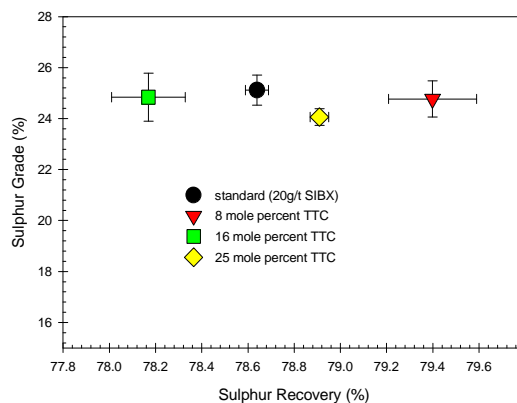


Figure 5.3 Sulphur grade-recovery combinations for the different SIBX/C₁₀ TTC mixtures tested

5.2.1.3 Uranium

Table 5.5 shows uranium flotation responses. Uranium grades showed a peak at 8 mole percent C₁₀ TTC (Figure 5.4 (a)). This was followed by a decline to almost identical responses at both 16 mole percent and 25 mole percent TTC. The recoveries however showed small increases each time more TTC was added (Figure 5.4 (b)). An assessment of Figure 5.4 (c) shows that all C₁₀ TTC /SIBX mixtures gave higher recoveries than the standard. This could have been a result of synergism between TTC and SIBX. 8 mole percent TTC gave

the highest grade of 721.5ppm while 25 mole percent TTC recorded the highest recovery of 15.6%.

Table 5.5 Uranium flotation responses for the SIBX/C₁₀ TTC combinations tested

C ₁₀ TTC (mole percent)	Concentrates		Tails		Uranium Recovery (%)	Std Error
	Uranium (ppm)	Std Error	Uranium Grade (ppm)	Std Error		
0	696.67	12.66	143.00	3.24	13.92	0.09
8	721.50	16.19	136.00	5.79	14.65	0.44
16	682.67	14.72	137.67	2.94	14.36	0.14
25	692.67	5.31	130.33	1.08	15.60	0.08

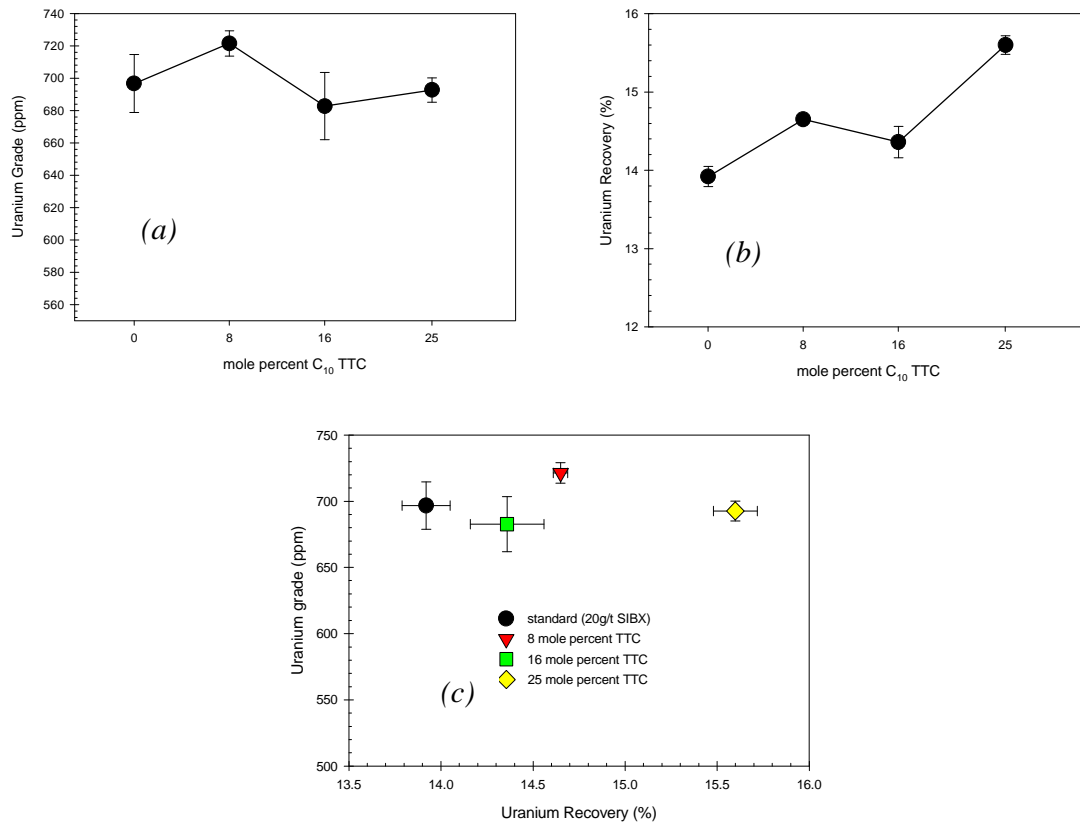


Fig. 5.4 Response of (a) uranium grade and (b) uranium recovery to different SIBX/C₁₀ TTC mixtures. (c) Corresponding uranium grade–recovery relationships

The best performance came from 25 mole percent TTC, which recovered 15.6% of uranium in the feed compared to 13.92% of the standard. This collector combination is in agreement with the findings reported by Davidtz

(2002). At this same point, the mass recovery rose from 3.21% to 3.36%. As for the grade, it fell marginally from 696.7ppm to 692.7ppm. This suggests that the increase in recovery might have been due to an improvement in the collecting power of the “collector” instead of being merely due to an increase in mass yield. Had this been the case, an increase in mass recovery is supposed to have reduced the grade by a reasonable magnitude. More uranium was indeed recovered by a combination of 25 mole percent C₁₀ TTC than with SIBX on its own.

5.2.1.4 Gold

Gold flotation responses are shown in Table 5.6. The standard gave the highest grade, which decreased as more TTC was added (Figure 5.5 (a)). Recovery on the other hand increased continuously from the standard to 25 mole percent (Figure 5.5 (b)). The difference between the flotation responses at 16 and at 25 mole percent TTC was marginal (Figure 5.6).

Table 5.6 Gold flotation data for SIBX/C₁₀ TTC mixtures tested

C ₁₀ TTC (mole percent)	Concentrates		Tails		Gold Recovery (%)	Std Error
	Gold Grade (g/t)	Std Error	Gold Grade (g/t)	Std Error		
0	5.43	0.04	0.21	0.01	38.21	1.30
8	5.40	0.22	0.26	0.01	40.51	0.13
16	5.20	0.07	0.24	0.01	42.66	0.74
25	5.00	0.14	0.23	0.01	43.45	1.34

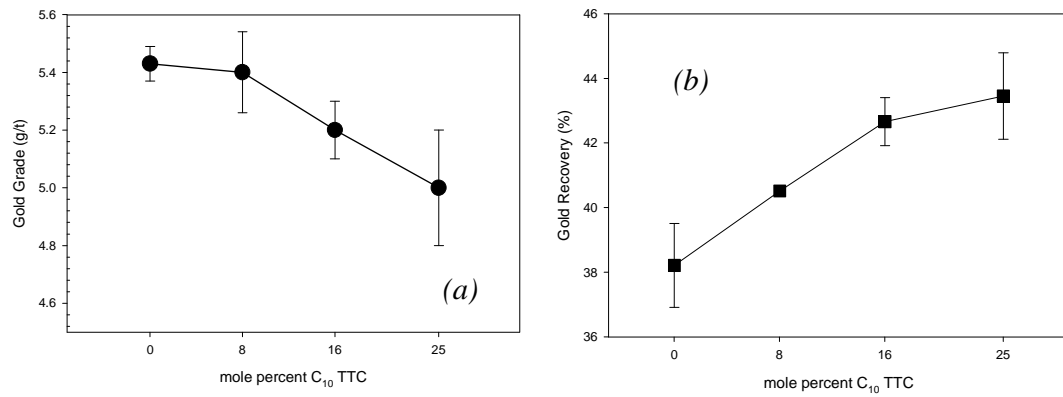


Fig. 5.5 (a) Gold grade and (b) recovery for SIBX/ C_{10} TTC mixtures

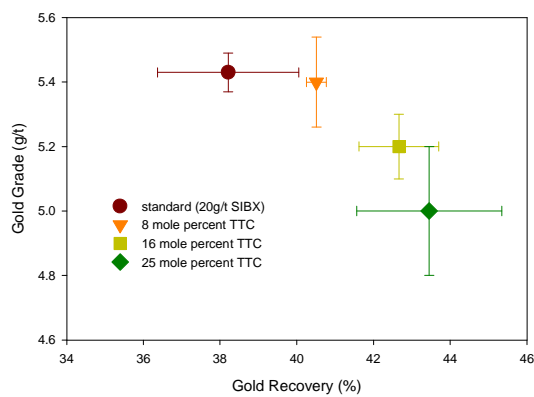


Figure 5.6 Gold grade–recovery relationships for SIBX/ C_{10} TTC combinations

5.2.1.5 Conclusions

The highest sulphur recovery was recorded at 8 mole percent TTC. Both uranium and gold recoveries increased with TTC mole percent, to give their highest readings at 25 mole percent TTC.

5.3 SIBX and C₁₂ TTC

5.3.1 Results and Discussion

The flotation results recorded for the various SIBX–C₁₂ TTC combinations tested are shown in Tables 5.7 to 5.10 and Figures 5.7 to 5.11. The same conditions of pH, frother, activator and depressant as previously used apply

5.3.1.1 Mass Recovery

The mass recoveries recorded for all the SIBX/C₁₂ TTC mixtures are shown in Table 5.7. A plot of these results in Figure 5.7 shows that mass recovery increased as the mole percent of C₁₂ TTC in the collector mixture was increased. As in the case of C₁₀ TTC/SIBX mixtures, this can be attributed to the increasing concentrations of a TTC collector that has more selectivity towards sulphides because of three sulphur atoms in its functional group that have a high affinity for metal ions on the minerals (Davidtz, 2005). Due to its long chain, the collector also has poor selectivity towards gangue (Fuerstenau, 1982b), which increases its flotation, and hence mass recovery.

Table 5.7 *Mass recovery*

C ₁₂ TTC (mole percent)	Mass Recovery (%)	Standard Error
0	3.20	0.06
8	3.31	0.03
16	3.41	0.10
25	3.46	0.12

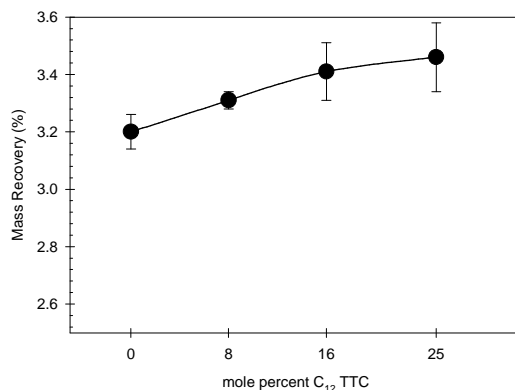


Figure 5.7 Response of mass recovery to increased C_{12} TTC mole percent

5.3.1.2 Sulphur

Sulphur flotation responses are shown in Table 5.8. Sulphur grade generally decreased with increases in C_{12} TTC mole percent used in the collector mixture (Figure 5.8 (a)). This can be accounted for using mass recoveries (Figure 5.7), which took an opposite trend. According to Fuerstenau (1982b), long chain collectors are known to exhibit poor selectivity so that increased mass recoveries result. This in turn implies that more gangue is floated and the concentrate grade falls. Sulphur recoveries were not significantly affected within the SIBX/TTC mole ratios tested (Figure 5.8 (b))

Table 5.8 Sulphur flotation responses for SIBX/ C_{12} TTC mole ratios

C_{12} TTC (mole percent)	Concentrates		Tails		Sulphur Recovery (%)	Std Error
	Sulphur Grade (%)	Std Error	Sulphur Grade (%)	Std Error		
0	25.7	0.29	0.22	0.01	79.3	0.8
8	25.3	0.44	0.22	0.00	79.7	0.3
16	24.7	0.78	0.22	0.00	79.6	0.2
25	24.3	0.73	0.23	0.01	79.2	0.5

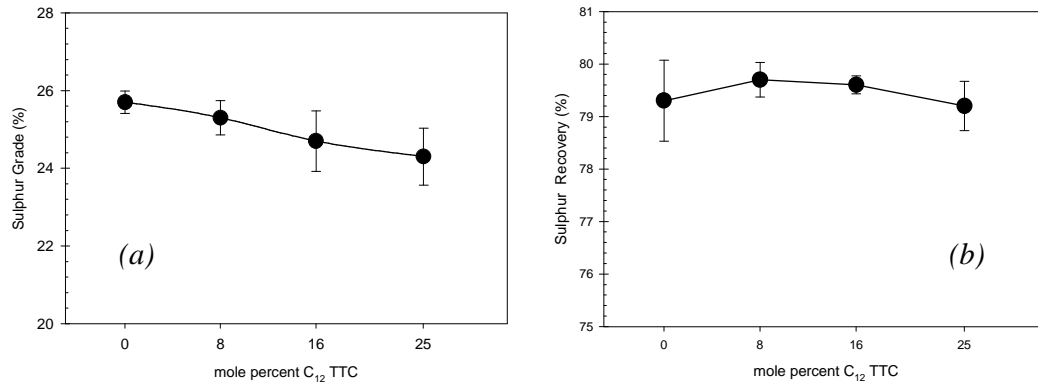


Figure 5.8 Sulphur (a) grade and (b) recovery plotted against C_{12} TTC mole percent in the collector mixture

5.3.1.3 Gold

Gold flotation responses are shown in Table 5.9. Grades fell at the onset of C_{12} TTC addition (Figure 5.9 (a)). Since this behaviour was not accompanied by a drop in recovery, it might have been caused by the poor selectivity of the long chain C_{12} collector towards gangue.

Table 5.9 Gold flotation data for SIBX/ C_{12} TTC mixtures

C_{12} TTC (mole percent)	Concentrates		Tails		Gold Recovery (%)	Std Error
	Gold Grade (g/t)	Std Error	Gold Grade (g/t)	Std Error		
0	5.1	0.1	0.24	0.02	39.0	0.68
8	5.0	0.2	0.24	0.00	41.6	1.45
16	4.9	0.2	0.22	0.01	43.5	1.25
25	4.7	0.2	0.21	0.01	45.3	1.18

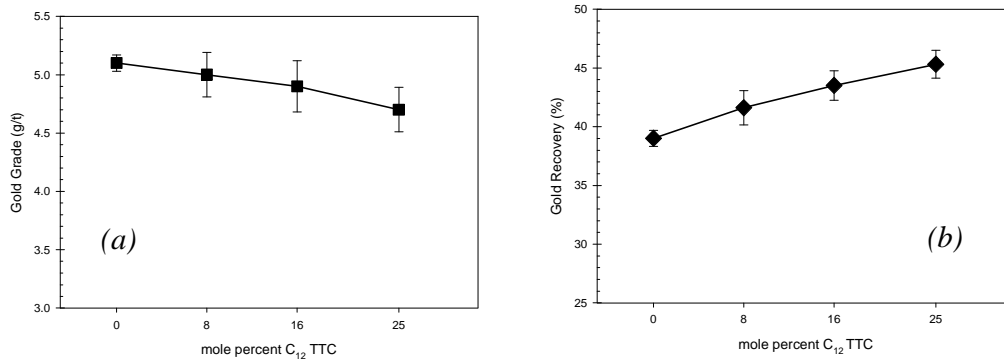


Figure 5.9 Response of gold (a) grade, and (b) gold recovery change in C₁₂ TTC mole percent in the collector

Recovery on the other hand improved as the mole fraction of TTC dosed was increased (Figure 5.9 (b)), giving the highest response at 25 mole percent TTC. From Figure 5.10, it can be seen that the standard gave the highest grade of 5.1g/t. As the mole percent TTC dosed was increased, grade decreased and recovery increased, reaching a maximum of 45.3% at 25 mole percent TTC. At this point, the grade had fallen to 4.7g/t. These progressive increases in recovery could be a result of synergism between SIBX and C₁₂ TTC. Introduction of 8 mole percent TTC increased recovery by a factor of 6% whereas 25 mole percent increased it by 16%.

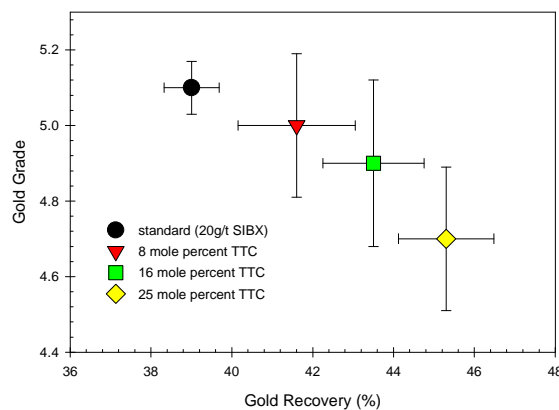


Figure 5.10 Gold recoveries and their corresponding grades for SIBX/C₁₂ mixtures

5.3.1.4 Uranium

Table 5.10 shows uranium flotation responses. Both grade and recovery did not show any significant change with TTC concentration in the collector (Figure 5.11). These results all show poor flotability of uranium bearing minerals under the prevailing conditions at least.

Table 5.10 Uranium flotation responses for different SIBX/C₁₂ TTC mixtures

C ₁₂ TTC (mole percent)	Concentrates		Tails		Uranium Recovery (%)	Std Error
	Uranium (ppm)	Std Error	Uranium Grade (ppm)	Std Error		
0	822.3	61.6	142.0	3.9	16.1	1.3
8	771.7	32.1	136.0	11.4	16.4	1.1
16	729.0	15.1	133.7	7.8	16.2	0.6
25	714.0	27.0	142.7	1.8	15.2	0.9

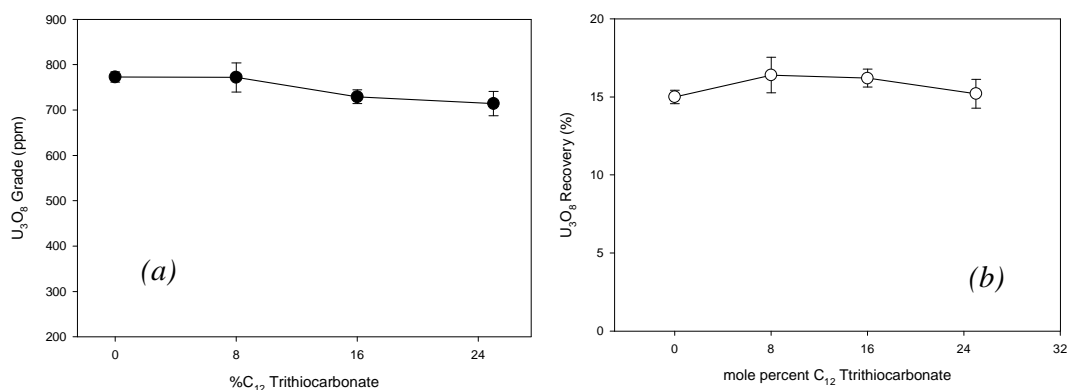


Figure 5.11 Response of uranium (a) grade and (b) recovery to change in C₁₂ TTC mole percent in the collector mixture dosed

5.3.1.5 Conclusions

Mass recoveries increased as the TTC mole percent in the collector mixture was increased. Sulphur and uranium recoveries did not change significantly while gold recoveries increased steadily to give the highest response at 25 mole percent TTC.

In all the flotation responses of SIBX/TTC mixtures presented so far, commercial TTC (20% wt TTC) was diluted to 1% wt stock solutions, which were used within 24 hours of preparation. It later emerged that TTC is stabilised by high pH and the decrease in pH that comes with dilution could have resulted in hydrolysis, reducing its activity (Davidtz, 2005). This necessitated the testing of fresh TTC to establish sulphur, gold and pyrite flotation responses. In the next section, C₁₂ TTC was chosen for the purpose.

5.4 Auriferous Pyrite Flotation with SIBX/Fresh C₁₂ TTC Mixtures

5.4.1 Introduction

In this section, single-point batch flotation experiments testing the effect of fresh C₁₂ TTC/SIBX mixtures on auriferous pyrite, gold and uranium flotation are presented. In section 5.3, C₁₂ TTC was diluted to a 1% wt solution before use. Its pH fell from 12.04 to 11.47 on dilution. Work conducted by Viljoen (1998) showed a half-life of 30 minutes for *i*C₃ TTC at pH 6. Even though the pH of the 1% wt C₁₂ TTC stock solution used in this present work did not fall this low, there is a possibility that activity could have been lost on dilution. A re-run of the experiments was therefore conducted. New feed material from No 2 Plant was used. Comparison between the XRD pattern of this ore and that used in earlier experiments (Figure 2.1) shows that they possess identical mineralogical compositions

As in the previous experiments, the percent replacement of the standard 20g/t SIBX has been expressed on a molar basis. SIBX and TTC were dosed according to Table 5.11, the values being calculated for a 2kg-dry ore sample used per batch test. All experiments were conducted at pH 7.2, 16g/t Dowfroth 200, 70g/t CuSO₄.5H₂O, 20g/t GEMPOLY GM4 and 6 minutes of flotation

Table 5.11 SIBX/C₁₂ TTC combinations and their corresponding reagent volumes

Test	SIBX			C ₁₂ TTC		
	%	μmol	1% wt Solution (ml)	%	μmol	20% wt Commercial TTC (μL)
1	100	233	4.0	0	0	0
2	92	214	3.7	8	19	27907
3	84	195	3.4	16	37	55814
4	75	174	3.0	25	58	87209

5.4.2 Results and Discussion

The flotation responses for the different SIBX/C₁₂ TTC mixtures tested are shown in Tables 5.12 to 5.16 and Figures 5.12 to 5.18.

5.4.2.1 Water Recovery

Water recoveries recorded for SIBX/C₁₂ TTC mixtures tested for their effect on auriferous pyrite flotation are shown in Table 5.12. A plot of this data against mole percent TTC shows an increase from the standard to eight mole percent (Figure 5.12). From this point forward, the change is not significant.

Table 5.12 Water recoveries

C ₁₂ TTC (mole percent)	Water Recovery (g)	Standard Error
0	229.4	3.8
8	297.7	16.9
16	301.7	4.5
25	300.0	24.0

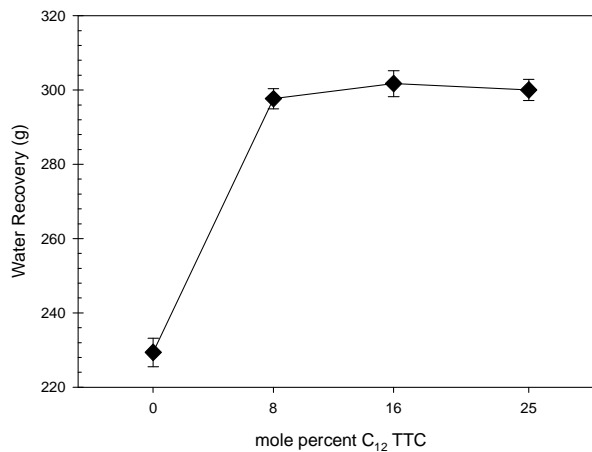


Figure 5.12 The response of water recovery to mole percent C₁₂ TTC

The water recovery for the standard is considerably lower than that for the eight mole percent C₁₂ TTC mixture by 29.8%. Since Kirjavainen (1996) has shown that water recoveries can be used as an indication of gangue flotation by entrainment, all the SIBX/TTC mixtures are likely to give higher mass recoveries and hence lower concentrate grades than the standard.

5.4.2.2 Mass Recovery

The mass recoveries recorded for SIBX/C₁₂ TTC combinations tested are shown in Table 5.13. A graph plotted from these data shows an increase from the standard to eight mole percent TTC (Figure 5.13(a)). The trend appears to be similar to that observed in Figure 5.12. In fact, mass recovery plotted against water recovery shows a strong correlation (Figure 5.13 (b)). This means that higher mass recoveries for all TTC mixtures could be attributed to gangue flotation since gangue entrainment is directly proportional to the water recovery.

Table 5.13 Mass recovery

C ₁₂ TTC (mole percent)	Mass Recovery (%)	Standard Error
0	2.78	0.11
8	3.34	0.07
16	3.38	0.07
25	3.35	0.20

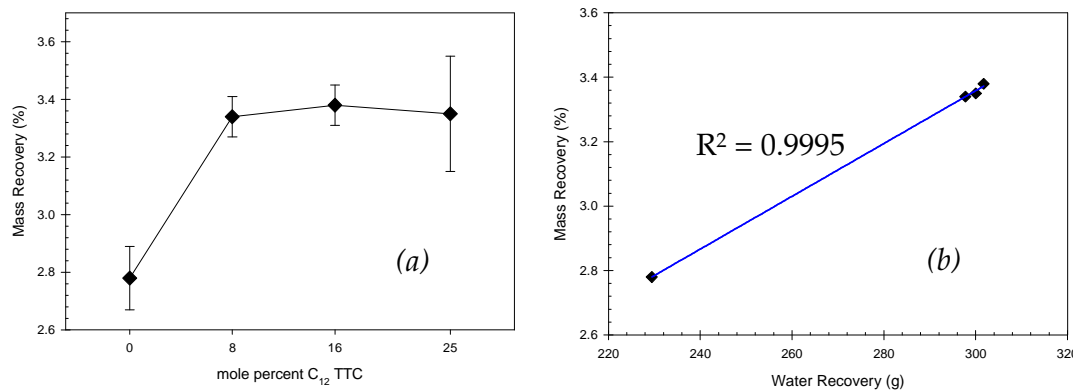


Figure 5.13 Variation of mass recovery with mole percent C₁₂ TTC of the mixture dosed and (b) linear relationship between mass and water recoveries

5.4.2.3 Sulphur

Sulphur flotation responses for SIBX/C₁₂ TTC mixtures are shown in Table 5.14. A plot of sulphur grade versus TTC mole percent shows a progressive decrease from the standard onwards (Figure 5.14 (a)). With the three SIBX/TTC mixtures exhibiting almost similar responses, the trend is opposite to that taken by mass recovery (Figure 5.13 (a)). The strong correlation shown in Figure 5.14 (b) suggests that the decrease in grade was a result of higher mass recovery, which is related to water recovery (Figure 5.13 (b)).

Table 5.14 Sulphur flotation responses for SIBX/C₁₂ TTC mixtures tested

C ₁₂ TTC (mole percent)	Concentrates		Tails		Sulphur Recovery (%)	Std Error
	Sulphur Grade (%)	Std Error	Sulphur Grade (%)	Std Error		
0	25.8	0.5	0.4	0.01	67.7	0.1
8	22.3	0.2	0.4	0.02	67.8	1.2
16	22.0	0.1	0.4	0.01	64.4	0.1
25	21.2	0.7	0.4	0.00	66.6	0.6

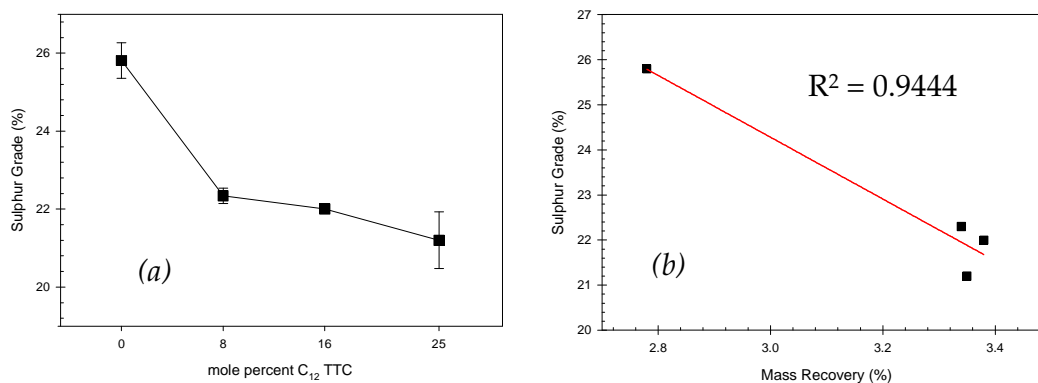


Figure 5.14 (a) Sulphur grade responses to amount of TTC dosed and (b) the linear relationship between sulphur grade and mass recovery

Sulphur recovery did not show significant change with TTC mole percent (Figure 5.15 (a)). This means that the increase in mass recovery that was accompanied by a decrease in sulphur grade was not due to more sulphide being floated. Since water recovery and mass recovery showed a correlation, the progressive decrease in sulphur grade and might have been due to increased gangue flotation. With the difference between the highest sulphur recovery and the lowest equal to 1.8%, sulphur flotation for all collector mixtures did not show any significant variation (Figure 5.15 (b)).

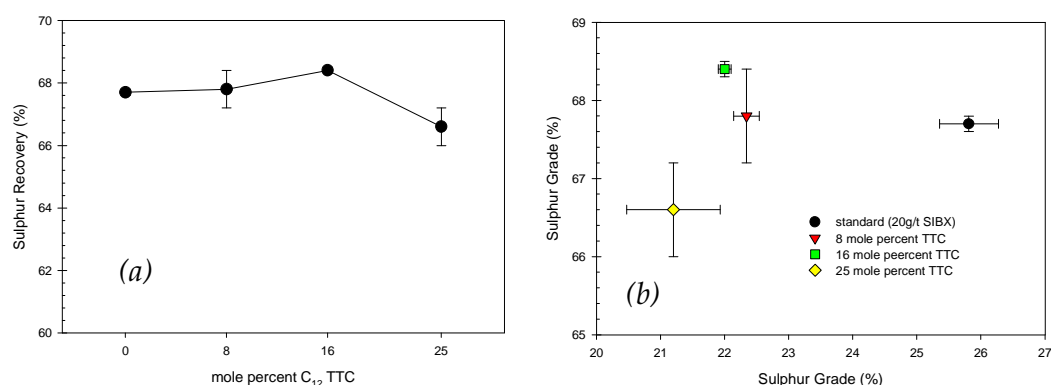


Figure 5.15 (a) Response of sulphur recovery to mole percent TTC dosed (b) Sulphur recoveries and their corresponding grades for the different collector combinations

5.4.2.4 Uranium

Uranium flotation responses are shown in Table 5.15. Plotting grade against reagent concentration shows a progressive decrease from the standard to twenty-five mole percent TTC (Figure 5.16 (a)). Based on a correlation with mass recovery (Figure 5.16 (b)), this trend might have been due to increased gangue flotation.

Table 5.15 Uranium flotation responses for different SIBX/C₁₂ TTC mixtures

C ₁₂ TTC (mole percent)	Concentrates		Tails		Uranium Recovery (%)	Std Error
	Uranium (ppm)	Std Error	Uranium Grade (ppm)	Std Error		
0	1355	35.0	90.0	0.00	30.1	0.45
8	1230	30.0	90.0	0.00	32.1	0.26
16	1200	0.0	90.0	0.00	31.8	0.82
25	1140	40.0	90.0	0.00	30.5	0.76

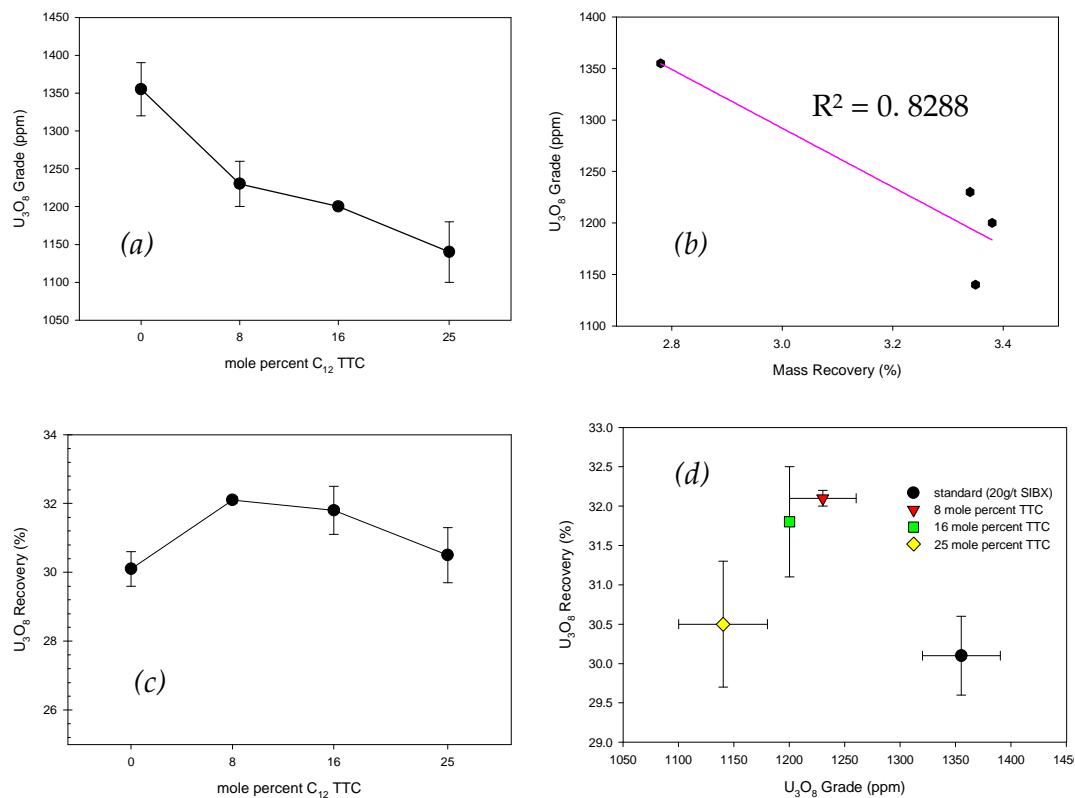


Figure 5.16 (a) Variation of uranium grade with mole percent C₁₂ TTC dosed, (b) linear correlation between uranium grade and mass recovery, (c) change in uranium recovery for varying TTC mole percent and (d) a summary of uranium flotation responses

From the standard to eight mole percent TTC, uranium recovery increased by 6% (Figure 5.16 (c)). Even though this appears small when experimental error is taken into account, a trend exists. Adjacent collector mixtures gave almost similar responses and both grade and recovery decreased as the mole percent

of TTC in the collector mixture was increased (Figure 5.16 (d)). Eight and sixteen mole percent TTC gave higher recoveries than the standard, which could be attributed to synergy between SIBX and TTC. The decrease in recovery that followed at twenty-five mole percent is smaller than the associated experimental error and is therefore non-existent.

5.4.2.5 Gold

Table 5.16 shows gold recoveries, concentrate and tails grades recorded for the SIBX/C₁₂ TTC mixtures tested. A plot of gold grade versus mole percent TTC shows a decrease from the standard to 8 mole percent (Figure 5.17 (a)). This is followed by almost similar responses from all three SIBX/TTC mixtures. The difference between the response of the standard and mixtures is most probably due to increased gangue recoveries. Between the standard and 8 mole percent TTC, gold recovery increased by a factor of 10.3% and it remained almost constant thereafter (Figure 5.17 (b)). The slight variation that followed was rendered insignificant by experimental error.

Table 5.16 Gold flotation data for SIBX/C₁₂ TTC mixtures tested

C ₁₂ TTC (mole percent)	Concentrates		Tails		Gold Recovery (%)	Std Error
	Gold Grade (g/t)	Std Error	Gold Grade (g/t)	Std Error		
0	5.90	0.10	0.2	0.01	46.4	0.03
8	5.30	0.04	0.2	0.00	51.2	1.49
16	5.36	0.03	0.2	0.00	51.7	1.61
25	5.36	0.04	0.2	0.00	44.1	1.92

As can be deduced from Figure 5.18, all the three SIBX/mixtures gave similar gold grades and recoveries. Eight mole percent TTC can be viewed as an optimum because of its lower TTC requirement.

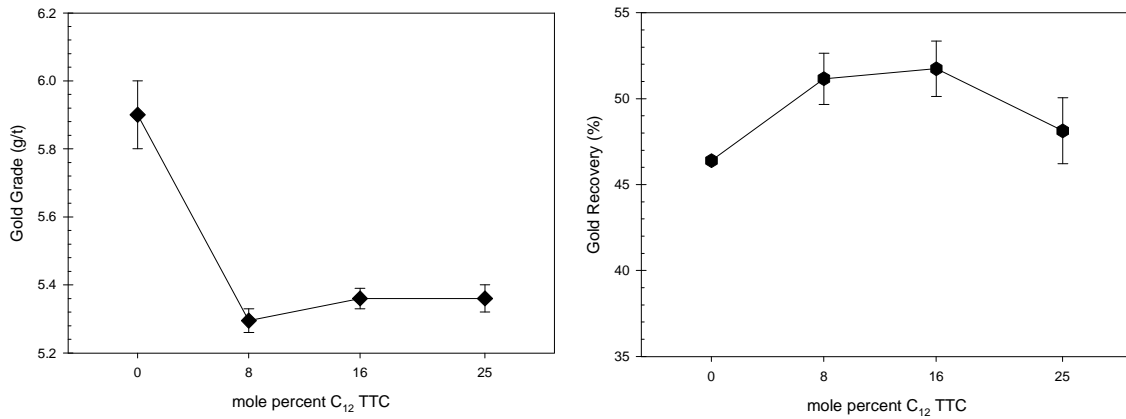


Figure 5.17 Change in (a) gold grade and (b) gold recovery with mole percent C₁₂ TTC

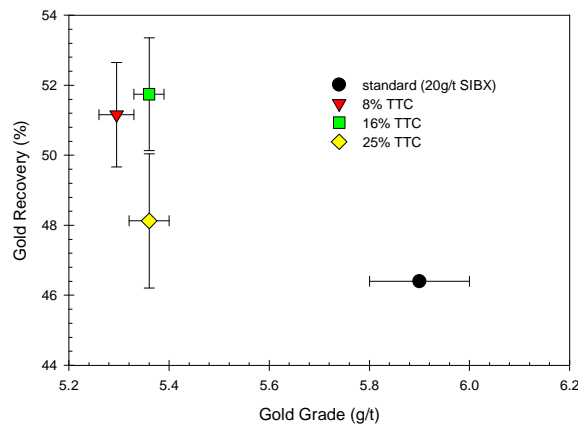


Figure 5.18 A summary of gold flotation responses for the different collector mixtures tested

5.4.2.6 Conclusions

All SIBX/C₁₂ TTC mixtures showed almost similar mass and water recoveries and these were significantly higher than the standard. Sulphur recovery did not change significantly with TTC mole fraction while uranium and gold recoveries recorded highest values at 8 mole percent TTC.

CHAPTER 6**EFFECT OF DILUTED AND AGED TTC ON SULPHUR, GOLD
AND URANIUM FLOTATION**

6.1 Introduction

The effect of using diluted and aged TTC on the flotation of sulphur, gold and uranium was investigated by means of release curve experiments in which the response of a 1% wt C₁₂ TTC solution was compared with that of fresh C₁₂ TTC (20% wt). Both reagents were used to substitute 8 mole percent of the standard since this was shown to be the optimum in the previous chapter. The dilute solution was aged for 24 hours before it was used. Its pH was initially 12.04 and after ageing, it was 11.47. The reason for this decrease in pH can be hypothesised to be decomposition illustrated by the reverse of equation 2.17, to give the mercaptide (RSNa) and carbon bi-sulphide (Davidtz, 2005). 8% C₁₂ mercaptan (C₁₂SH) was also tested for reference purposes.

6.2 Results and Discussion**6.2.1 Water and Mass recovery**

Table 6.1 below shows water final recovery (R_{max}) and flotation initial rate (k) data for the standard and the three collector mixtures tested. Included is an R^2 term, which is an indicator of the how well the data fit this particular rate equation. As seen from the data in table 6.1, the fit was good.

Table 6.1 Water initial rates and final recoveries

Experimental Condition	R ²	k (min ⁻¹)	R _{max} (g)
Standard (20g/t SIBX)	0.9957	0.11	379.0
8% C ₁₂ mercaptan	0.9958	0.12	339.6
8% diluted C ₁₂ TTC and aged for 24 hours	0.9994	0.17	436.5
8% fresh C ₁₂ TTC	0.9983	0.17	443.9

The two TTC mixtures gave similar initial rates. Their final recoveries were separated by 1.7% of the smaller value. Kirjavainen (1996) showed that water recoveries can be used for predicting gangue entrainment. They have been previously shown to correlate with mass recovery in Figure 5.13 (b).

Final mass recoveries and initial rates are shown in Table 6.2. The standard and 8 mole percent C₁₂ mercaptan gave identical initial rates that were significantly lower than for both TTC reagents. This is consistent with predictions from water recovery initial rates shown in Table 6.1.

Table 6.2 Mass final recoveries and initial rates

Experimental Condition	R ²	k (min ⁻¹)	R _{max} (%)
Standard (20g/t SIBX)	0.9859	0.33	3.1
8% C ₁₂ mercaptan	0.9928	0.33	2.7
8% diluted C ₁₂ TTC and aged for 24 hours	0.9780	0.40	3.3
8% fresh C ₁₂ TTC	0.9828	0.45	3.1

At long flotation times that are associated with equilibrium recovery, the standard and 8 mole percent fresh TTC gave similar final recoveries. This is useful because it allows a more realistic comparison between the two. Though not significant, 8 mole percent diluted and aged TTC gave a slightly higher final recovery than the fresh reagent. The mercaptan mixture gave the lowest mass final recovery, which is also consistent with water final recoveries. During the flotation experiments, it was noticed that the mercaptan mixture gave relatively smaller bubbles than the standard. Both TTC mixtures gave

the largest bubbles. The froth height increased in the order: mercaptan mixtures < the standard < the two SIBX/TTC mixtures.

6.2.2 Sulphur Recovery

Table 6.3 shows sulphur initial rates and final recoveries. For all four collector combinations, 8 mole percent fresh TTC gave the highest initial rate and final recovery. For both responses the SIBX/diluted C₁₂ TTC mixture differed by 3.5%. Compared to the standard, the 8% Mercaptan mixture gave a much lower initial rate and almost identical final recovery.

Table 6.3 *Sulphur initial rates and final recoveries*

Experimental Condition	R ²	k (min ⁻¹)	R _{max} (%)
Standard (20g/t SIBX)	0.9953	1.03	65.52
8% C ₁₂ mercaptan	0.9982	0.82	67.70
8% diluted C ₁₂ TTC and aged for 24 hours	0.9997	1.42	67.02
8% fresh C ₁₂ TTC	0.9998	1.47	69.39

Figure 6.1 shows sulphur recovery-grade curves. 8 mole percent fresh TTC showed the best performance. This was followed by substituted C₁₂ mercaptan, and diluted TTC and lastly, the standard. The curve for fresh TTC/SIBX mixture was above that of the standard throughout. This shows that the collector mixture was superior all through.

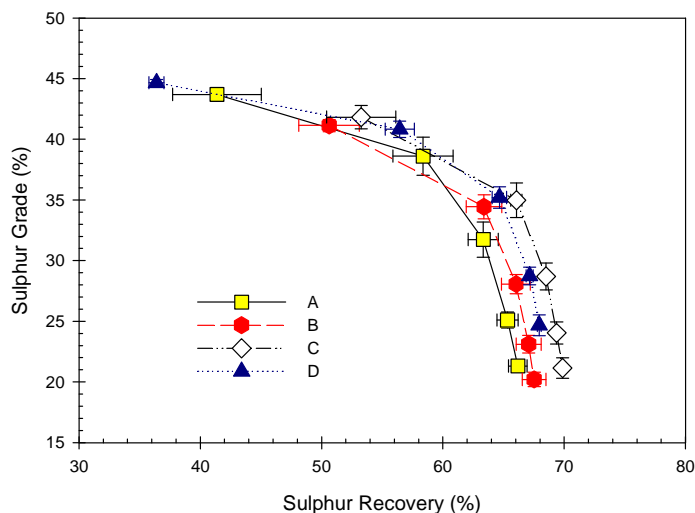


Figure 6.1 Sulphur recovery-grade curves for [A] the standard, [B] 8 mole percent C_{12} TTC, diluted and aged for 24 hours, [C] 8 mole percent fresh C_{12} TTC and [D] 8 mole percent C_{12} mercaptan

6.2.3 Uranium Recovery

Uranium initial rates and final recoveries are shown in Table 6.4. The mercaptan mixture gave the lowest responses. Both TTCs gave higher initial rates and final recoveries than the standard. The initial rate for the diluted and aged TTC/SIBX mixture was lower than that for the fresh TTC/SIBX combination by 10% while their final recoveries differed by only 0.5%. Based on initial rates, it appears that the fresh TTC/SIBX mixture gave better performance.

Table 6.4 Uranium final recoveries and initial rates for the standard and the three collector mixtures tested.

Experimental Condition	R^2	k (min^{-1})	R_{max} (ppm)
Standard (20g/t SIBX)	0.9953	0.70	27.47
8% C_{12} mercaptan	0.9962	0.62	24.30
8% diluted C_{12} TTC and aged for 24 hours	0.9952	0.83	28.4
8% fresh C_{12} TTC	0.9966	0.92	28.3

Figure 6.2 shows uranium recovery-grade curves. The standard showed the highest grade throughout. Its recoveries were however lower than for both SIBX/TTC mixtures, which showed almost identical recoveries and grades all through. 8 mole percent mercaptan gave the poorest uranium flotation response.

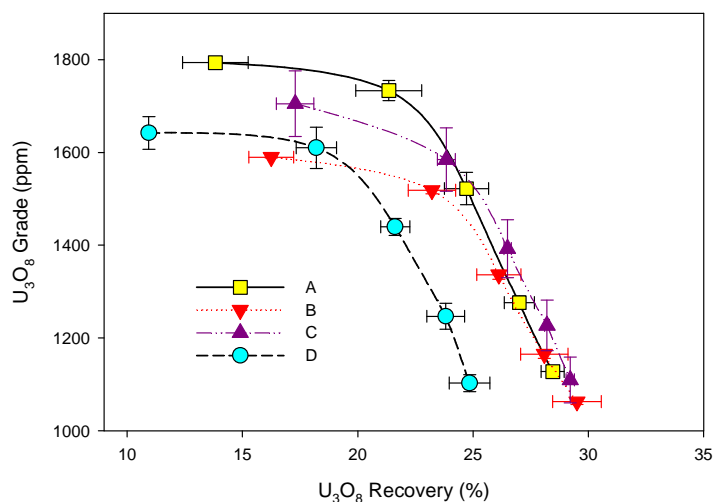


Figure 6.2 Uranium recovery-grade curves for [A] the standard, [B] 8 mole percent C_{12} TTC, diluted and aged for 24 hours, [C] 8 mole percent fresh C_{12} TTC and [D] 8 mole percent C_{12} Mercaptan

6.2.5 Gold

Gold flotation initial rates and final recoveries are shown in Table 6.5. Initial rates for both SIBX/TTC mixtures differed by 4% and their final recoveries by 5%. Comparison between the recovery-grade curves of the two shows that the differences are insignificant (Figure 6.3). Comparing the standard and the two TTC mixtures shows that the standard progressively gave higher concentrate grades and much lower recoveries. Its initial rate was 0.63 min^{-1} while the fresh TTC/SIBX mixture recorded 0.74 min^{-1} , which indicates an increase by a factor of 17%.

Table 6.5 Gold flotation responses for 8 mole percent substitution of the standard

Experimental Condition	R ²	k (min ⁻¹)	R _{max} (g/t)
Standard (20g/t SIBX)	0.9967	0.63	42.4
8% C ₁₂ Mercaptan	0.9961	0.59	39.4
8% diluted C ₁₂ TTC and aged for 24 hours	0.9942	0.71	47.4
8% fresh C ₁₂ TTC	0.9956	0.74	45.0

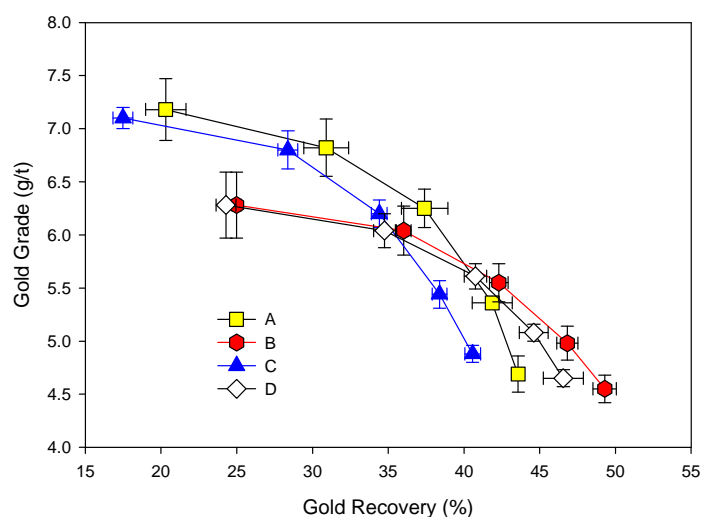


Figure 6.3 Gold recovery-grade curves for [A] the standard, [B] 8 mole percent C₁₂ TTC, diluted and aged for 24 hours, [C] 8 mole percent C₁₂ Mercaptan and [D] 8 mole percent fresh C₁₂ TTC

6.2.6 Conclusions

Based on the measurement of flotation initial rates and final recoveries, together with comparison between plotted recovery-grade curves, it is clear that by combining SIBX and fresh C₁₂ TTC, a better flotation activity is obtained than with SIBX alone. This is in agreement with earlier plant trials by Davidtz (2002). It has generally been concluded that the promoting effect is a synergistic one. Previous conclusions have been that the surface density of collector packing of dixanthogen is promoted by the long chain TTC (Breytenbach, 2003; Davidtz, 1999). Furthermore, the addition of TTC at the dosage levels studied does not reduce the effectiveness of SIBX. The 1% wt solution of TTC marginally lost activity when compared to the fresh TTC solution. This is probably due to the hydrolysis of TTC. The product of

decomposition would then be a mercaptan. The mercaptan reference sample showed a distinct reduction in grade recovery and kinetics. The conclusion therefore is that when dosed as such, mercaptan is detrimental to SIBX activity.

du Plessis (2003) suggested that the TTC dimmer and adsorbed mercaptan, which results from a surface decomposition of an adsorbed TTC are responsible for a strong hydrophobic state. This data also suggests the mercaptan most likely has to be generated via the adsorbed TTC. Thereafter decomposition of the adsorbed TTC leads to the presence of a metal mercaptide salt.

Gibbs Excess Free Energy calculations show that the calculated hydrophobicity of a TTC adsorbed is the same as that of a mercaptan adsorbed (Davidtz, 2005), so that either the TTC or mercaptan when adsorbed on their own would generate equivalent states of hydrophobicity. However, this is a mixed xanthate TTC system with only a small fraction of the collector being TTC and mercaptan. Consequently one has to conclude that the presence of these are enhancing or promoting the effectiveness of the xanthate.

Although there was not much difference between the fresh and aged TTC the decrease in activity could be more severe if the concentrations were lower. Fresh operations are between 2 and 5 mole percent TTC in SIBX. It is therefore possible that these results are still within this region. However, pH is the dominant factor and a stability time phase diagram with pH included is needed to predict the aged TTC behaviour. Certainly the mercaptan on its own is not effective in synergism, but in fact has a depressing effect.

CHAPTER 7**EFFECT OF CONDITIONING pH ON SULPHUR, GOLD AND URANIUM FLOTATION**

7.1 Introduction

The feed treated at No 2 Gold Plant consists of a mixture of tailings from the cyanidation of run-of-mine ore and reclaimed dump material. Exposure of this feed to air and water, coupled with the use of air during leaching all subject the sulphide minerals to surface oxidation. Oxidized surfaces inhibit their reaction with collector molecules. For optimal recovery, the negative effect of surface oxidation has to be overcome.

Examination of thermodynamic data for metal-water systems shows certain E_h -pH conditions in which metals are more stable in their cationic form (Jackson, 1986). Subjecting oxides to these conditions promotes their dissolution in order to achieve the thermodynamically supported species. In this view, treatment of the oxidised flotation feed at low pH in the presence of dissolved oxygen should favour the removal of iron oxides formed on pyrite, thereby exposing underlying fresh sulphide. This is likely to improve interaction with SIBX, and hence flotation response.

Based on this background, the effect of a low pH treatment prior to flotation was investigated on No. 2 Gold Plant feed. After the initial conditioning for 1 minute, 1.25kg/t of sulphuric acid was added and the pH decreased from 7.8 to 1.9. At the same time, the pulp potential increased from 0.3V to 0.6V^Ω. The pulp was conditioned for 10 minutes, the pH rose to 3.7 and the potential decreased to 0.5V. A caustic solution was added to achieve the standard

^Ω All pulp potentials are reported versus the standard hydrogen electrode

flotation pH of 7.2. At this point, the pulp potential was 0.3V. Flotation was then carried out using the reagent suite of the standard.

7.2 Results and Discussion

7.2.1 Sulphur

Table 7.1 shows sulphur flotation initial rates and corresponding final recoveries for the two conditioning pHs. The initial rate of 0.91min^{-1} at pH 1.9^φ indicates significantly higher sulphur flotation kinetics compared to the 0.66min^{-1} recorded at pH 7.2. This shows that conditioning at this low pH activated sulphide surfaces, which improved interaction with flotation reagents.

Table 7.1 *Sulphur final recoveries and initial rates*

Conditioning pH	k (min ⁻¹)	R _{max} (%)	R ²
1.9	0.91	72.5	0.9995
7.2	0.66	77.4	0.9987

Table 7.2 shows pulp potential and pH values recorded during conditioning. Superimposing these data on the Pourbaix diagram of the Fe-S-H₂O system can give an indication of the thermodynamically stable species, and hence reactions that took place during conditioning.

Table 7.2 *Pulp pH and potentials recorded during conditioning*

	Natural E _h -pH	After acid dosage	After 10 min conditioning	After caustic dosage	During Flotation
pH	7.8	1.9	3.7	7.2	7.2
Potential (V)	0.3	0.6	0.5	0.3	0.04

^φ This will be referred to as “pH 1.9 conditioning” throughout this discussion even though pH rose throughout conditioning until it stabilised at 3.7

Figure 7.1 shows that the natural pulp pH and potential recorded for the flotation feed (point A) coincide with the domain in which ferric oxide⁸ is thermodynamically stable. Immediately after sulphuric acid was added, the two responses shifted to point B, which lies in the domain of ferrous ion stability.

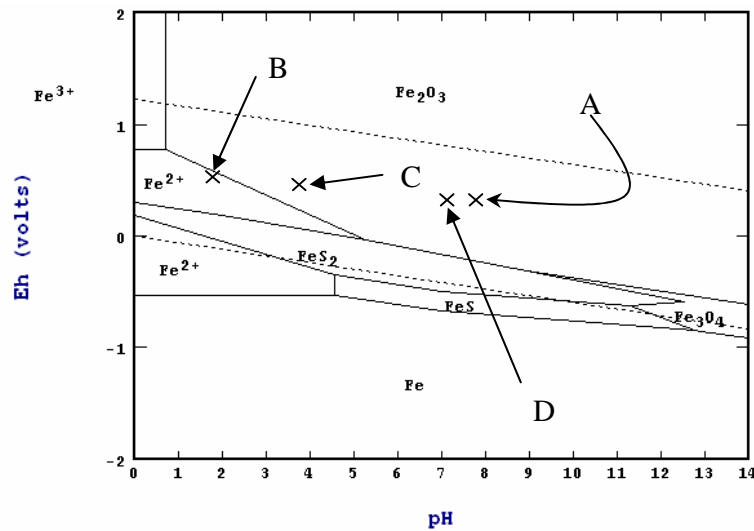


Figure 7.1 A Pourbaix diagram for the Fe-S-H₂O system at 25°C, 10⁻⁴M [Fe], 10⁻⁴M [S] showing E_h-pH conditions prevailing during conditioning [A] natural pulp E_h-pH, [B] after addition of 1.25kg/t sulphuric acid, [C] after 10 minutes of conditioning, [D] after dosage of a caustic solution to attain standard flotation pH

Any superficial iron oxide on pyrite particles should leach to form ferrous ions. This exposes the underlying sulphide, so that it can interact freely with flotation reagents. This probably accounts for the higher flotation kinetics.

Figure 7.2 shows sulphur recovery-grade curves plotted for the two conditioning pHs. Even though pH 1.9 seemed superior at the beginning of the experiment, the difference was small. By the end of both flotation experiments, pH 7.5 had recorded a higher final recovery (Table 7.1). Figure 7.1 shows that after addition of caustic, the new pulp pH and potential fell in the domain of ferric oxide (point C). If solubility limits were exceeded, then ferric hydroxide should have precipitated. Because precipitation is not

⁸ Under normal conditions, the hydrated form of this oxide is formed

selective between sulphide and gangue, the hydroxide could have formed on pyrite, which is likely to depress it. For the iron ions that remained in solution, they can form a number of hydroxyl complexes with caustic. These are likely to affect pyrite flotation with xanthate.

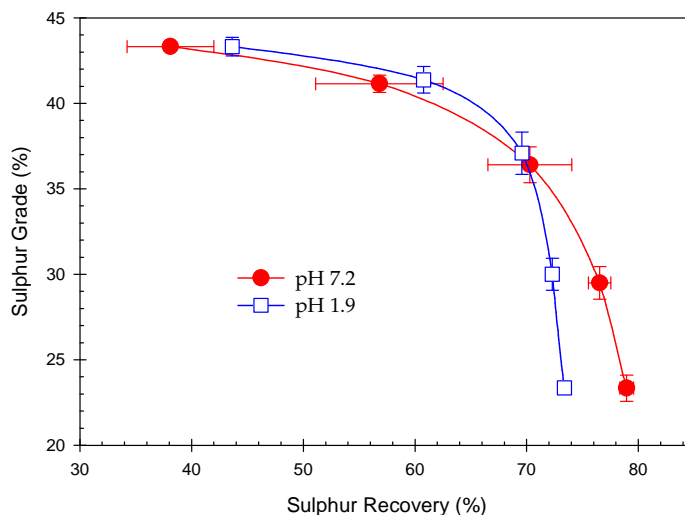


Figure 7.2 Sulphur recovery-grade curves

Jiang and co-workers (1998) observed significant depression in the neutral pH range after $2 \times 10^{-3}\text{M}$ Fe^{3+} ions were added to ore pyrite at pH 3, which was followed by adjustment of pulp pH to flotation pH and dosage of $3.3 \times 10^{-4}\text{M}$ ethyl xanthate and 50mg l^{-1} MIBC. A similar exercise using ferrous ions showed more significant depression in the same pH range. Examination of speciation diagrams in Figures 7.3 and 7.4 plotted using STABCAL software for the concentration of ferrous and ferric ions tested by Jiang et al. (1998) predicts Fe^{2+} , FeOH^+ and $\text{Fe}(\text{OH})_3$ to be the stable species in the neutral pH range.

By using iron-xanthate-water system distribution diagrams, the authors showed that in neutral to weakly alkaline conditions (pH 5-9.5), some hydroxyl xanthate species are formed, namely $(\text{Fe}(\text{OH})\text{X})_2$ and $\text{Fe}(\text{OH})\text{X}$. Since FTIR measurements by Wang (1995) suggested that ferric xanthate is

adsorbed on pyrite, Jiang and co-workers (1998) attributed the lower recoveries to the lower hydrophobicity exhibited by the two complexes.

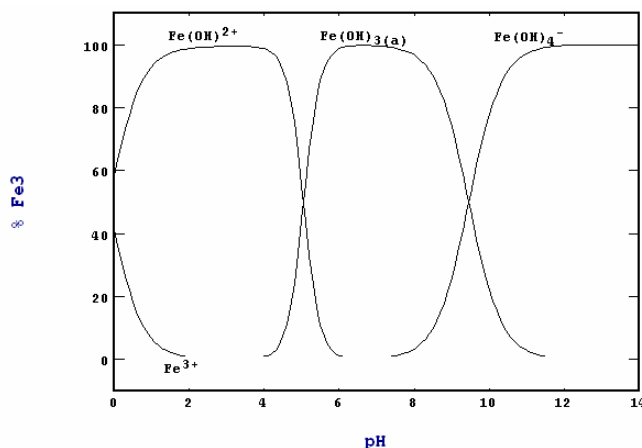


Figure 7.3 Speciation diagram for $2 \times 10^{-3}M$ Fe(III) as a function of pH at 25°C. STABCAL Software, NBS Database

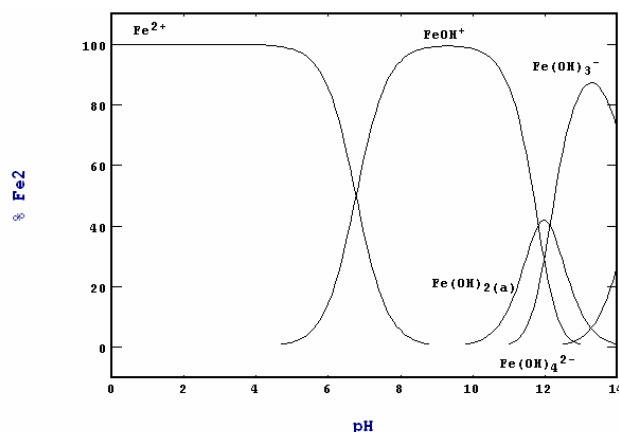


Figure 7.4 Speciation diagram for $2 \times 10^{-3}M$ Fe(II) as a function of pH at 25°C. STABCAL Software, NBS Database

The depression of pyrite flotation following conditioning at pH 1.9 is probably due to the two hydroxyl-xanthate species. The above speciation diagrams suggest that conditioning at pH 1.9 promotes the formation of $Fe(OH)^{2+}$, Fe^{2+} and $Fe(OH)^+$ in the pulp. When pH is raised to 7.2 using a caustic solution, only $Fe(OH)_3$ is the stable iron (III) species formed. Iron (II)

forms FeOH^+ and Fe^{2+} only. Addition of xanthate results in the formation of $(\text{Fe}(\text{OH})\text{X})_2$ and $\text{Fe}(\text{OH})^+\text{X}$ and ferrous xanthate as well. Due to its high solubility, ferrous xanthate is unlikely to precipitate. For enhancement of pyrite flotation, all these complexes have to either form on the surface or adsorb after formation in solution (Davidtz, 2005). Failure to interact with the surface will give poor flotation response since there will be less xanthate available to impart hydrophobicity to pyrite. Since it is not always possible that all the ferrous hydroxyl xanthates formed in solution will adsorb onto pyrite, the presence of ferrous ions might have contributed to the lower sulphide final recoveries in Figure 7.2.

Jiang et al. (1998) have showed that at a modest degree of oxidation; pyrite surfaces behave like iron oxide with a PZC at pH 7. This is due to the presence of ferric hydroxide formed during oxidation. The surface will acquire electrokinetic features of the iron hydroxide. The authors showed that in the presence of $2 \times 10^{-3}\text{M}$ ferric ions and $6.6 \times 10^{-4}\text{M}$ ethyl xanthate, the zeta potential of pyrite exhibited less positive charge below pH 7.5 compared with that in the presence of ferric xanthate alone. At $\text{pH} > 7.5$, there was no noticeable difference between the two. This implies that in the presence of ferric ions, adsorption of xanthate onto pyrite is favoured in acidic conditions. In the present work, flotation tests were run at pH 7.2. The speciation diagram in Figure 7.9 has shown that under these conditions, all iron (III) will form ferric hydroxide as a stable species so that it did not affect the flotation response in the manner described above.

The work by Jiang et al. (1998) also showed that the PZC of pyrite in the presence of $2 \times 10^{-3}\text{M}$ ferrous ions is pH 9. Addition of $6.6 \times 10^{-4}\text{M}$ ethyl xanthate reduced it to pH 6. The authors observed that at $\text{pH} < 6$, the zeta potential curve was identical to that in the presence of xanthate only and at $\text{pH} > 6$, it was identical to that in the presence of only ferrous ions. From these results, they concluded that ferrous ions do not undergo significant reaction with

xanthate at pH < 6 and the flotation of pyrite in this region is mainly due to the adsorption of xanthate on the surface. At pH > 6, the adsorption of xanthate was reduced, which was in agreement with their flotation results. Similarly, the presence of ferrous ions from low pH treatment in this present work could have affected flotation recoveries by reducing xanthate adsorption. This could have been due to the formation of ferrous hydroxyl xanthate complexes in solution, rather than on the surface.

7.2.2 Uranium

The R and k values for uranium recovery are reported in Table 7.3 and the grade recovery data is presented in Figure 7.5.

Table 7.3 *Uranium final recoveries and initial rates*

Conditioning pH	k (min ⁻¹)	R _{max} (%)	R ²
1.9	0.53	21.9	0.9954
7.2	0.59	23.4	0.9947

Conditioning the plant feed at pH 7.2 prior to flotation resulted in a higher initial rate of 0.59 min⁻¹ compared to 0.53 min⁻¹ at pH 1.9 (Table 7.3). With a factor of almost 11%, the difference between the two is significant. The final recovery for pH 7.2 was also higher than that for pH 1.9 by a factor of 6.8%. Recovery-grade curves also show that pH 7.5 gave a much better flotation response throughout since its curve was always above that for pH 1.9 (Figure 7.5)

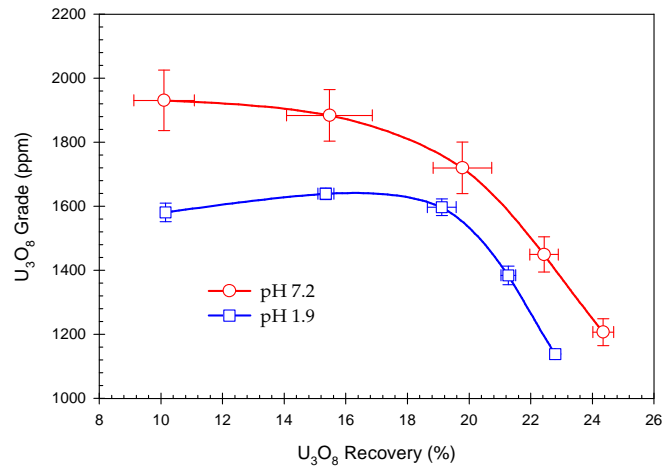


Figure 7.5 Uranium grade-recovery curves recorded following conditioning at two pH values prior to flotation.

Ores mined from the Vaal Reef contain uranium predominantly in the form of uraninite (Ford, 1993). Brannerite is also present but in much lower quantities (Brown, 2002). These are oxides, yet are floated with a sulphide collector. The effective recovery by sulphide flotation agents is probably due to the association with other minerals that respond to xanthates, or due to some activating species present on the uraninite surface.

Back-scattered Electron Imaging (BEI) and Energy Dispersive Spectroscopy (EDS) have been used to identify the minerals in concentrates recovered with SIBX. An EDS spectrum (Figure 7.7 (a)) of phase A (Figure 7.6) shows that it contains $78.95 \pm 0.83\%$ wt U as uraninite. Phase B (Figure 7.6) on the other hand contains vast amounts of sulphur and iron (Figure 7.7 (b)) as pyrite. The darkest particles (C for instance) consist of aluminosilicates, free quartz and some pyrophyllite (Figure 7.7 (c)).

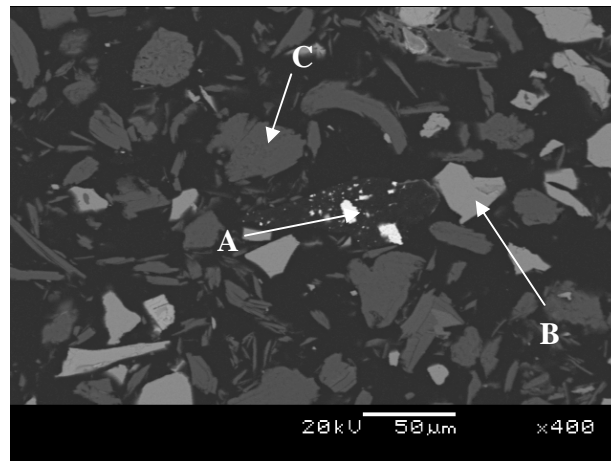


Figure 7.6 A back-scattered electron image taken from a concentrate recovered with 20g/t SIBX^{sr}

^{sr} More back-scattered images are shown in Appendix A

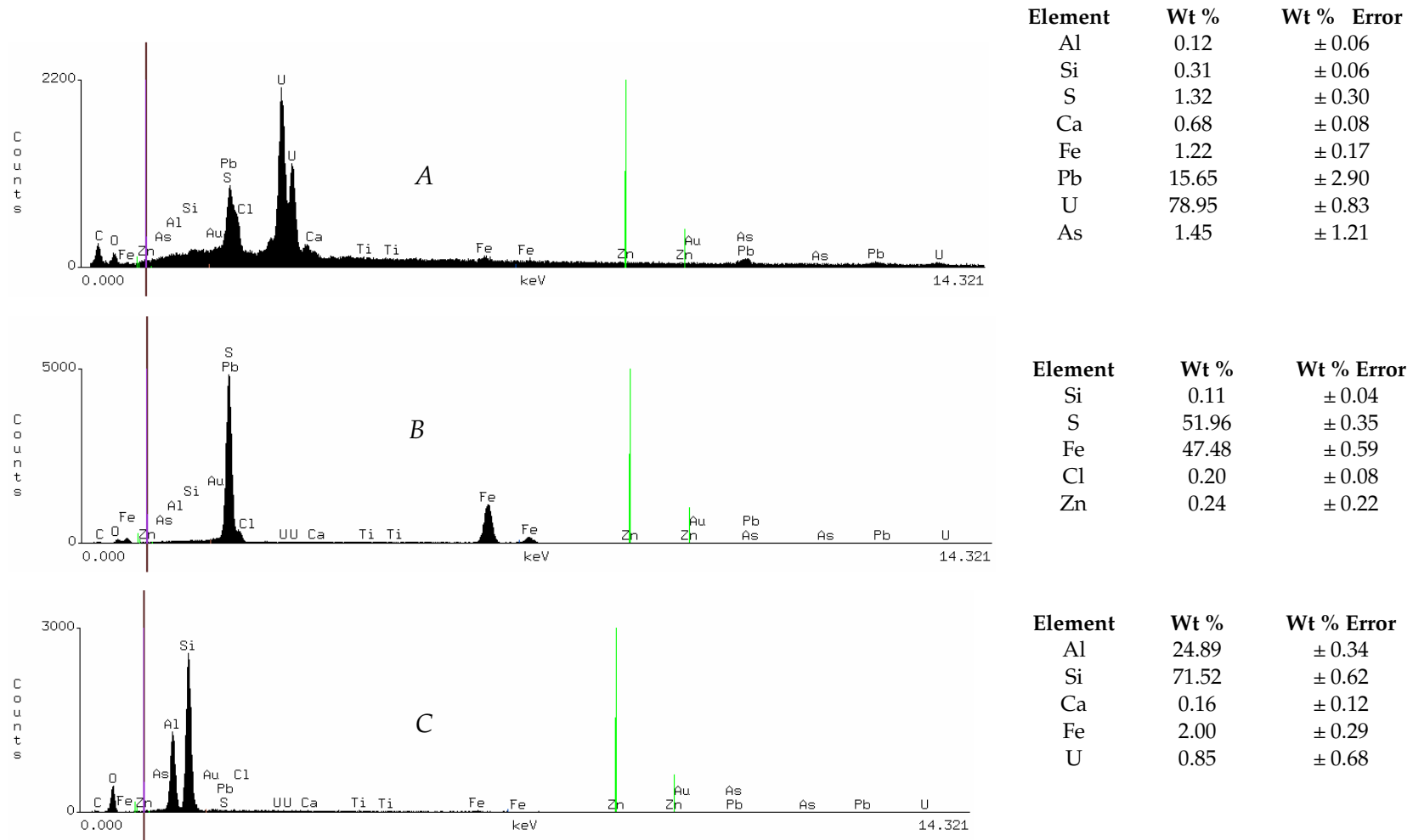


Figure 7.7 (a), (b) and (c) EDS spectra showing the elemental compositions of the corresponding phases shown in the back scattered electron image in Figure 4.32.

The presence of lead ($15.65 \pm 2.90\%$ wt) and sulphur (1.32 ± 0.30 wt %) in the EDS spectra (Figure 7.7 (a)) of phase A (Figure 7.6) suggests the presence of galena. This sulphide responds very well to flotation with xanthates (O'Dea et al., 2001; Woods, 1971; Tolun and Kitchener, 1963). Presumably the presence of lead acts as a good activator for thiol collectors.

Because of a mineralogical association between uraninite and galena, one may expect a relationship between lead and uranium recovery. Plots of lead and uranium recoveries versus mole percent of TTC dosed are shown in Figures 7.8 and 7.9. There does appear to be a relationship.

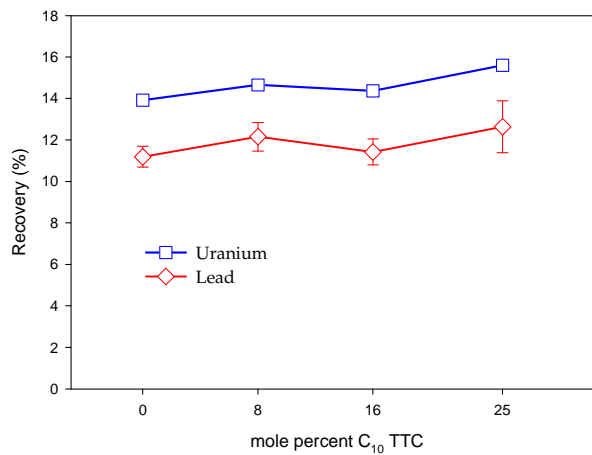


Figure 7.8 Lead and uranium recoveries for C₁₀ TTC/SIBX mixtures

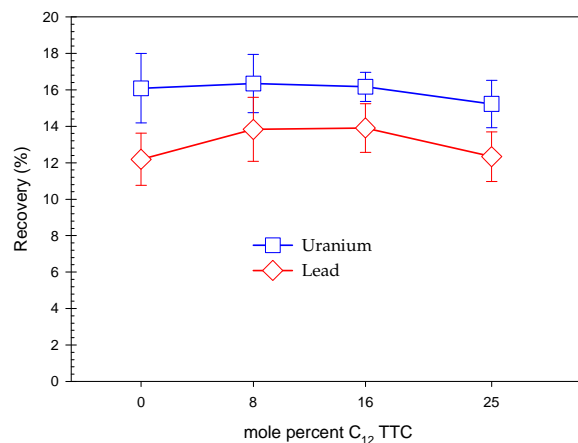


Figure 7.9 Lead and uranium recoveries for C₁₂ TTC/SIBX mixtures

Particle A in Figure 7.6 shows that it is part of a dispersion of fine particles that is surrounded by a dark matrix. If the borders of the latter are traced, they compound to a particle. This is more visible in another BEI shown in Figure 7.10 below. During micro-probe analysis of a similar particle (Figure 7.11), while resin used to mount the sample was charred by the electron beam of the instrument, this matrix did not respond. This shows that the matrix differs from resin.

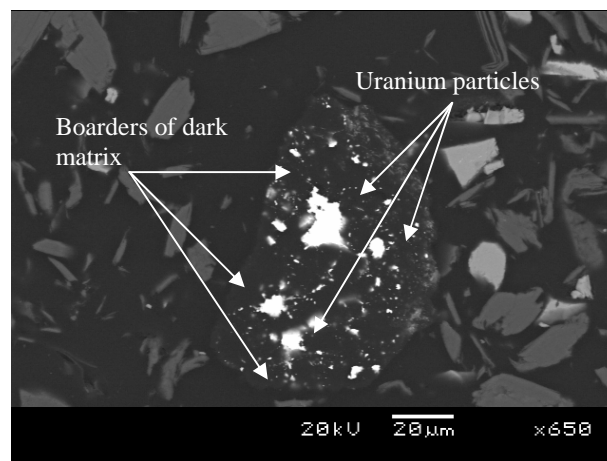


Figure 7.10 A dispersion of fine uranium-containing particles embedded in a larger particle found in a concentrate floated with 20g/t SIBX

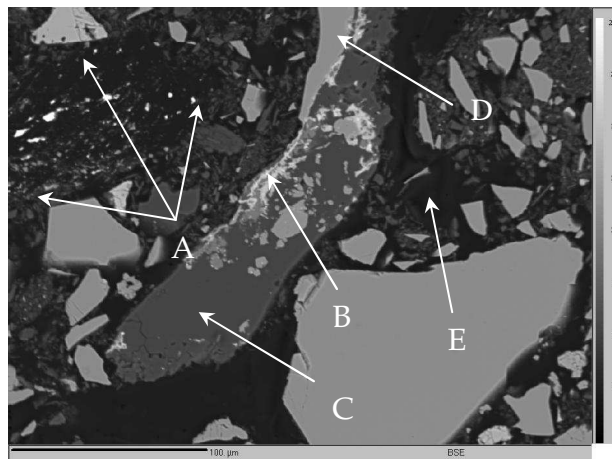


Figure 7.11 A BEI taken from the micro-probe analysis of concentrates floated with 20g/t SIBX, (A) boundaries of a dark matrix carrying a fine dispersion of uranium particles, (B) uranium particles, (C) siliceous phase, (D) pyrite and (E) charring of resin after exposure to electron beam

EDS spectra (Figure 7.13) generated from the micro-probe analysis of phase A (Figure 7.11) showed a carbon peak. Comparison between this peak⁹⁸ and that on spectra from an iron-sulphide (Figure 7.12) eliminates the effect of carbon introduced to increase the conductivity of the sample. Since the peak is larger, the dark matrix is carbonaceous in nature and it could be the karogen (or thucolite) that constitutes carbon seams found in the Witwatersrand Basin (Rob and Meyer, 1995; Anhaeusser et al., 1987; Simpson and Bowels, 1977). Since the carbonaceous matter is organic, it possesses natural hydrophobicity.

Another observation from the back-scattered electron image in Figure 7.11 is that uranium and pyrite co-exist in a single particle. This implies that uranium could at least partially be recovered with pyrite. The flotation behaviour following pre-flotation conditioning at pH 1.9 can be accounted for through the mineralogical relationships with pyrite, karogen and galena.

⁹⁸ Note that the peak labelled [O] in Figure 4.39 is actually a carbon peak

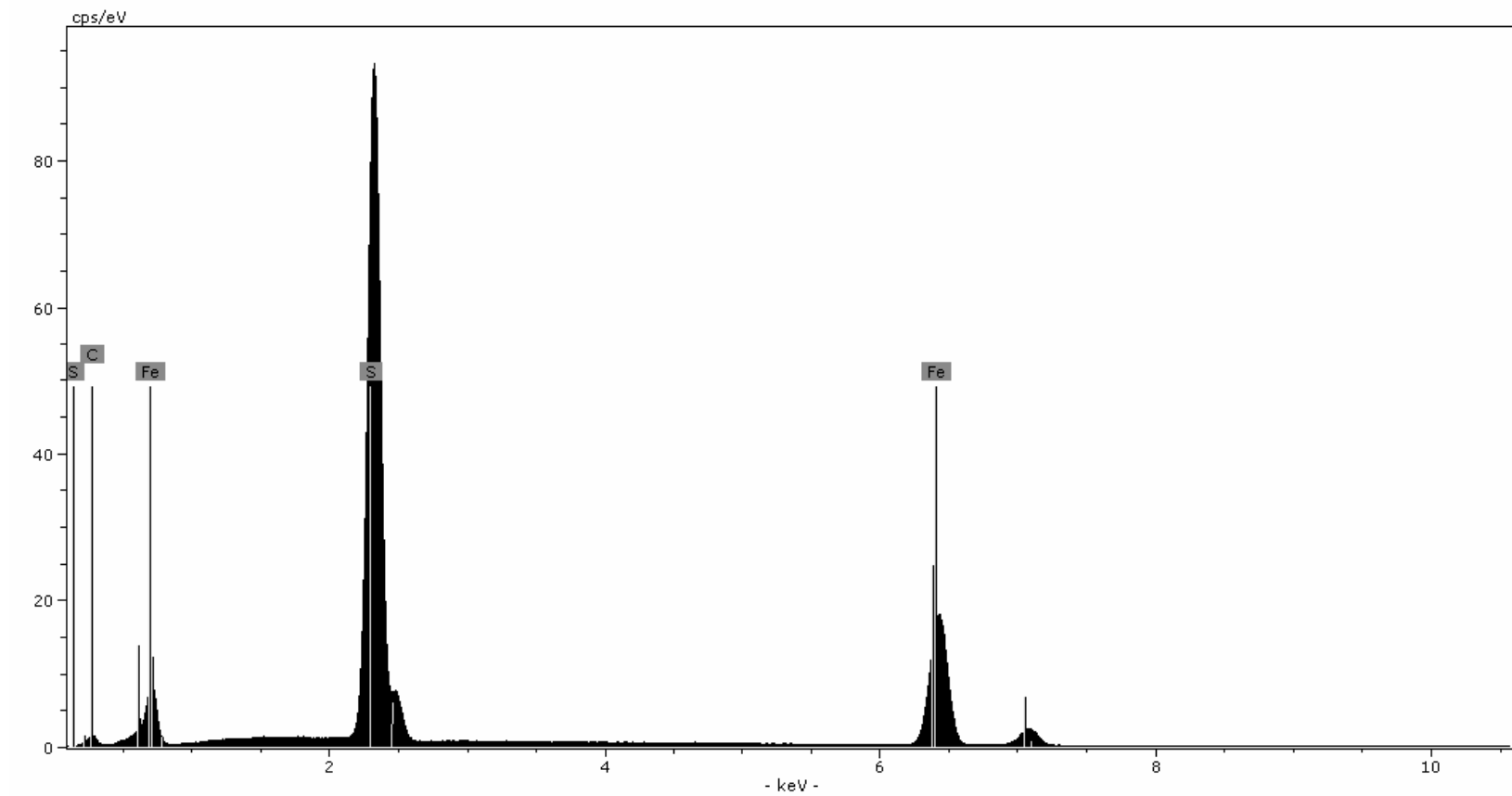


Figure 7.12 EDS spectra generated from the microprobe analysis of an iron sulphide

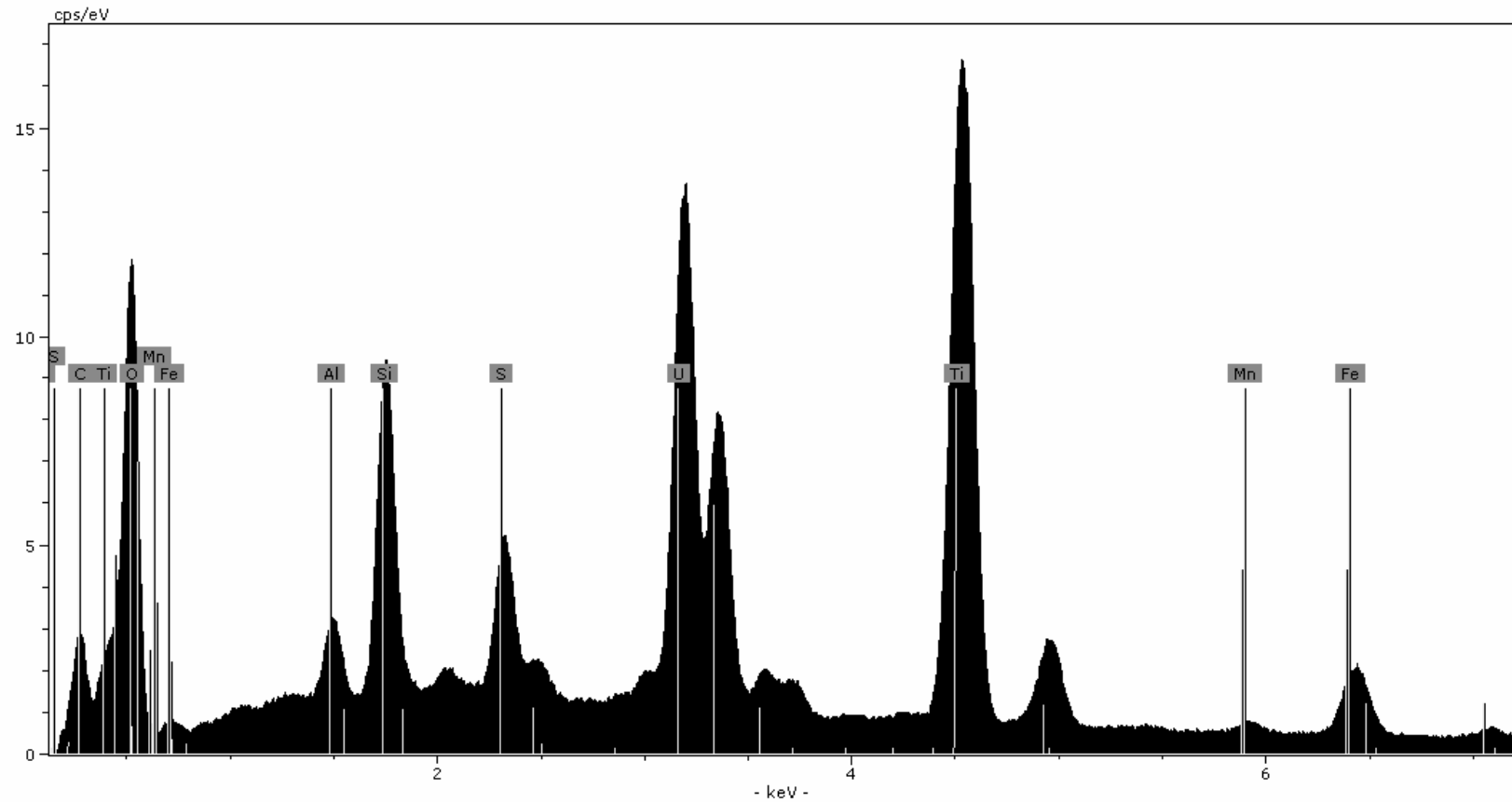
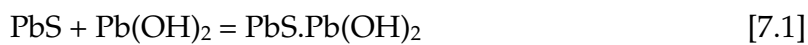


Figure 7.13 EDS spectra generated from the microprobe analysis of the dark phase found in a concentrate recovered with 20g/t SIBX.

Karogen is not expected to undergo chemical change at low pH because it is essentially carbon. It might however adsorb ferric hydroxide, ferrous ions and the respective hydroxyl complexes. Interaction between xanthate and the adsorbed species will form hydroxyl xanthate complexes, which will enhance flotation of karogen. This would consequently improve flotation of the hosted uranium.

The flotation response of galena can be predicted by using thermodynamic data to establish the species formed on the surface. Figure 7.13 shows a Pourbaix diagram for the Pb-S-H₂O system in which E_h-pH conditions encountered in each conditioning stage (Table 7.2) have been superimposed. Natural pulp potential and pH (point A) fall in the domain of Pb(OH)₂ stability so that galena is likely to be coated by lead hydroxide. Conditions prevailing immediately after acid addition and 10 minutes of conditioning (points B and C) both predict the formation of PbSO₄. After addition of a caustic solution to adjust pH to the standard flotation pH, Pb(OH)₂ is formed. This implies that the flotation behaviour of galena is controlled by interactions between lead hydroxide and the collector. O'Dea and co-workers (2001) have proposed a mechanism in which the hydroxide attaches to the surface of galena (equation 7.1). An exchange reaction between xanthate and hydroxide may then take place (equation 7.2). Oxidation of xanthate to dixanthogen accompanied by oxygen reduction may follow (equation 4.3).



In this way, a mineralogical association between galena and uranium minerals should enhance recoveries after low pH conditioning.

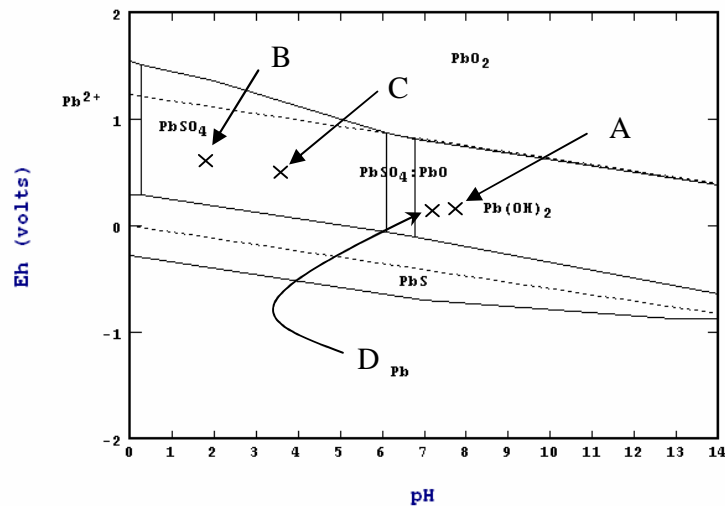


Figure 7.13 A Pourbaix diagram for the Pb-S-H₂O system at 25°C, 10⁻³M [Pb], 10⁻³M [S] showing E_h-pH conditions prevailing during conditioning [A] natural pulp E_h-pH, [B] soon after addition of 1.25kg/t sulphuric acid, [C] after 10 minutes of conditioning, [D] after addition of a caustic solution to attain standard flotation pH

4.4.3 Gold

Table 7.4 shows gold final recoveries and initial rates for the two conditioning pHs tested. Corresponding recovery-grade curves are shown in Figure 7.14. The curve for pH 1.9 is above that for pH 7.2 throughout, which implies a better flotation response. This is also evidenced by their flotation initial rates; pH 1.9 recorded 0.65min⁻¹ while the latter gave 0.53min⁻¹. A similar trend was observed in the final recoveries, 43.9% compared to 41.5 %.

Table 7.4 Gold final recoveries and initial rates

Conditioning pH	k (min ⁻¹)	R _{max} (%)	R ²
1.9	0.65	43.9	0.9931
7.2	0.53	41.5	0.9956

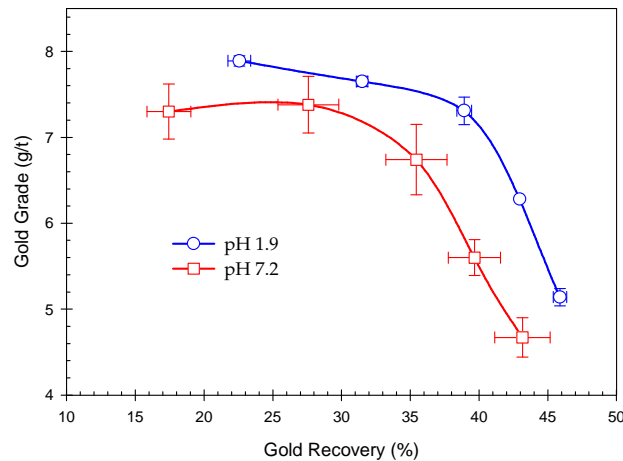


Figure 7.14 Gold recovery–grade curves plotted from data recorded from experiments in which No 2 Gold Plant feed was conditioned at pH 1.9 and pH 7.5 prior to flotation

Since gold is associated with cyanide insoluble pyrite (Parnell, 2001; Rob and Meyer, 1995; Ford, 1993), recovery of this sulphide accounts for the recovery of gold from leach residues (de Wet et al., 1995). Part of the feed to the plant consists of reclaimed old dump material so that the sulphide is likely to be oxidised. This is further influenced by air that is introduced to meet the oxygen requirement of the cyanidation process. Low pH treatment prior to flotation has already been shown to result in higher kinetics and lower final recoveries. Rob and Meyer (1995) have also mentioned the presence of gold in quartz veins in the Witwatersrand basin. This fraction, if partially liberated will not be fully soluble in cyanide. Acid conditioning could have polished the gold, and improved interaction with flotation reagents.

7.2.4 Conclusions

Based on release curve experiments, conditioning at pH 1.9 gave significantly higher sulphur flotation kinetics and slightly lower final recoveries compared to the standard pH of 7.2. Uranium initial rates were higher although recovery-grade curves showed that the standard pH was better all through. In fact, uranium lost flotability considerably because the curve for the standard was above throughout. Gold initial rates and final recoveries were significantly improved by the low pH treatment. This was also shown in the corresponding recovery-grade curve that was above the standard throughout.

Through use of EDS analysis and back-scattered electron images from microprobe analysis and scanning electron microscopy, all uranium-bearing particles recovered with SIBX were shown to have an association with pyrite, galena and/or karogen. The flotation of uranium was therefore attributed to these relationships since all these minerals are floatable.

CHAPTER 8

ACTIVATION OF PYRITE BY Pb^{2+} and Cu^{2+} IN THE PRESENCE OF CYANIDE

8.1 Introduction

The feed to the flotation circuit at No 2 Gold Plant consists of de-slimed cyanidation tailings. Cyanide acts as a depressant in pyrite flotation (De Wet et al., 1997; O'Connor et al., 1988; Janetski et al., 1977, Elgillani and Fuerstenau, 1968). This effect is partially overcome by oxidation of the cyanide using SO_2 -containing calcine water followed by activation with copper sulphate. Work conducted by Miller (2003) indicated that in the presence of cyanide, Pb^{2+} ions in lead nitrate proved to be a better pyrite activator than Cu^{2+} in copper sulphate. In this section, the two activators are compared using release curves. After addition of $2 \times 10^{-3}M$ (100ppm) sodium cyanide and three minutes of conditioning, the respective activators were dosed at 440mmol/t (equivalent to 70g/t copper sulphate and 145.7g/t lead nitrate). Flotation was carried out at pH 7.2. There was no flotation with either copper or lead addition.

8.2 Results and Discussion

8.2.1 Copper Sulphate

In order to understand the possible mechanisms contributing to the failure of copper sulphate to activate pyrite, it is necessary to review the response of pyrite surfaces to the presence of cyanide and copper (II) ions. The Pourbaix diagram of the Fe-S-CN- H_2O system in Figure 8.1 shows that $Fe(CN)_6^{3-}$ and $Fe(CN)_6^{4-}$ are the stable species formed at pH 7.2 used in the present study.

Seke (2005) has highlighted that most practical pulp potentials are in the range where the formation of $Fe(CN)_6^{2-}$ is thermodynamically favourable. This implies that when cyanide was dosed to the flotation feed in the experiment, ferrocyanide should have formed. Early work by Elgillani and Fuerstenau (1968) has shown that in the presence of cyanide, the depression of pyrite is a result of the formation of ferrocyanide (equation 4.4) followed by the precipitation of ferric ferrocyanide ($Fe_4[Fe(CN)_6]_3$) on the sulphide surface.

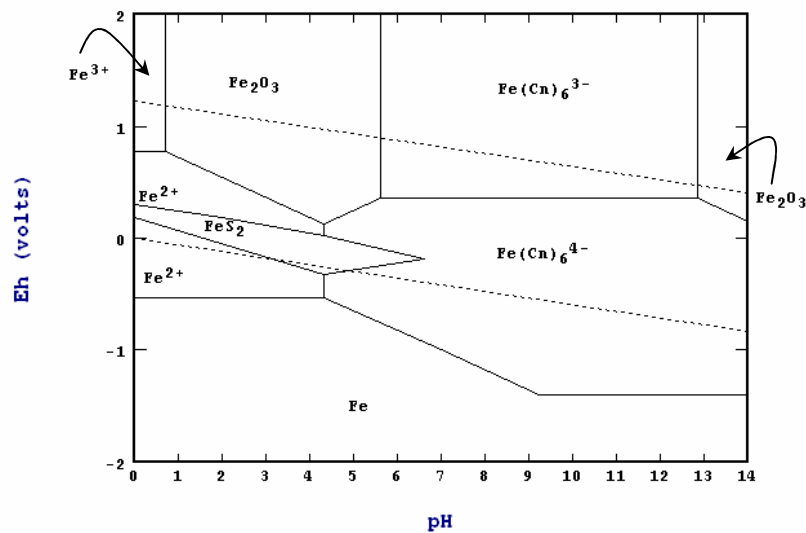
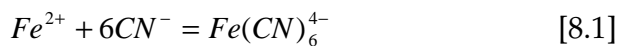


Figure 8.1 A Pourbaix diagram for the Fe-S-CN- H_2O system drawn using STABCAL software for $10^{-4}M [S]$, $10^{-4}M [Fe]$ and $2 \times 10^{-3}M [CN^-]$, NBS Database

The speciation of copper (II) at different pH values is shown in Figure 8.2. It is clear that at around pH 7, approximately 70% of the copper is available in the form of Cu^{2+} while the balance exists as aqueous $Cu(OH)_2$ and a very small proportion in complex form: $CuOH^+$. Since Cu^{2+} makes up the largest proportion, it is bound to have a strong influence on the behaviour of copper (II) at the flotation pH used in the experiment.

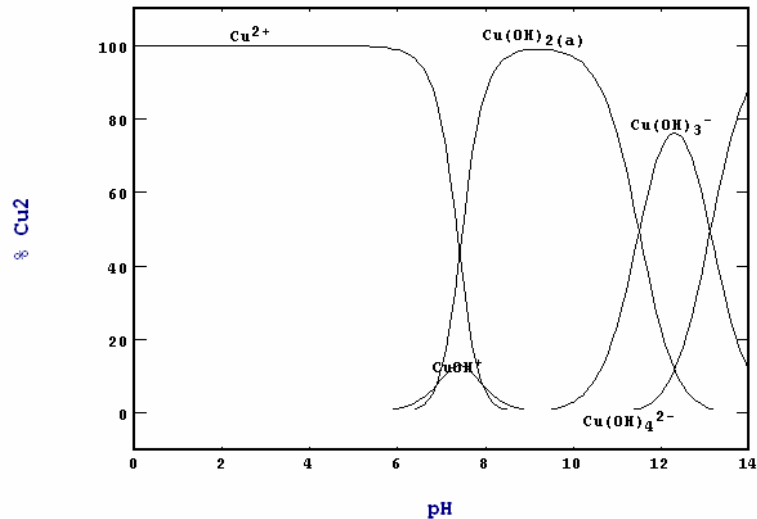
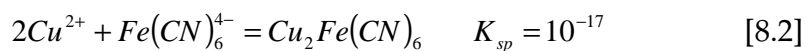


Figure 8.2 Copper (II) speciation at different pH values. Diagram drawn using STABCAL Software for $2 \times 10^{-4}M [Cu^{2+}]$, NBS Database

Reference has been made to the formation of ferrocyanide at E_h -pH conditions typical of most pyrite flotation circuits. Any interaction between Cu^{2+} and the iron cyanide complex is likely to affect the capacity of copper sulphate to activate pyrite. In the work conducted by Bellomo (1970), titration of copper (II) with ferrocyanide yielded a reddish brown precipitate of $Cu_2Fe(CN)_6$ according to:



Bellomo (1970) also showed that the copper ferrocyanide precipitate formed has a solubility of $2 \times 10^{-6} M$ and its formation was accompanied by a change in standard free energy of $-75kJ/mol$. This present work tested $2 \times 10^{-4}M$ copper sulphate. Considering the negative free energy change, it is reasonable to assume that copper ferrocyanide was formed spontaneously when copper sulphate was dosed to the flotation slurry. Since the resulting concentration of copper (II) was greater than the solubility, some of the salt formed should have precipitated. This shows that copper sulphate dosed was consumed in the formation of copper ferrocyanide salt so that none was available to adsorb

on pyrite and activate it. Consequently, xanthate could not adsorb and pyrite could not float.

Addition of copper sulphate to flotation streams treating cyanidation tailings has been reported to enhance pyrite recovery through formation of copper-cyanide complexes (O'connor et al., 1988). These eliminate free cyanide so that it cannot depress pyrite. Westwood and co-workers (1970) have however emphasised that treatment with copper sulphate alone is not sufficient to render pyrite floatable. This is consistent with the findings of this present work where $2 \times 10^{-4}M$ copper (II) failed to activate pyrite in the presence of $2 \times 10^{-3}M$ sodium cyanide. The authors also mentioned that low pH treatment is essential for pyrite to float. It is most likely that the low pH destroys cyanide through hydrolysis; completely eliminating ferrocyanide (Figure 8.1) so that copper (II) can adsorb and activate pyrite without any interference from complex ion formation. Since Elgillani and Fuerstenau (1968) proposed that precipitation of ferric ferrocyanide in flotation pulps containing cyanide depresses pyrite, there is a possibility that copper ferrocyanide has a similar effect. Given that gold and uranium are hosted by pyrite, their flotation responses are bound to be affected as well.

8.2.2 Lead Nitrate

The complete depression of pyrite observed despite the dosage of 0.44mol/t lead nitrate (equivalent to $2 \times 10^{-4}M$ Pb^{2+}) activator can possibly be understood by studying the speciation of lead (II) at the flotation pH of 7.2. Figure 8.3 shows that at around pH 7, approximately 80% of lead (II) at the concentration dosed in the experiment [$2 \times 10^{-4}M$] exists in the form of $PbOH^+$ and only about 20% as Pb^{2+} . Because lead (II) does not interact with cyanide (Miller, 2003), the probability that it will activate pyrite essentially depends on the dominant species: $PbOH^+$. Since complete depression of pyrite was

observed in the experiment, it appears that this species is incapable of activating pyrite.

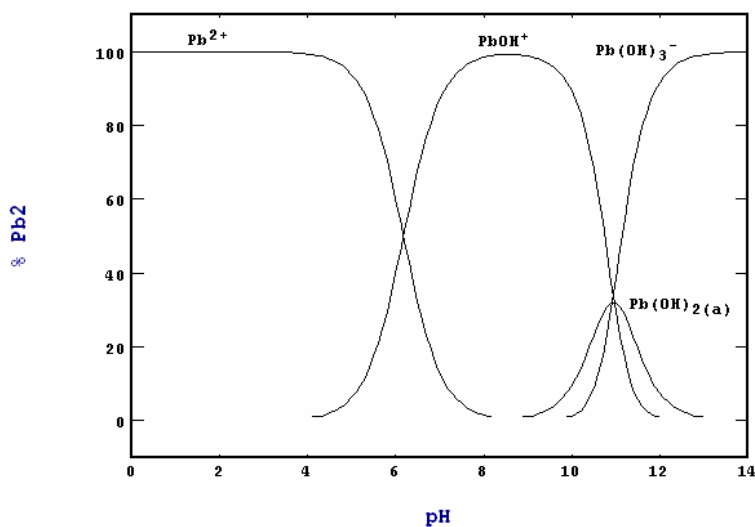
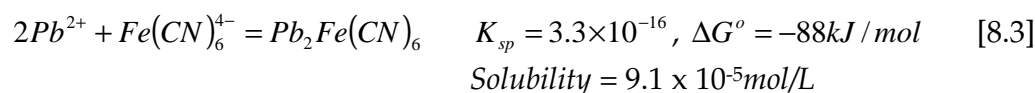


Figure 8.3 Lead (II) speciation at $2 \times 10^{-4}M [Pb^{2+}]$. Diagram drawn with STABCAL software, NBS database

Electrochemically controlled contact angle measurements by Miller (2003) on pyrite using potassium amyl xanthate in the presence of cyanide showed high contact angles in lead nitrate-treated pyrite compared to untreated sulphide. This work was conducted at pH 4.7 and from Figure 8.3; almost 100% of lead (II) is as a cation (Pb^{2+}). It appears that for lead (II) to activate pyrite, it is essential that it must be in this form. In view of this background, the flotation experiment was repeated at pH 5.5. Approximately 90% of lead (II) would be in the form: Pb^{2+} (Figure 8.3) and 100% of copper (II) as Cu^{2+} (Figure 8.2). Viljoen (1998) has shown that SIBX has a half life of 63.2 hours at pH 6 so that at pH 5.5, there is little risk of collector losses through hydrolysis. As in Cu^{2+} , Bellomo (1970) reported that Pb^{2+} reacts with ferrocyanide to give $Pb_2Fe(CN)_6$, a white powdery precipitate soluble in strong acids and bases.



The author however noted that the kinetics of the reaction are very slow at room temperature so that its effects might be insignificant within the time frame of the flotation experiment.

8.2.3 Copper Sulphate at pH 5.5

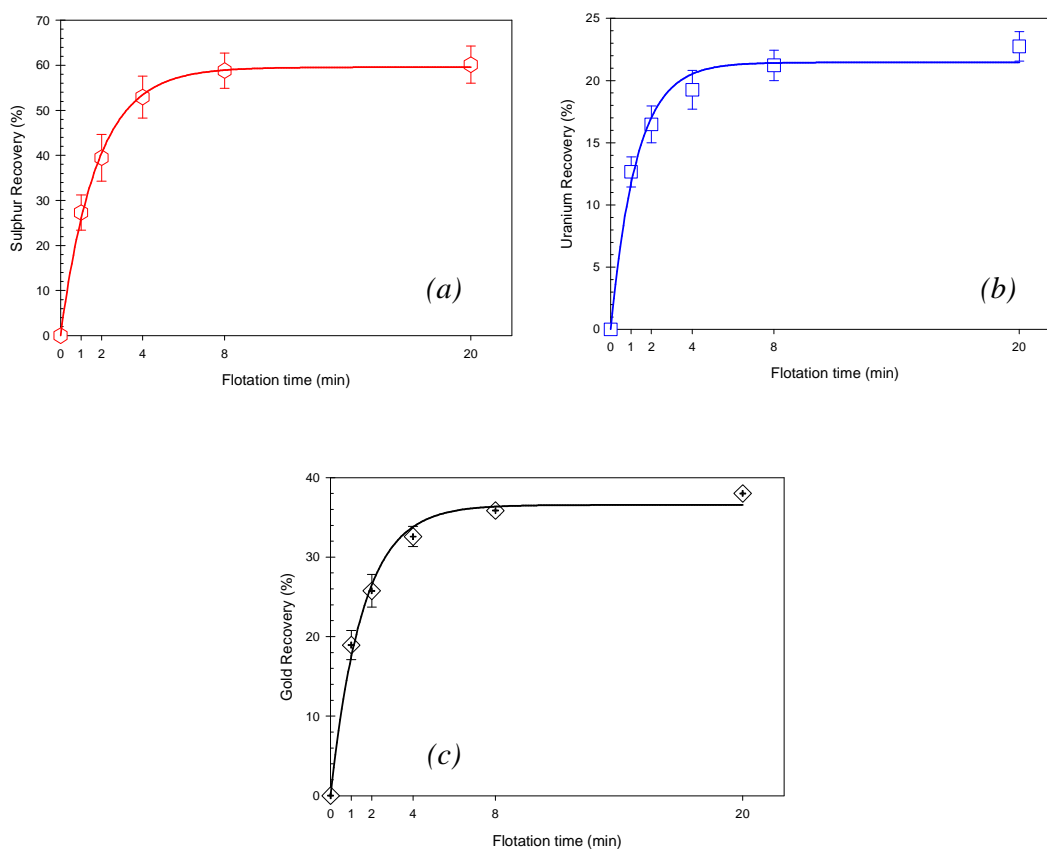
Flotation at pH 5.5 using 0.44mol/t copper sulphate as an activator in the presence of 100ppm cyanide still failed to recover pyrite. There was no froth build-up and any bubbles formed were barren and they broke down as soon as they reached the surface. Throughout conditioning, cyanide could still be smelled from the flotation pulp. Examination of the Pourbaix diagram of the Fe-S-CN-H₂O system in Figure 8.1 shows that flotation at pH 5.5 was still in the Eh-pH conditions where ferrocyanide is stable. It appears that the pH 5.5 was not low enough to destroy cyanide through hydrolysis and stabilize the ferrous ion. This means that the mechanisms thought to be operative at pH 7.2 presented earlier still dominated the flotation experiment. The presence of cyanide is so detrimental to pyrite flotation that standard practice at No 2 Gold Plant is to keep its concentration below 4ppm (Brooks, 2005).

8.2.4 Lead Nitrate at pH 5.5

The flotation responses for sulphur gold and uranium following flotation at pH 5.5 with lead nitrate as an activator are shown in Table 8.1 and Figure 8.4. The lack of interaction between the lead (II) in cationic form (Pb^{2+}) and cyanide enabled it to adsorb onto pyrite so that it was amenable to xanthate adsorption, and hence floatable (Miller 2003). The nature of the xanthate species formed on adsorption of SIBX is essentially dixanthogen (Sui *et al.*, 1997).

Table 8.1 Sulphur, gold and uranium flotation responses recorded following activation with lead nitrate in the presence of cyanide at pH 5.5

Component	Activator	k (min^{-1})	R_{max} (%)	R^2
Sulphur	Lead nitrate	0.57	59.54	0.9990
	Copper sulphate	0.00	0.00	0.0000
Uranium	Lead nitrate	0.79	21.40	0.9870
	Copper sulphate	0.00	0.00	0.0000
Gold	Lead nitrate	0.57	59.54	0.9990
	Copper sulphate	0.00	0.00	0.0000

**Figure 8.4** (a) Sulphur (b) uranium and (c) gold recovery-time graphs recorded for flotation with 440mmol/t $Pb(NO_3)_2$ in the presence of 0.001M NaCN at pH 5.5

8.2.5 Conclusions

In the presence of 100ppm sodium cyanide, and pH 5.5 lead (II) recovered sulphur, gold and uranium but copper (II) did not. Therefore the Pb^{2+} cation was necessary for activation.

The destruction of cyanide at No 2 Gold Plant is based on the INCO SO_2 /AIR process. This not only enhances the flotation of pyrite, it also removes the poisonous chemical from the system so that tailings from the flotation circuit can be dumped without any risk of contaminating the environment. Substitution of copper sulphate with lead nitrate means that the tailings will still contain cyanide and this will pose a serious environmental problem. A plan to destroy cyanide before the tailings leave the plant will have to be put in place. Whether lead nitrate is a better activator than copper sulphate therefore depends on whether any improvements in flotation performance outweigh the cost of setting up extra facilities to handle cyanide from tailings.

CHAPTER 9

CONCLUSIONS AND RECOMMENDATIONS

This thesis is an investigation of chemicals in the flotation of auriferous pyrite. Gold uranium and sulphur from AngloGold Ashanti's No 2 Gold were optimised using SIBX and mixtures of SIBX and TTC.

The effect of conditioning at low-pH (1.9-3.7) prior to flotation, the activation of pyrite with lead nitrate and copper sulphate in the presence of cyanide and possible mechanisms contributing to uranium flotation were studied. The following conclusions have been made:

- A steady increase in sulphur, uranium and gold recovery was found in SIBX doses from 10g/t to 40g/t. The gold grade was unaffected by dosage between these limits.
- Synergism was shown to occur in gold flotation at 25 mole percent C₁₂ TTC and 75 mole percent SIBX. Gold recovery improved from 39% to 45.3%. At a similar mole ratio, 15.6% uranium recovery was recorded with a C₁₀ TTC/SIBX mixture. This was an increase by a factor of 12% when compared to 13.92% recorded with the standard.
- A re-run of bulk flotation experiments testing fresh SIBX/C₁₂ TTC mixtures recorded almost similar mass recoveries for all three collector mixtures. These were all higher than the standard. Water recoveries indicated that the higher mass recoveries were due to increased gangue recovery. Almost similar sulphur recoveries were observed for the standard and all three SIBX/TTC mixtures. The highest uranium and gold recoveries were observed at 8 mole percent TTC. This is close to dosages of 2 - 5 mole percent TTC in SIBX used in commercial operations. The

results also indicated that SIBX/C₁₂ TTC had more effect on gold than on either sulphur or uranium.

- Based on time/recovery studies, initial rates and final recoveries shown that the combination of 92 mole percent SIBX and 8 mole percent commercial C₁₂ TTC performed better than SIBX alone. A combination of SIBX and a diluted and aged 1% wt solution of TTC marginally lost activity when compared to that of SIBX and fresh commercial TTC. This was attributed to the hydrolysis of TTC. The product of decomposition would then be a mercaptan. The mercaptan/SIBX reference sample showed a distinct reduction in grade recovery and kinetics. The conclusion therefore is that when dosed as such, mercaptan is detrimental to flotation activity. The mercaptan on its own is not an effective flotation agent and exhibits no synergism, but rather has a depressing effect.
- Micro-probe analysis, back-scattered electron images, and EDS analysis showed that all the uranium recovered in flotation concentrates was associated with either pyrite, galena or a carbonaceous material (called karogen). Since the sulphides respond to xanthates and karogen is naturally hydrophobic, its flotation of the uranium oxide minerals (brannerite and uraninite) was attributed to these mineralogical associations. It is however recommended that more work be done to quantify the distribution of uranium in each of the host minerals using instruments like the QEM SCAN. Once the mineral that hosts the largest proportion of uranium is established, further work to maximise recoveries through flotation of the host can be undertaken.
- A preconditioning step at pH 1.9-3.7 gave higher gold, sulphur and uranium initial rates. Sulphur and uranium final recoveries were lower while gold final recovery was higher than the standard. Grade-recovery curves indicated that uranium lost flotability considerably after the low-pH treatment while gold improved significantly.

- In the presence of 0.001M cyanide, 70g/t copper sulphate (440 mmol/t) Cu^{2+} failed to activate pyrite at both pH 5.5 and the standard flotation pH of 7.2. At a similar dosage an equi-molar dose Pb^{2+} did not activate the sulphide at pH 7.2 either. It was only functional at pH 5.5. The lack of activation at the alkaline pH is contrary to work by Sui et al. (1997) who observed enhanced xanthate uptake with lead-activated pyrite at pH 10.5. Since lead does not complex with cyanide, it was expected to aid xanthate uptake in the present work. The investigation by Miller (2003) that was used as a precursor to this study was run at pH 4.7. Examination of speciation diagrams showed at this pH, the Pb^{2+} species is prevalent. In this view, it is recommended that further work be done to characterise the lead adsorption onto pyrite in the presence of cyanide in order to determine whether the cationic state is a requirement for lead to activate pyrite, and possible reasons for the lack of activation at alkaline pH.

REFERENCES

Agar, G. E., and Barret, J. J., 1983. The use of flotation rate data to evaluate reagents. *CIM Bulletin*, **76** (851), pp 157-162

Agar, G. E., Stratton-Crawley, R., and Bruce, T. G., 1980. Optimising the design of flotation circuits. *CIM Bulletin*, **73** (824), pp 173

Ackerman P. K., Harris, G. H., Klimpel, R. R. and Aplan, F. F., 1987. Evaluation of flotation collectors for copper sulphides and pyrite , I. Common sulphhydryl collectors. *Int. J. Miner. Process.*, **21**, pp 105-127

Alison, S. A., 1982. Interactions between sulphide minerals and metal ions in the activation, deactivation and depression of mixed sulphide ores during the flotation process, Report No M9, Published by Council for Mineral Technology, Randburg, South Africa

Allison, S., and Finkelstein, N. P., 1971. Study of the products of reactions between galena and aqueous xanthate solutions. *Trans. Inst. Min. Metall.*, **80**, pp C235-C239

Anhaeusser, C. R., Feather, C. E., Liebenburg, W. R., Smits, G., and Snegg, J. A., 1987. Geology and mineralogy of the principal goldfields in South Africa, in Stanley, G. G., (Ed.), *The Extractive Metallurgy of Gold in South Africa*, Vol. 1, The South African Institute of Mining and Metallurgy, Johannesburg, pp 1-67

Avotins, P. V., Wang, S. S., and Nagaraj, D. R., 1994. Recent advances in sulphide collector development, in Mulukutla, P. S., (Ed.), *Reagents for better metallurgy*, Society for Mining, Metallurgy and Exploration, Inc., Littleton, USA, pp 81-90

Bellomo, A., 1970. Formation of Copper (II), Zinc (II), Silver (I) and Lead (II) Ferrocyanides, *Talanta*, **17**, pp1109-1114

Benzaazoua, M. and Kongolo, M., 2003. Physico-chemical properties of tailing slurries during environmental desulphurisation by froth flotation. *Int. J. Miner. Process.*, **69**, pp 221-234

Boschkova, K., 2002, *Adsorption and Frictional Properties of Surfactant Assemblies at Solid Surfaces*, Institute of Surface Chemistry, Stockholm, PhD Thesis

Bradshaw, D. J., 1997. Synergistic effect between thiol collectors used in the flotation of pyrite, PhD Thesis, University of Cape Town

Broekman, B. R., Carter, L. A. E., and Dunne, R. C., 1987. Flotation, in Stanley, G. G., (Ed.), *The Extractive Metallurgy of Gold in South Africa*, South African Institute of Mining and Metallurgy, Johannesburg, pp 235-276

Brooks, M., 2005, Personal Communication

Browne, B., 2002. Personal Communication

REFERENCES

- Breytenbach, W., Vermaak, M. K. G. and Davidtz, J. C., 2003. Synergistic effects among dithiocarbonates (DTCs), dithiophosphate (DTP) and trithiocarbonates (TTCs) in the flotation of Merensky ores, *S. Afr. Inst. Min. Metall.*, pp 667-670
- Bushell, C. G. H., Kraus, G. J and Brown, G., 1961. Some reasons for selectivity of copper activations of minerals, *Trans. SME/AIME*, **46**, pp 177-184
- Chander, S., 1999. Fundamentals of sulphide mineral flotation, in B. K. Parekh and J. D. Miller (Eds.), *Advances In Flotation Technology*, Society for Mining, Metallurgy and Exploration Inc. Littleton, USA, pp 129-145
- Chen, Z., 1999. Electrochemical studies of copper-activation of sphalerite and pyrite, Virginia Polytechnic Institute and State University, PhD Thesis
- Coetzer, G., and Davidtz, J. C., 1989. Sulphydryl collectors in bulk and selective flotation. Part I: Covalent trithiocarbonate derivatives. *J. S. Afr. Inst. Min. Metall.*, **89** (10), pp 307-311
- Critchley, J. K. and Riaz, M., 1991. Study of synergism between xanthate and dithiocarbamate collectors in flotation of heazlewoodite. *Trans. Instn. Min. Metall.*, **100**, pp C55-C57
- Crozier, R. D., 1991. Sulphide collector mineral bonding and the mechanism of flotation. *Min. Eng.*, **4** (7-11), pp 839-858
- Crozier, R.D., 1992. *Flotation - theory, reagents, ore testing*. Pergamon Press, Oxford, New York, Seoul, Tokyo
- Cullinan, V. J., Grano, S. R., Greet, C. J., Johnson, N. W. and Ralston, J., 1999. Investigating fine galena recovery problems in the lead circuit of Mount Isa Mines lead/zinc concentrator. Part I: Grinding effects. *Miner. Eng.*, **12** (2), pp 147-163
- Davidtz, J. C., 1999, Quantification of Flotation Activity by Means of Excess Gibbs Free Energies, *Miner. Eng.*, **12**, (10), pp. 1147-1161
- Davidtz, J. C., 2002, Personal Communication
- Davidtz, J. C., 2004, Personal Communication
- Davidtz, J. C., 2005, Personal Communication
- de Donato, P., Cases, J. M., Kongolo, M., Cartier, A., and Rivail, J. L., 1989. Stability of the amyloxanthate ion as a function of pH: Modelling and comparison with the ethylxanthate ion. *Int. J. Min. Proc.*, **25**, pp 1-16
- de Wet J. R., Pistorius P. C. and Sandenbergh R. F., 1997. The influence of cyanide on pyrite flotation from gold leach residues with sodium *iso*-butyl xanthate. *Int. J. Min. Proc.*, **49** (3-4), pp 149-169

REFERENCES

- du Plessis, R., 2003. The thiocarbonate flotation chemistry of auriferous pyrite. PhD Thesis, The University of Utah
- du Plessis, R., Miller, J. D., and Davidtz, J. C., 2000. Preliminary examination of electrochemical and spectroscopic features of trithiocarbonate collectors for sulphide mineral flotation, *Trans. Nonferrous Met. Soc. China*, **10**, pp 12-18
- Dumisa, L., 2002. Personal Communication
- Elgillani, D. A., and Fuerstenau M. C., 1968. Mechanisms involved in cyanide depression of pyrite. *Trans. AIME, Soc. Min. Eng.*, **241**, pp 437-445
- Ford, M. A., 1993. Uranium in South Africa. *J. S. Afr. Inst. Min. Metall.*, **93**, (2), pp 37-58
- Fuerstenau, D. W., and Raghavan, S., 1976. Some aspects of the thermodynamics of flotation, in Fuerstenau, M. C., (Ed.), Flotation - A. M. Gaudin Memorial Volume, AIME, New York, pp 1-21
- Fuerstaenau, M. C., 1982a, Chemistry of collectors in solution, in King, R. P., (Ed.), Principles of Flotation, South African Institute of Mining and Metallurgy, Johannesburg, pp 1 - 16
- Fuerstenau, M. C, 1982b, Sulphide Mineral Flotation, in King, R. P., (Ed.), Principles of flotation, South African Institute of Mining and Metallurgy, Johannesburg.
- Fuerstenau, M. C., 1982c. Mineral-water interfaces and the electrical double layer, in King R. P., (Ed.), Principles of flotation, South African Institute of Mining and Metallurgy, Monograph Series No 3, Johannesburg pp 17
- Fuerstenau, M. C., Kuhn, M. C., and Elgillani, D. A., 1968. The Role Of Dixanthogen In Xanthate Flotation Of Pyrite. *Trans Am. Inst. Min. Eng.* **241**, pp 148-156
- Jackson, E., 1986. Hydrometallurgical Extraction and Reclamation, John Wiley and Sons, New York, pp 30
- Janetski, N. D., Woodburn, S. I., Woods, R., 1977. Electrochemical investigation of pyrite flotation and depression. *Int. J. Min. Proc.*, **4** (3), pp 227-239
- Jiang, C. L., Wang X. H., Parekh, B. K., and Leonard, J. W., 1998. The surface and solution chemistry of pyrite flotation with xanthate in the presence of iron ions. *Coll. and Surf. A: Physic. Eng. Aspects*, **136**, pp 51-62
- Kirjavainen, V. M., 1996. Review and analysis of factors controlling the mechanical flotation of gangue minerals. *Int. J. Miner. Process.* **46**, pp 21-34.
- Klimpel, R. R, 1980, Selection of chemical reagents for flotation, in Mular, A. and Bhappu, R. (Eds), Mineral Processing Plant Design, 2nd Edition, AIME, NY, pp907-934

REFERENCES

- Klimpel, R. R, 1984a, Froth flotation: A kinetic approach, Proceedings of the International Conference on Mineral Science and Technology, Sandton, South Africa, Vol. 1, pp 385-392
- Klimpel, R. R, 1984b, Use of chemical reagents in flotation, *Chem. Eng. (September 1984)*, pp 75-79
- Klimpel, R. R., 1999. A review of sulphide mineral collector practice, in Parekh, B. K. and Miller, J. D (Eds.), *Advances in Flotation Technology*, 1st Edition, Society of Mining, Metallurgy and Exploration Inc., Littleton, USA, pp 115-127
- Leppinen, J. O., 1990. FTIR and flotation investigation of the adsorption of ethyl xanthate on activated and non-activated sulphide minerals. *Int. J. Miner. Process*, **30**, pp 245-263
- Leppinen, J., Laajalehto, K., Kartio, I and Souminen, E., 1995. FTIR and XPS studies of surface chemistry of pyrite in flotation, *Int. Miner. Process Congr. XIXth Soc. Min. Metal. Explor.*, Littleton, Vol. 3, pp 35-38
- Levin, J., and Veitch, M. L., 1970. Laboratory tests on the flotation of pyrite from Witwatersrand gold ores by a cationic collector. *J. S. Afr. Inst. Min. Metall.*, **70**, pp 259-271
- Livshits, A. K., and Dudenkov, S. V., 1965. Some factors in flotation froth stability. *Proc. 7th Int. Min. Proc. Congress*, New York, pp 367-371
- Lloyd, P. J. D., 1981. The flotation of gold, uranium and pyrite from Witwatersrand ores. *J. S. Afr. Inst. Min. Metall.*, pp 41-47
- Majima, H., and Takeda, N., 1968. Electrochemical studies of the xanthate-dixanthogen system on pyrite. *Trans. Amer. Inst. Min. Metall. Engrs.*, **241**, pp 431-436
- Marsden, J., and House, I., 1992. *The chemistry of gold extraction*. Ellis Horwood, New York, London, Toronto, Sydney, Tokyo, Singapore, pp 183-185
- Mellgren, O., 1966. Heat of adsorption and surface reactions of potassium amyl xanthate on galena. *Trans. Am. Inst. Min. Engrs.*, **235**, pp 46-60
- Miller, J. D., 2003. Thiocarbonate collectors for pyrite flotation. Presented during a seminar on Developments in Flotation at The University of Pretoria on June 17, 2003, Pretoria, South Africa
- Mitrofanov, S. I., Kuz'kin, A. S. And Filimonov, V. N., 1985. Theoretical and practical aspects of using combinations of collectors and frothing agents for sulphide flotation, *Proceedings of 15th Congr. Int. Metall.*, St. Etienne, France, Vol. 2, pp 65-73
- O'Connor, C. T., and Dunne, R. C., 1991. The practice of pyrite flotation in South Africa And Australia. *Min. Eng.*, **4**, (7-11), pp 1057-1069

REFERENCES

O'Connor, C. T. and Dunne, R. C., 1994, The flotation of gold bearing ores – A review, *Miner. Eng.*, **7**, (7), pp 839-849

O'Connor, C. T., Botha, C., Walls, M. J., and Dunne, R. C., 1988. The role of copper sulphate in pyrite flotation, *Min. Eng.*, **1** (3), pp 203-212

O'Dea, A. R., Prince, K. E., Smart, R. C., and Gerson, A. R., 2001. Secondary ion mass spectrometry investigation of the interaction of xanthate with galena. *Int. J. Min. Proc.*, **61**, pp 121-143

Parnell, J., 2001. Paragenesis of mineralisation within fractured pebbles of the Witwatersrand conglomerates. *Mineralium Deposita*, **36**, pp 689-699

Plaskin, I. N., Glembotskii, V. A. And Okolovich, A. M., 1954. Investigations of the possible intensification of the flotation process using combinations of collectors. (Mintek translation Feb. 1989). Naachnye Soobshcheniya Institut Gonnogo del Imeni AA Skochinskogo, Akademiya Nauk SSSRm No. 1, pp 213-224

Robb, L. J., and Meyer, F. M., 1995. The Witwatersrand basin, South Africa: geological framework and mineralisation processes. *Ore Geology Reviews*, **10**, pp 67-94

Robbins, G. H., 1996. Historical development of the INCO SO₂/AIR cyanide destruction process. CIM Bulletin, **89**, pp 63-69

Salamy, S. G., and Nixon, J. C., 1952. The application of electrochemical methods to flotation research, in *Recent Developments in Mineral Dressing*, Institute of Mining And Metallurgy, London, pp 503-516

Seke, M. D., 2005. Optimisation of the selective flotation of galena and sphalerite at Rosh Pinar Mine, PhD Thesis, University of Pretoria

Simpson, P. R., and Bowles, J. F. W., 1977. Uranium mineralisation of the witwatersrand and dominion reef systems. *Phil. Trans. R. Soc. Lond. A.* **286**, pp 527-548

Slabbert, W., 1985. The role of trithiocarbonates and thiols on the flotation of some selected south african sulphide ores. MSc. Dissertation, Potchefstroom University, South Africa

Sui, C. S., Brienne, S. H. R., Xu, Z. and Finch. J. A., 1997. Xanthate adsorption on lead contaminated pyrite, *Int. J. Miner. Process.*, **49**, pp 207-221

Sutherland, K. L., and Wark, I. W., 1955. Principles of flotation, Australian Institute of Mining and Metallurgy (Inc.) Melbourne

The Nuclear History Site, 2002,

http://nuclearhistory.tripod.com/images/diagrams/decay_chain.jpg

REFERENCES

- Tolun, R., and Kitchener, J. A., 1963. Electrochemical study of the galena-xanthate-oxygen flotation system. *Trans. Inst. Min. Metall.*, **73**, pp 313-322
- Usul, A. H., and Tolun, R., 1974. Electrochemical study of the pyrite-oxygen-xanthate system. *Int. J. Min. Proc.*, **1**, pp 135-140
- Valdiviezo, E. and Oliviera, J. F., 1993. Synergism in aqueous solutions of surfactant mixtures and its effect on the hydrophobicity of mineral surfaces. *Miner. Eng.*, **6**, (6), pp 655-661
- Viljoen, G. P., 1998. The Development and Implementation of New TTC Flotation Chemicals, MENG Thesis, Potchefstroom University
- Voigt, S., Szargan, R. and Souninen, E., 1994. Interaction of copper (II) with pyrite and its influence on ethyl xanthate adsorption, *Surf. Int. Anal.* **21**, pp 526-536
- Wang, X. H., 1994. Interfacial electrochemistry of pyrite oxidation and flotation II. FTIR studies of xanthate adsorption on pyrite surfaces in neutral pH solutions. *J. Coll. Int. Sci.* **171**, pp 413-428
- Wang, X, Forssberg, E. and Bolin, J. N., 1989. The aqueous surface chemistry of activation in flotation of sulphide minerals – A Review Part I: An electrochemical model, *Miner Process and Extr. Metall. Review*, **4** (3-4), pp 134-165
- Westwood, R. J., Stander, G. P and Carlisle, H. P., 1970. Recovery of pyrite at Government Gold Mining Areas Ltd. *J. S. Afr. Inst. Min. Metall.*, **70**, pp 213-228
- Woods, R., 1976. Electrochemistry of sulphide flotation, in Fuerstenau, M. C., (Ed.), A. M. Gaudin Memorial Volume, Volume 1, American Institute of Mining and Metallurgical Engineers, New York, pp 298-333
- Yarar, B. (Section Ed.), 1985. Flotation, in Gerhartz, W., (Exec. Ed.), Ullmann's Encyclopedia Of Industrial Chemistry, 5th Completely Revised Edition, Volume **B2**, Unit Operations I, VCH Publishers, New York, pp 23-1 to 23-30
- Zhang, Q., Xu, Z., Bozkurt, V. and Finch, J. A., 1997. Pyrite flotation in the presence of metal ions and sphalerite, *Int. J. Miner. Process.*, **52**, pp 187-201

Appendix A – Back – Scattered Electron Images

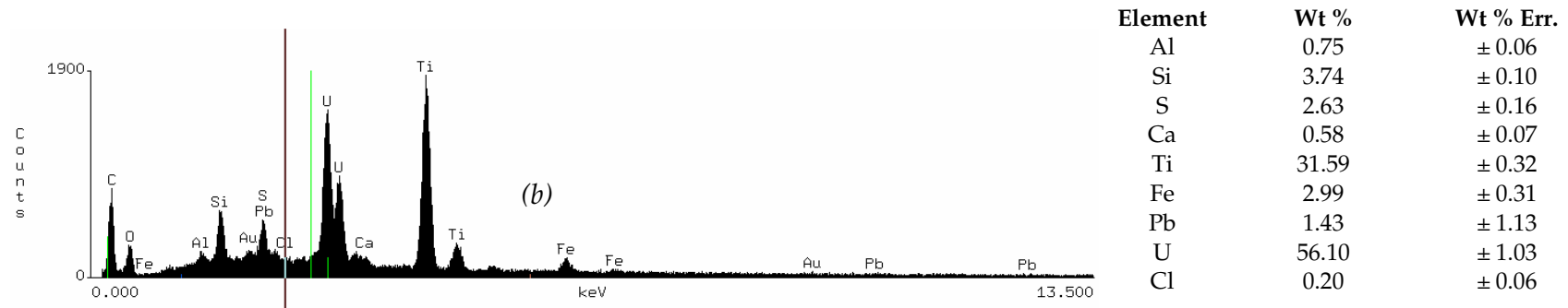
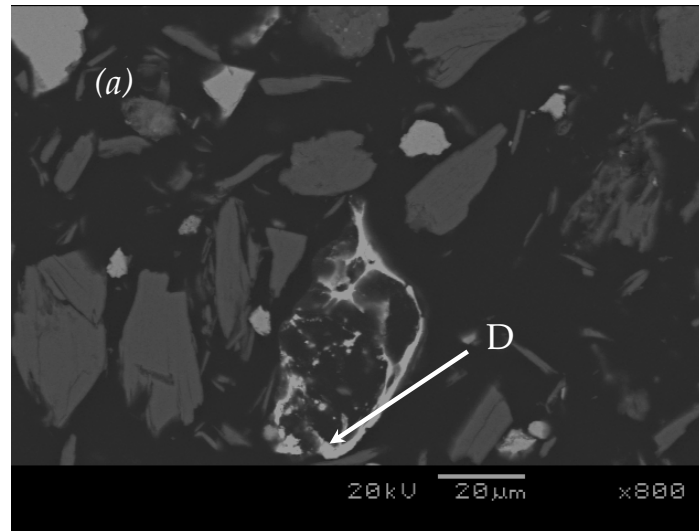
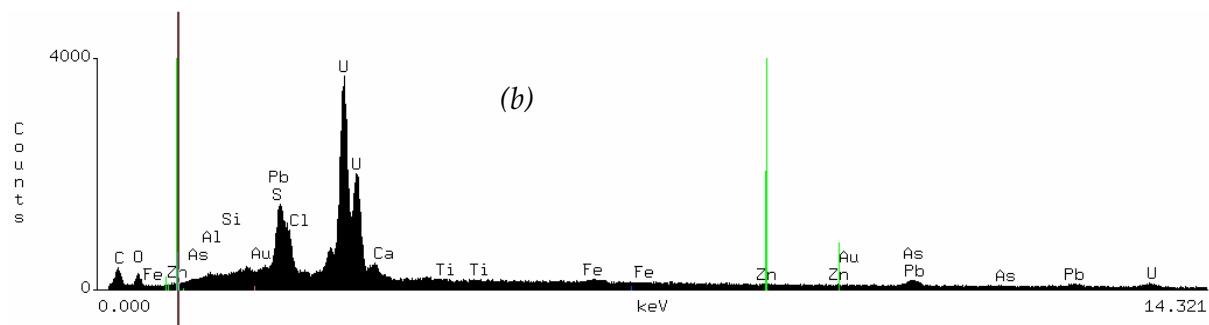
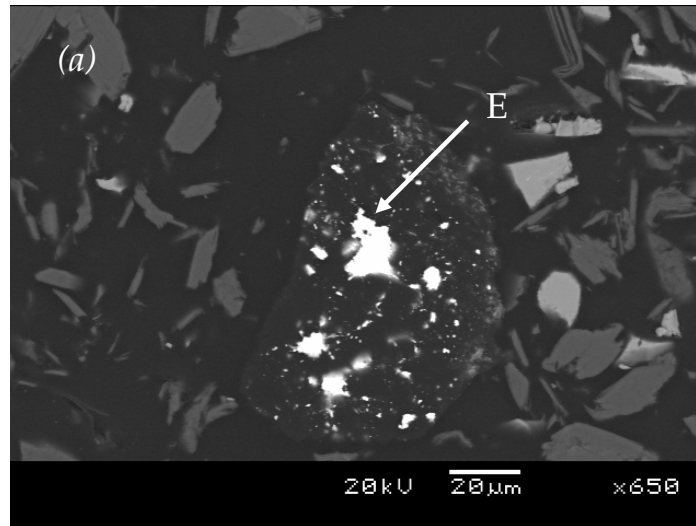


Figure A1 (a) BEI of a uranium-bearing particle and (b) corresponding EDS spectra showing its elemental composition

Appendix A – Back – Scattered Electron Images



Element	Wt%	Wt % Err.
Al	0.12	± 0.04
S	1.05	± 0.22
Fe	0.60	± 0.13
Pb	17.90	± 2.69
U	78.58	± 1.06
Cl	0.90	± 0.16
Zn	0.58	± 0.21

Figure A2 (a) BEI of a uranium-containing particle and (b) corresponding EDS spectra showing its elemental composition

Appendix A – Back – Scattered Electron Images

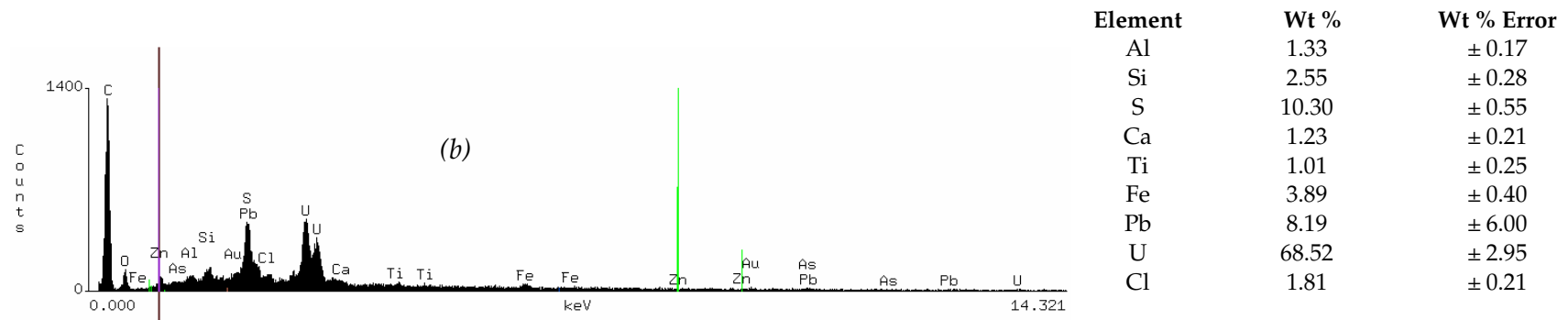
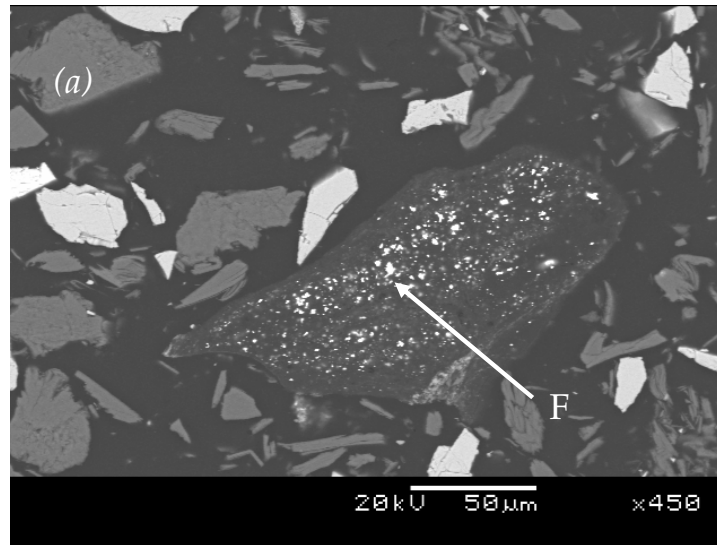


Figure A3 (a) BEI of a uranium-containing particle and (b) corresponding EDS spectra showing its elemental composition

Appendix A – Back – Scattered Electron Images

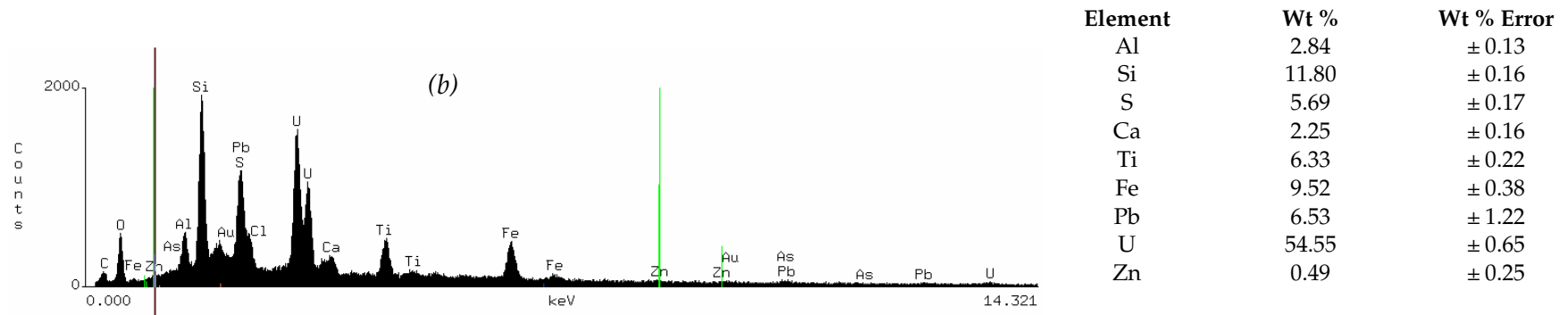
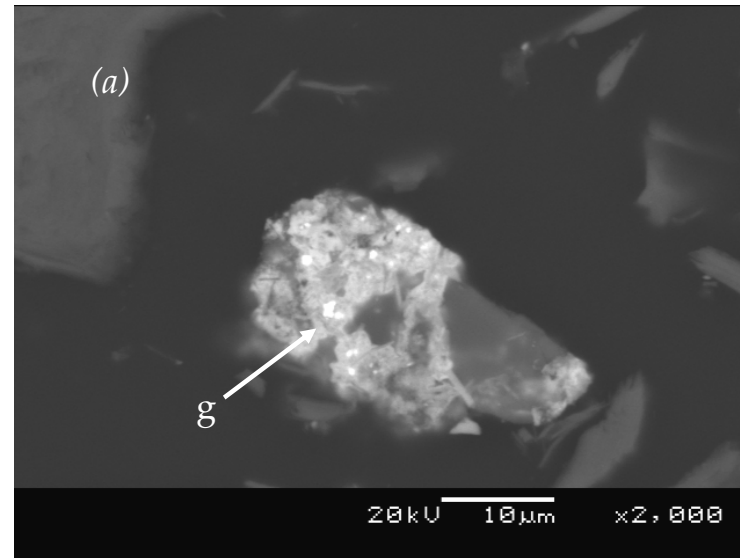


Figure A4 (a) BEI of a uranium-containing particle and (b) corresponding EDS spectra showing its elemental composition